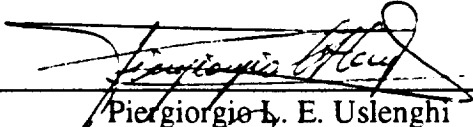


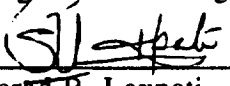
GRANT NAG2-544
COMPUTER CODE FOR
SCATTERING FROM IMPEDANCE BODIES OF
REVOLUTION
PART III: SURFACE IMPEDANCE WITH S AND PHI
VARIATION - ANALYTICAL AND NUMERICAL
RESULTS

June 1993

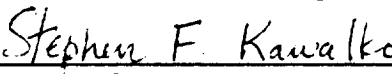
Principal Investigator: _____


Piergiorgio L. E. Uslenghi

Co-Principal Investigator: _____


Sharad R. Laxpati

Research Assistant: _____


Stephen F. Kawalko

Report EML-93-6-1
Electromagnetics Laboratory
Department of Electrical Engineering and Computer Science (M/C 154)
University of Illinois at Chicago
P.O. Box 4348
Chicago, Illinois 60680

ACKNOWLEDGEMENT

This work was partially supported by the National Science Foundation under Grant ECS930000N and utilized the Cray Y-MP 4/64 at the National Center for Supercomputing Applications, University of Illinois at Urbana-Champaign.

TABLE OF CONTENTS

Chapter		Page
1.	Introduction	1
2.	Analytical Results	4
2.1	Introduction	4
2.2	Statement of Problem	4
2.3	Derivation of Integral Equations	7
2.4	Integral Equations for Body of Revolution	14
2.4.1	Preliminary Remarks	14
2.4.2	Electric Field Integral Equation	15
2.4.3	Magnetic Field Integral Equation	18
2.4.4	Combined Field Integral Equation	21
2.5	Far Field and Radar Cross Section	23
2.5.1	Far Scattered Fields	23
2.5.2	Radar Cross Section	25
3.	Numerical Methodology	27
3.1	Introduction	27
3.2	Method of Moments	27
3.3	Description of Scatterer Geometry and Surface Impedance	29
3.4	Hermite Expansion Functions	30
3.5	Hermite Expansion Functions on Rectangles	32
3.6	Expansion of Surface Currents	36
3.7	Selection of Sampling and Integration Points	41
4.	Numerical Results	47
4.1	Organization of Computer Code	47
4.2	Sample Results	50
	Bibliography	81

LIST OF FIGURES

Figure	Page
2.2.1 Geometry of Problem.....	5
2.2.2 Geometry of generating curve.....	5
3.5.1 Domain of two-dimensional Hermite expansion functions.....	33
3.6.1 Expansion function domains for components of the surface current.....	37
3.6.2 Construction of local coordinate system at $s = 0$	38
3.7.1 Location of sampling points for a continuous function.....	42
3.7.2 Location of sampling points for discontinuous functions.....	44
4.1.1 Cross section of cone-sphere geometry.....	49
4.1.2 Cross section of cone-cylinder geometry.....	49
4.2.1 Graphical representation of relative surface impedance given by eq. (4.2.1).....	53
4.2.2 Graphical representation of relative surface impedance given by eq. (4.2.2).....	53
4.2.3 Bistatic radar cross section for perfectly conducting cone-cylinder: TE polarization, $\phi_i = 0^\circ$ and $\theta_i = 45^\circ$	54
4.2.4 Bistatic radar cross section for perfectly conducting cone-cylinder: TM polarization, $\phi_i = 0^\circ$ and $\theta_i = 45^\circ$	55
4.2.5 Bistatic radar cross section for cone-cylinder with piecewise constant surface impedance: TE polarization, $\phi_i = 0^\circ$ and $\theta_i = 45^\circ$	56
4.2.6 Bistatic radar cross section for cone-cylinder with piecewise constant surface impedance: TM polarization, $\phi_i = 0^\circ$ and $\theta_i = 45^\circ$	57
4.2.7 Bistatic radar cross section for cone-cylinder with piecewise constant surface impedance: TE polarization, $\phi_i = 0^\circ$ and $\theta_i = 45^\circ$	58
4.2.8 Bistatic radar cross section for cone-cylinder with piecewise constant surface impedance: TM polarization, $\phi_i = 0^\circ$ and $\theta_i = 45^\circ$	59
4.2.9 Side view of cone-cylinder 2 with surface impedance given by eq. (4.2.3) showing the impedance patch.....	60
4.2.10 Bistatic radar cross section for perfectly absorbing cone-cylinder: TE polarization, $\phi_i = 270^\circ$ and $\theta_i = 0^\circ$	61
4.2.11 Bistatic radar cross section for perfectly absorbing cone-cylinder: TM polarization, $\phi_i = 270^\circ$ and $\theta_i = 0^\circ$	62
4.2.12 Bistatic radar cross section for perfectly absorbing cone-cylinder: TE polarization, $\phi_i = 270^\circ$ and $\theta_i = 45^\circ$	63

4.2.13	Bistatic radar cross section for perfectly absorbing cone-cylinder: TM polarization, $\phi_i = 270^\circ$ and $\theta_i = 45^\circ$	64
4.2.14	Bistatic radar cross section for perfectly absorbing cone-cylinder: TE polarization, $\phi_i = 270^\circ$ and $\theta_i = 90^\circ$	65
4.2.15	Bistatic radar cross section for perfectly absorbing cone-cylinder: TM polarization, $\phi_i = 270^\circ$ and $\theta_i = 90^\circ$	66
4.2.16	Bistatic radar cross section for perfectly absorbing cone-cylinder: TE polarization, $\phi_i = 270^\circ$ and $\theta_i = 135^\circ$	67
4.2.17	Bistatic radar cross section for perfectly absorbing cone-cylinder: TM polarization, $\phi_i = 270^\circ$ and $\theta_i = 135^\circ$	68
4.2.18	Bistatic radar cross section for perfectly absorbing cone-cylinder: TE polarization, $\phi_i = 270^\circ$ and $\theta_i = 180^\circ$	69
4.2.19	Bistatic radar cross section for perfectly absorbing cone-cylinder: TM polarization, $\phi_i = 270^\circ$ and $\theta_i = 180^\circ$	70
4.2.20	Bistatic radar cross section for cone-cylinder with impedance patch: TE polarization, $\phi_i = 270^\circ$ and $\theta_i = 0^\circ$	71
4.2.21	Bistatic radar cross section for cone-cylinder with impedance patch: TM polarization, $\phi_i = 270^\circ$ and $\theta_i = 0^\circ$	72
4.2.22	Bistatic radar cross section for cone-cylinder with impedance patch: TE polarization, $\phi_i = 270^\circ$ and $\theta_i = 45^\circ$	73
4.2.23	Bistatic radar cross section for cone-cylinder with impedance patch: TM polarization, $\phi_i = 270^\circ$ and $\theta_i = 45^\circ$	74
4.2.24	Bistatic radar cross section for cone-cylinder with impedance patch: TE polarization, $\phi_i = 270^\circ$ and $\theta_i = 90^\circ$	75
4.2.25	Bistatic radar cross section for cone-cylinder with impedance patch: TM polarization, $\phi_i = 270^\circ$ and $\theta_i = 90^\circ$	76
4.2.26	Bistatic radar cross section for cone-cylinder with impedance patch: TE polarization, $\phi_i = 270^\circ$ and $\theta_i = 135^\circ$	77
4.2.27	Bistatic radar cross section for cone-cylinder with impedance patch: TM polarization, $\phi_i = 270^\circ$ and $\theta_i = 135^\circ$	78
4.2.28	Bistatic radar cross section for cone-cylinder with impedance patch: TE polarization, $\phi_i = 270^\circ$ and $\theta_i = 180^\circ$	79
4.2.29	Bistatic radar cross section for cone-cylinder with impedance patch: TM polarization, $\phi_i = 270^\circ$ and $\theta_i = 180^\circ$	80

ABSTRACT

This report is on the third phase of the development of the computer codes for scattering by coated bodies that has been part of an ongoing effort in the Electromagnetics Laboratory of the Electrical Engineering and Computer Science Department at the University of Illinois at Chicago. The work reported here discusses the analytical and numerical results for the scattering of an obliquely incident plane wave by impedance bodies of revolution with phi variation of the surface impedance.

Integral equation formulation of the problem is considered. All three types of integral equations, electric field, magnetic field and combined field, are considered. These equations are solved numerically via the method of moments with parametric elements. Both TE and TM polarization of the incident plane wave are considered. The surface impedance is allowed to vary along both the profile of the scatterer and in the phi direction.

Computer code developed for this purpose determines the electric surface current as well as the bistatic radar cross section. The results obtained with this code have been validated by comparing the results with available results for specific scatterers such as the perfectly conducting sphere. Results for the cone-sphere and cone-cylinder-sphere for the case of an axially incident plane have been validated by comparing the results with the results with those obtained in the first phase of this project. In this report results for body of revolution scatterers with an abrupt change in the surface impedance along the both the profile of the scatterer and the phi direction are presented.

1. INTRODUCTION

The availability of new artificial dielectric and absorbing materials during the last decade has resulted in increased activity and interest in the formulation and analysis of reflection, transmission and scattering by such materials and bodies coated with these anisotropic materials [Graglia et. al., 1984, 1987a, 1987b] The very nature of these problems require that, except for very special cases of material parameters and geometries, a numerical solution be performed. Finite difference, finite element and integral equation formulations are the techniques employed most frequently in such cases. In this study the scattering problem is formulated in terms of an integral equation. This technique well suited to problems involving anisotropic and inhomogeneous materials. The integral equation formulation leads to a set of coupled integro-differential equations which can be solved numerically using the method of moments [Harrington, 1968]. From a computation stand point a method of moments solution of an integral equation is particularly effective when parametric elements are employed [Graglia, 1988a, 1989].

This report describes the details of the development of a set of computer codes for scattering by a body of revolution with arbitrary surface impedance. This is the third phase of an ongoing effort at the University of Illinois at Chicago to develop codes that would allow the numerical computation of electromagnetic scattering by and the radar cross section (RCS) of an arbitrary body coated with a variety of artificial materials. The present phase of the study presented in this report is the development of analytical results, numerical codes and results for the scattering of an obliquely incident plane wave by a body of revolution with an impedance boundary condition. This phase differs from the previous phase in that the surface impedance is allowed to vary not only along the profile of the scatterer but also in the ϕ direction.

The analytical results presented in Chapter 2 are applicable to a scatterer which has a body of revolution symmetry. The profile of the scatterer is readily described by a generating curve described parametrically in cylindrical coordinates by a pair of functions $\rho(s)$ and $z(s)$ where s is the arclength along the profile (generating curve) of the scatterer. The surface of the scatterer is generated by rotating the generating curve in the ϕ direction around the z axis. The surface impedance is allowed to vary as a function of both the arclength s and the cylindrical coordinate ϕ .

The integral equation formulation leads to vector integro-differential equations for the unknown electric surface current density on the scatterer. All three types of integral equations, electric field integral equation (EFIE), magnetic field integral equation (MFIE) and combined field integral equation (CFIE) are derived. These integral equations are then specialized for the case where the scatterer has body of revolution symmetry. This specialization transforms the vector integral equations into a pair of coupled scalar integral equations in terms of the vector components of the electric surface current density. Expressions for the incident fields with arbitrary angle of polarization and arbitrary angles of incidence are derived in parallel with the corresponding integral equation. Finally, expressions for the far scattered fields and the bistatic radar cross sections in terms of the electric surface current density are derived for the geometry under consideration.

In Chapter 3, after a brief discussion of the method of moments to introduce the terminology and notations, specific details of geometry and surface impedance descriptions are presented. This is followed by an overview of the Hermite expansion functions utilized in the method of moments implementation. The discussion covers Hermite expansion functions in one-dimension and its extension to two-dimensions. This is followed by details of the representation of the surface currents and some practical

considerations involving the testing procedure used in this method of moments implementation. The discussions presented in this chapter delineate explicitly the expressions needed for numerical implementation of the scheme and shed some light on the development of the computer code.

The numerical results obtained from the code developed based on the discussions found in Chapters 2 and 3 are presented in Chapter 4. Results validating the code have been previously presented in the report for Phase II of this study [Uslenghi et al., 1991b]. The results presented here will concentrate on cases where the surface impedance is allowed to have abrupt discontinuities in either the s direction only or in both the s and ϕ directions (i.e. impedance patch). The data presented was generated on a Cray Y-MP with 64 megawords (512 megabytes) of memory. Future plans include the parallelization of the code for shared memory parallel processor systems like the Cray Y-MP and also for massively parallel processor systems like the Thinking Machines CM5.

2. ANALYTICAL RESULTS

2.1 Introduction

This chapter deals with the derivation of the analytical results for the problem of scattering of an electromagnetic plane wave by a scatterer with body of revolution symmetry. The material properties of the scatterer are specified through the use of a surface impedance boundary condition. General integral equations for a scatterer with arbitrary geometry and arbitrary surface impedance are derived. Three integral equations, electric field integral equation, magnetic field integral equation and combined field integral equation, are presented. These integral equations are then specialized to the geometry of interest. Finally, expressions for the far field and bistatic radar cross section are presented.

2.2 Statement of Problem

Given a scatterer geometry, the material properties of the scatterer and the form of the incident electromagnetic fields the problem is to determine the fields which arise when the incident fields interact with the scatterer. The geometry of the problem under consideration is shown in Figure 2.2.1. The scatterer consists of a body of revolution with a surface impedance boundary condition. The surface impedance is allowed to vary arbitrarily over the surface of the scatterer. The incident electromagnetic wave is taken to be a linearly polarized plane wave with arbitrary angle of polarization and arbitrary angles of incidence. Throughout this work, a time harmonic variation of the form $e^{j\omega t}$ is implicitly assumed.

The geometry of the scatterer is defined by specifying a generating curve which is parameterized in terms of the arclength along the generating curve as shown in Figure 2.2.2. To allow for rather complex scatterer geometries the generating curve is defined by specifying two profile functions $\rho(s)$ and $z(s)$ where s is the arclength coordinate of the point (ρ, z) on the generating curve and ρ and z are the usual cylindrical

coordinates. The surface of the scatterer is then defined by rotating the generating curve about the z axis through an angle of 360° . Since ρ and z are functions of s , each point on the surface of the scatterer is uniquely defined by its s and ϕ coordinates. The surface of the scatterer can then be easily mapped to a rectangular region in the s - ϕ plane.

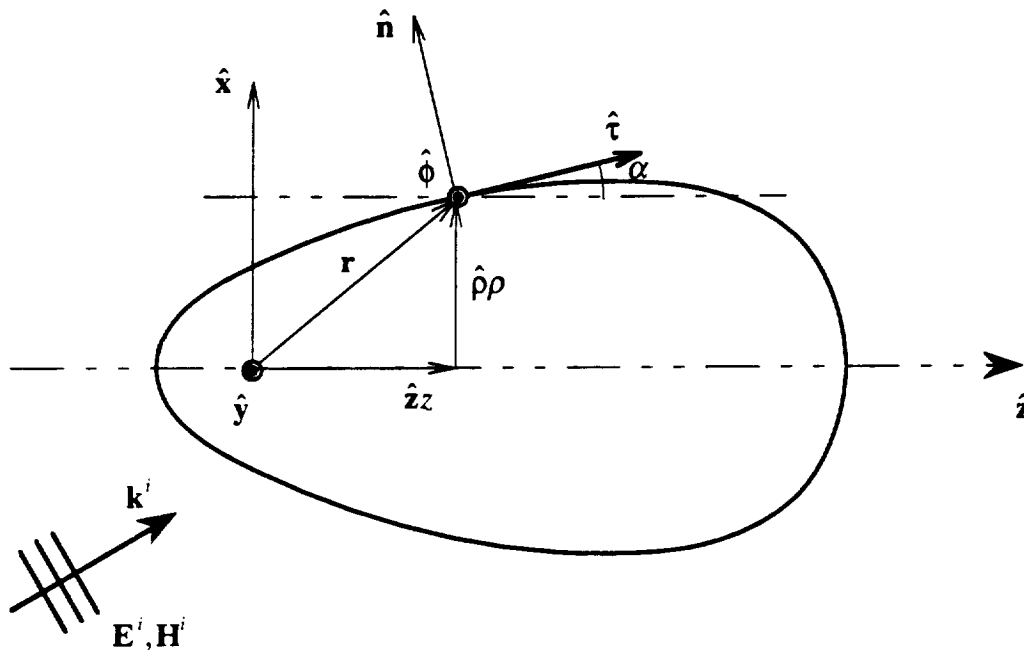


Figure 2.2.1 Geometry of Problem

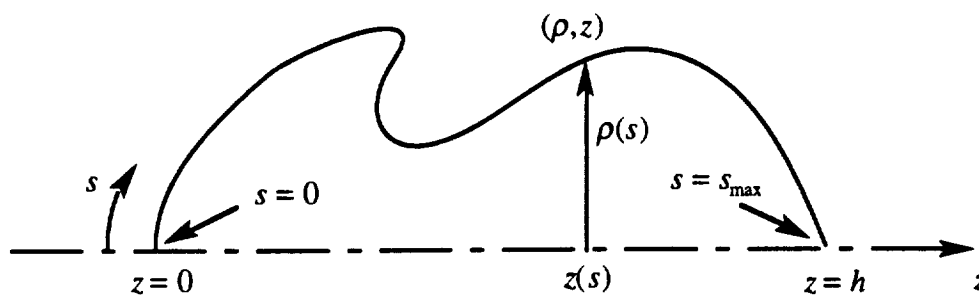


Figure 2.2.2 Geometry of generating curve.

The direction of propagation of the incident fields is specified by two angles of incidence, θ_i and ϕ_i where θ_i is the angle between the propagation vector, \mathbf{k}^i , and the positive z axis and ϕ_i is the angle between the projection of the propagation vector on to the x - y plane and the positive x axis. Using θ_i and ϕ_i , define the following set of orthogonal unit vectors

$$\hat{\mathbf{x}}_i = \hat{\rho} \cos(\theta_i) \cos(\Delta_i) + \hat{\phi} \cos(\theta_i) \sin(\Delta_i) - \hat{\mathbf{z}} \sin(\theta_i) \quad (2.2.1)$$

$$\hat{\mathbf{y}}_i = -\hat{\rho} \sin(\Delta_i) + \hat{\phi} \cos(\Delta_i) \quad (2.2.2)$$

$$\hat{\mathbf{z}}_i = \hat{\rho} \sin(\theta_i) \cos(\Delta_i) + \hat{\phi} \sin(\theta_i) \sin(\Delta_i) + \hat{\mathbf{z}} \cos(\theta_i) \quad (2.2.3)$$

where $\Delta_i = \phi_i - \phi$. These unit vectors define a coordinate system in which the incident fields propagate along $\hat{\mathbf{z}}_i$ and have components which lie only in the x_i - y_i plane. The incident electric field, \mathbf{E}^i , and the incident magnetic field, \mathbf{H}^i , can be written in terms of the coordinate system defined by eqs. (2.2.1), (2.2.2) and (2.2.3) as

$$\mathbf{E}^i(\mathbf{r}) = [\hat{\mathbf{x}}_i \cos(\nu) + \hat{\mathbf{y}}_i \sin(\nu)] e^{-j\mathbf{k}^i \cdot \mathbf{r}} \quad (2.2.4)$$

$$\mathbf{H}^i(\mathbf{r}) = \frac{1}{Z_0} [-\hat{\mathbf{x}}_i \sin(\nu) + \hat{\mathbf{y}}_i \cos(\nu)] e^{-j\mathbf{k}^i \cdot \mathbf{r}} \quad (2.2.5)$$

where $\mathbf{k}^i = k_0 \hat{\mathbf{k}}_i = k_0 \hat{\mathbf{z}}_i$, $\mathbf{r} = \hat{\rho} \rho + \hat{\mathbf{z}} z$, Z_0 is the impedance of free space, k_0 is the free space wave number and ν is the polarization angle. The incident plane wave is said to have transverse magnetic polarization (TM polarization) when the incident electric field has a component only in the $\hat{\mathbf{y}}_i$ direction ($\nu = \pm \pi/2$) and transverse electric polarization (TE polarization) when the incident magnetic field has a component only in the $\hat{\mathbf{y}}_i$ direction ($\nu = 0, \pi$)

In general, η the relative surface impedance can be an arbitrary function of s and ϕ . However, some care must be taken so that the definition of η does not lead to an ambiguous value for the surface impedance at the points $s = 0$ and $s = s_{\max}$. For example, $\eta(s, \phi) = \cos(\phi)$ leads to an ambiguous surface impedance at $s = 0$ and $s = s_{\max}$, that is, η

has an infinite number of values at these two points. However, if $\eta(s, \phi) = u(\phi - \pi)$, $0 \leq \phi \leq 2\pi$, where $u(t)$ is the unit step function, then η has two values at $s = 0$ and $s = s_{\max}$ but this is an acceptable form since it corresponds to a scatterer with a surface which is perfectly conducting in the half space $y > 0$ and has a relative surface impedance equal to 1 in the half space $y < 0$.

2.3 Derivation of Integral Equations

In the phasor domain, Maxwell's equations can be written as follows:

$$\nabla \times \mathbf{H} = \mathbf{J}_e + j\omega\mathbf{D} \quad (2.3.1)$$

$$\nabla \times \mathbf{E} = -\mathbf{J}_m - j\omega\mathbf{B} \quad (2.3.2)$$

$$\nabla \cdot \mathbf{D} = \rho_e \quad (2.3.3)$$

$$\nabla \cdot \mathbf{B} = \rho_m \quad (2.3.4)$$

where \mathbf{E} , \mathbf{H} , \mathbf{D} , \mathbf{B} are the electric field, magnetic field, electric flux density and the magnetic flux density respectively, \mathbf{J}_e , \mathbf{J}_m , ρ_e , and ρ_m are the electric current density, magnetic current density, electric charge density and magnetic charge density respectively and a time dependence of $e^{j\omega t}$ has been assumed.

A solution of Maxwell's equations in free space for the electric field, \mathbf{E} , and the magnetic field, \mathbf{H} , in terms of the electric sources, ρ_e and \mathbf{J}_e and the magnetic sources, ρ_m and \mathbf{J}_m can be written as follows [Elliott, 1981]

$$\mathbf{E}(\mathbf{r}) = -\nabla\Phi_e(\mathbf{r}) - j\omega\mathbf{A}_e(\mathbf{r}) - \frac{1}{\epsilon_0}\nabla \times \mathbf{A}_m(\mathbf{r}) \quad (2.3.5)$$

$$\mathbf{H}(\mathbf{r}) = -\nabla\Phi_m(\mathbf{r}) - j\omega\mathbf{A}_m(\mathbf{r}) + \frac{1}{\mu_0}\nabla \times \mathbf{A}_e(\mathbf{r}) \quad (2.3.6)$$

where

$$\Phi_e(\mathbf{r}) = \frac{1}{4\pi\epsilon_0} \int_V G(\mathbf{r}, \mathbf{r}') \rho_e(\mathbf{r}') dV' \quad (2.3.7)$$

$$\Phi_m(\mathbf{r}) = \frac{1}{4\pi\mu_0} \int_V G(\mathbf{r}, \mathbf{r}') \rho_m(\mathbf{r}') dV' \quad (2.3.8)$$

$$\mathbf{A}_e(\mathbf{r}) = \frac{\mu_0}{4\pi} \int_V G(\mathbf{r}, \mathbf{r}') \mathbf{J}_e(\mathbf{r}') dV' \quad (2.3.9)$$

$$\mathbf{A}_m(\mathbf{r}) = \frac{\epsilon_0}{4\pi} \int_V G(\mathbf{r}, \mathbf{r}') \mathbf{J}_m(\mathbf{r}') dV' \quad (2.3.10)$$

ϵ_0 is the permittivity of free space, μ_0 is the permeability of free space, $k_0 = \omega\sqrt{\mu_0\epsilon_0}$ is the free space wave number and $G(\mathbf{r}, \mathbf{r}')$ is the free space Green's function which is given by

$$G(\mathbf{r}, \mathbf{r}') = G(R) = \frac{e^{-jk_0R}}{R}; \quad R = |\mathbf{r} - \mathbf{r}'| \quad (2.3.11)$$

The terms Φ_e , Φ_m , \mathbf{A}_e , and \mathbf{A}_m are referred to as the electric scalar potential, magnetic scalar potential, electric vector potential and the magnetic vector potential respectively. Additionally, the charge densities ρ_e and ρ_m are related to the current densities \mathbf{J}_e and \mathbf{J}_m by the following continuity equations

$$\nabla \cdot \mathbf{J}_e(\mathbf{r}) + j\omega\rho_e(\mathbf{r}) = 0 \quad (2.3.12)$$

$$\nabla \cdot \mathbf{J}_m(\mathbf{r}) + j\omega\rho_m(\mathbf{r}) = 0 \quad (2.3.13)$$

The scattering problem under consideration is formulated by invoking the equivalence theorem [Harrington, 1961], [Elliott, 1981]. The scatterer is removed and is replaced by an equivalent electric surface current density \mathbf{J}_{es} , an equivalent electric surface charge density ρ_{es} , an equivalent magnetic surface current density \mathbf{J}_{ms} , and an equivalent magnetic surface charge density ρ_{ms} . The surface currents \mathbf{J}_{es} and \mathbf{J}_{ms} and the surface charge densities ρ_{es} and ρ_{ms} exist on the surface S where S corresponds to the surface of the scatterer. The original fields on S and the equivalent surface currents satisfy the following boundary conditions

$$\mathbf{J}_{es} = \hat{\mathbf{n}} \times \mathbf{H} \quad (2.3.14)$$

$$\mathbf{J}_{ms} = -\hat{\mathbf{n}} \times \mathbf{E} \quad (2.3.15)$$

where $\hat{\mathbf{n}}$ is the outward pointing surface normal and \mathbf{H} and \mathbf{E} are the total magnetic field and total electric field respectively over the surface S . For the problem under consideration the scatterer is taken to be an impenetrable scatterer so the fields are equal to zero inside the scatterer. The total electric field and total magnetic field are then given by $\mathbf{E} = \mathbf{E}^i + \mathbf{E}^s$ and $\mathbf{H} = \mathbf{H}^i + \mathbf{H}^s$ where \mathbf{E}^s and \mathbf{H}^s are the scattered electric and magnetic fields respectively.

Since the sources are confined to the surface of the scatterer the potentials associated with the equivalent surface current densities and surface charge densities can be obtained from eqs. (2.3.7), (2.3.8), (2.3.9) and (2.3.10) by replacing the current densities, \mathbf{J}_e and \mathbf{J}_m , and the charge densities, ρ_e and ρ_m , by the equivalent surface current densities, \mathbf{J}_{es} and \mathbf{J}_{ms} , and the equivalent surface charge densities, ρ_{es} and ρ_{ms} respectively. Also, the volume integral $\int_V dV'$ is replaced by the surface integral $\oint_S dS'$.

Then, the scattered electric and magnetic fields due to the equivalent sources can be written as

$$\begin{aligned} \mathbf{E}^s(\mathbf{r}) = & -\frac{1}{4\pi\epsilon_0} \nabla \oint_S G(\mathbf{r}, \mathbf{r}') \rho_{es}(\mathbf{r}') dS' - \frac{j\omega\mu_0}{4\pi} \oint_S G(\mathbf{r}, \mathbf{r}') \mathbf{J}_{es}(\mathbf{r}') dS' \\ & - \frac{1}{4\pi} \nabla \times \oint_S G(\mathbf{r}, \mathbf{r}') \mathbf{J}_{ms}(\mathbf{r}') dS' \end{aligned} \quad (2.3.16)$$

$$\begin{aligned} \mathbf{H}^s(\mathbf{r}) = & -\frac{1}{4\pi\mu_0} \nabla \oint_S G(\mathbf{r}, \mathbf{r}') \rho_{ms}(\mathbf{r}') dS' - j \frac{\omega\epsilon_0}{4\pi} \oint_S G(\mathbf{r}, \mathbf{r}') \mathbf{J}_{ms}(\mathbf{r}') dS' \\ & + \frac{1}{4\pi} \nabla \times \oint_S G(\mathbf{r}, \mathbf{r}') \mathbf{J}_{es}(\mathbf{r}') dS' \end{aligned} \quad (2.3.17)$$

Interchanging the order of differentiation and integration in eqs. (2.3.16) and (2.3.17), making use of the following relations

$$\nabla \int G(\mathbf{r}, \mathbf{r}') f(\mathbf{r}') dS' = \int f(\mathbf{r}') \nabla G(\mathbf{r}, \mathbf{r}') dS' \quad (2.3.18)$$

$$\nabla \times \int G(\mathbf{r}, \mathbf{r}') \mathbf{F}(\mathbf{r}') dS' = \int \nabla G(\mathbf{r}, \mathbf{r}') \times \mathbf{F}(\mathbf{r}') dS' \quad (2.3.19)$$

noting that $\nabla G = -\nabla' G$ and using the continuity equations given by eqs. (2.3.12) and (2.3.13) to write the charge densities in terms of the surface current densities, the scattered electric and magnetic fields can be written as

$$\mathbf{E}^s(\mathbf{r}) = \frac{jZ_0}{4\pi k_0} \oint_S [\nabla' G(\mathbf{r}, \mathbf{r}')][\nabla' \cdot \mathbf{J}_{es}(\mathbf{r}')] dS' - \frac{jk_0 Z_0}{4\pi} \oint_S G(\mathbf{r}, \mathbf{r}') \mathbf{J}_{es}(\mathbf{r}') dS' + \frac{1}{4\pi} \oint_S \nabla' G(\mathbf{r}, \mathbf{r}') \times \mathbf{J}_{ms}(\mathbf{r}') dS' \quad (2.3.20)$$

$$\mathbf{H}^s(\mathbf{r}) = \frac{jY_0}{4\pi k_0} \oint_S [\nabla' G(\mathbf{r}, \mathbf{r}')][\nabla' \cdot \mathbf{J}_{ms}(\mathbf{r}')] dS' - \frac{jk_0 Y_0}{4\pi} \oint_S G(\mathbf{r}, \mathbf{r}') \mathbf{J}_{ms}(\mathbf{r}') dS' - \frac{1}{4\pi} \oint_S \nabla' G(\mathbf{r}, \mathbf{r}') \times \mathbf{J}_{es}(\mathbf{r}') dS' \quad (2.3.21)$$

where $Z_0 = \sqrt{\mu_0/\epsilon_0}$ is the characteristic impedance of free space and $Y_0 = 1/Z_0$ is the characteristic admittance of free space.

If the current densities \mathbf{J}_{es} and \mathbf{J}_{ms} were known eqs. (2.3.20) and (2.3.21) could be used to calculate the scattered electric and magnetic fields. However for a scattering problem \mathbf{J}_{es} and \mathbf{J}_{ms} are generally not known in advance and so a direct calculation of the scattered fields is not possible. Since the incident electric and magnetic fields are known it is conceivable that one might try to construct a pair of integral equations for the unknown surface current densities by substituting eqs. (2.3.20) and (2.3.21) into the electromagnetic boundary conditions given by eqs. (2.3.14) and (2.3.15). However, one important piece of information for this problem has not been considered. The material properties of the scatterer do not appear in the expression for the either the scattered electric field or the scattered magnetic field. They also do not appear in either of the two electromagnetic boundary conditions.

If one were considering the problem of scattering from a dielectric scatterer the material properties of the scatterer would appear in the Green's function used to write the potentials for the fields inside the scatterer. For an impedance scatterer the material

properties are specified through the use of the surface impedance boundary condition. Repeated for convenience, the surface impedance boundary condition is given by

$$\mathbf{E}_{\text{tan}} = \mathbf{E} - (\mathbf{E} \cdot \hat{\mathbf{n}})\hat{\mathbf{n}} = \eta Z_0 \hat{\mathbf{n}} \times \mathbf{H} \quad (2.3.22)$$

where Z_0 is the impedance of free space, η is the relative surface impedance and $\hat{\mathbf{n}}$ is the outward pointing surface normal. Taking the cross product of $\hat{\mathbf{n}}$ with eq. (2.3.22) and making use of the following relation

$$\hat{\mathbf{n}} \times \mathbf{E}_{\text{tan}} = \hat{\mathbf{n}} \times [\mathbf{E} - (\mathbf{E} \cdot \hat{\mathbf{n}})\hat{\mathbf{n}}] = \hat{\mathbf{n}} \times \mathbf{E} \quad (2.3.23)$$

one obtains the following expression

$$\hat{\mathbf{n}} \times \mathbf{E} = \eta Z_0 \hat{\mathbf{n}} \times \hat{\mathbf{n}} \times \mathbf{H} \quad (2.3.24)$$

Making use of the electric and magnetic boundary conditions given by eqs. (2.3.14) and (2.3.15) the magnetic surface current density \mathbf{J}_{ms} can be written in terms of the electric surface current density \mathbf{J}_{es} as follows

$$\mathbf{J}_{ms} = -\eta Z_0 \hat{\mathbf{n}} \times \mathbf{J}_{es} \quad (2.3.25)$$

Substituting eq. (2.3.25) into eqs. (2.3.20) and (2.3.21) one obtains the following expressions for the scattered fields

$$\begin{aligned} \mathbf{E}^s(\mathbf{r}) = & \frac{jZ_0}{4\pi k_0} \oint_S [\nabla' G(\mathbf{r}, \mathbf{r}')][\nabla' \cdot \mathbf{J}_{es}(\mathbf{r}')] dS' - \frac{jk_0 Z_0}{4\pi} \oint_S G(\mathbf{r}, \mathbf{r}') \mathbf{J}_{es}(\mathbf{r}') dS' \\ & - \frac{Z_0}{4\pi} \oint_S \nabla' G(\mathbf{r}, \mathbf{r}') \times [\eta(\mathbf{r}') \hat{\mathbf{n}}' \times \mathbf{J}_{es}(\mathbf{r}')] dS' \end{aligned} \quad (2.3.26)$$

$$\begin{aligned} \mathbf{H}^s(\mathbf{r}) = & -\frac{j}{4\pi k_0} \oint_S [\nabla' G(\mathbf{r}, \mathbf{r}')][\nabla' \cdot (\eta(\mathbf{r}') \hat{\mathbf{n}}' \times \mathbf{J}_{es}(\mathbf{r}'))] dS' \\ & + \frac{jk_0}{4\pi} \oint_S G(\mathbf{r}, \mathbf{r}') [\eta(\mathbf{r}') \hat{\mathbf{n}}' \times \mathbf{J}_{es}(\mathbf{r}')] dS' \\ & - \frac{1}{4\pi} \oint_S \nabla' G(\mathbf{r}, \mathbf{r}') \times \mathbf{J}_{es}(\mathbf{r}') dS' \end{aligned} \quad (2.3.27)$$

The electric field integral equation (EFIE) for the unknown surface current density \mathbf{J}_{es} can be derived in the usual manner [Poggio and Miller, 1973] from the boundary condition for the total electric field given by eq. (2.3.15). Substituting eq. (2.3.26) in eq. (2.3.15), making use of eq. (2.3.25) and taking the limit as the field point \mathbf{r} approaches \mathbf{r}' on the surface S the following electric field integral equation is obtained

$$\begin{aligned} \eta(\mathbf{r})Z_0\hat{\mathbf{n}} \times \mathbf{J}_{es}(\mathbf{r}) = & 2\hat{\mathbf{n}} \times \mathbf{E}^i(\mathbf{r}) + \frac{jZ_0}{2\pi k_0} \hat{\mathbf{n}} \times \oint_S [\nabla' G(\mathbf{r}, \mathbf{r}')] [\nabla' \cdot \mathbf{J}_{es}(\mathbf{r}')] dS' \\ & - \frac{jk_0 Z_0}{2\pi} \hat{\mathbf{n}} \times \oint_S G(\mathbf{r}, \mathbf{r}') \mathbf{J}_{es}(\mathbf{r}') dS' \\ & - \frac{Z_0}{2\pi} \hat{\mathbf{n}} \times \oint_S \nabla' G(\mathbf{r}, \mathbf{r}') \times [\eta(\mathbf{r}') \hat{\mathbf{n}}' \times \mathbf{J}_{es}(\mathbf{r}')] dS' \end{aligned} \quad (2.3.28)$$

where \oint_S represents the principle value of the surface integral \oint_S .

In a similar manner, the magnetic field integral equation (MFIE) can be derived from the boundary condition for the total magnetic field given by eq. (2.3.14) and the expression for the scattered magnetic field given by eq. (2.3.27). The resulting magnetic field integral equation is given below.

$$\begin{aligned} \mathbf{J}_{es}(\mathbf{r}) = & 2\hat{\mathbf{n}} \times \mathbf{H}^i(\mathbf{r}) - \frac{j}{2\pi k_0} \hat{\mathbf{n}} \times \oint_S [\nabla' G(\mathbf{r}, \mathbf{r}')] [\nabla' \cdot (\eta(\mathbf{r}') \hat{\mathbf{n}}' \times \mathbf{J}_{es}(\mathbf{r}'))] dS' \\ & + \frac{jk_0}{2\pi} \hat{\mathbf{n}} \times \oint_S G(\mathbf{r}, \mathbf{r}') [\eta(\mathbf{r}') \hat{\mathbf{n}}' \times \mathbf{J}_{es}(\mathbf{r}')] dS' \\ & - \frac{1}{2\pi} \hat{\mathbf{n}} \times \oint_S \nabla' G(\mathbf{r}, \mathbf{r}') \times \mathbf{J}_{es}(\mathbf{r}') dS' \end{aligned} \quad (2.3.29)$$

Following Mitzner [1968] and Oshiro et. al. [1970], the combined field integral equation (CFIE) can be derived from the superposition of the magnetic field boundary condition given by eq. (2.3.14) and a modified form of the electric field boundary condition given by eq. (2.3.15). This form of the integral equation is also discussed in

detail by Jones [1979]. Using $\mathbf{E}_{\text{tan}} = -\hat{\mathbf{n}} \times \hat{\mathbf{n}} \times \mathbf{E}$, an alternate form of the electric field boundary condition can be written as follows

$$\hat{\mathbf{n}} \times \mathbf{J}_{ms} = \mathbf{E}_{\text{tan}} \quad (2.3.30)$$

Now construct a combined field boundary condition by the superposition of the usual magnetic field boundary condition, eq. (2.3.14) and the electric field boundary condition given by eq. (2.3.30) as follows

$$\mathbf{J}_{es} + \frac{\alpha_{\text{CFIE}}}{Z_0} (\hat{\mathbf{n}} \times \mathbf{J}_{ms}) = \hat{\mathbf{n}} \times \mathbf{H} + \frac{\alpha_{\text{CFIE}}}{Z_0} \mathbf{E}_{\text{tan}} \quad (2.3.31)$$

where α_{CFIE} is a scalar constant. The combined field integral equation can then be derived by substituting the expressions for the scattered electric and magnetic fields given by eqs. (2.3.26) and (2.3.27) into eq. (2.3.31). However, it is more convenient to write the combined field integral equation by utilizing the results for the electric and magnetic field integral equations.

Using the notation of Poggio and Miller [1968] the electric field integral equation and the magnetic field integral equation can be written in operator notation as

$$L_E[\mathbf{J}_{es}(\mathbf{r}')] = 2\hat{\mathbf{n}} \times \mathbf{E}^i(\mathbf{r}) \quad (2.3.32)$$

$$L_H[\mathbf{J}_{es}(\mathbf{r}')] = 2\hat{\mathbf{n}} \times \mathbf{H}^i(\mathbf{r}) \quad (2.3.33)$$

where the electric field integral operator L_E and the magnetic field integral operator L_H are given by

$$\begin{aligned} L_E[\mathbf{J}_{es}(\mathbf{r}')] = & \eta(\mathbf{r})\hat{\mathbf{n}} \times \mathbf{J}_{es}(\mathbf{r}) \\ & - \frac{jZ_0}{2\pi k_0} \hat{\mathbf{n}} \times \oint_S \nabla' G [\nabla' \cdot \mathbf{J}_{es}(\mathbf{r}')] dS' \\ & + \frac{jk_0 Z_0}{2\pi} \hat{\mathbf{n}} \times \oint_S G \mathbf{J}_{es}(\mathbf{r}') dS' \\ & + \frac{Z_0}{2\pi} \hat{\mathbf{n}} \times \oint_S \nabla' G \times [\eta(\mathbf{r}')\hat{\mathbf{n}}' \times \mathbf{J}_{es}(\mathbf{r}')] dS' \end{aligned} \quad (2.3.34)$$

and

$$\begin{aligned}
L_H[\mathbf{J}_{es}(\mathbf{r}')] &= \mathbf{J}_{es}(\mathbf{r}) \\
&+ \frac{j}{2\pi k_0} \hat{\mathbf{n}} \times \int_S \nabla' G [\nabla' \cdot \eta(\mathbf{r}') \hat{\mathbf{n}}' \times \mathbf{J}_{es}(\mathbf{r}')] dS' \\
&- \frac{jk_0}{2\pi} \hat{\mathbf{n}} \times \oint_S \eta(\mathbf{r}') G [\hat{\mathbf{n}} \times \mathbf{J}_{es}(\mathbf{r}')] dS' \\
&+ \frac{1}{2\pi} \hat{\mathbf{n}} \times \int_S \nabla' G \times \mathbf{J}_{es}(\mathbf{r}') dS'
\end{aligned} \tag{2.3.35}$$

The combined field integral equation can then be written in terms of the electric and magnetic field integral equations as

$$L_c[\mathbf{J}_{es}(\mathbf{r}')] = 2\hat{\mathbf{n}} \times \left(\mathbf{H}^i(\mathbf{r}) - \frac{\alpha_{\text{CFIE}}}{Z_0} \hat{\mathbf{n}} \times \mathbf{E}^i(\mathbf{r}) \right) \tag{2.3.36}$$

where the combined field integral operator L_c is given by

$$L_c[\mathbf{J}_{es}(\mathbf{r}')] = L_H[\mathbf{J}_{es}(\mathbf{r}')] - \frac{\alpha_{\text{CFIE}}}{Z_0} \hat{\mathbf{n}} \times L_E[\mathbf{J}_{es}(\mathbf{r}')] \tag{2.3.37}$$

The electric field, magnetic field and combined field integral equation given by eqs. (2.3.32), (2.3.33) and (2.3.36) respectively are valid for scatterers with arbitrary shape and arbitrary surface impedance. In the following sections these integral equation will be specialized to the case where the shape of the scatterer is a body of revolution.

2.4 Integral Equations for Body of Revolution

2.4.1 Preliminary Remarks

The integral equations obtained in Section 2.3 are valid for an arbitrarily shaped scatterer with arbitrary surface impedance. In Sections 2.4.2, 2.4.3 and 2.4.4 these integral equations will be simplified for the case of a scatterer with body of revolution symmetry.

At each point $P = (\rho, \phi, z)$ on the surface of a body of revolution it is possible to construct a local right handed coordinate system (τ, n, ϕ) as shown in Figure 2.2.1. The unit vectors for the local coordinate system at the point P can be written as

$$\hat{\tau} = \hat{\rho} \sin(\alpha) + \hat{z} \cos(\alpha) \quad (2.4.1)$$

$$\hat{n} = \hat{\rho} \cos(\alpha) - \hat{z} \sin(\alpha) \quad (2.4.2)$$

$$\hat{\phi} = -\hat{x} \sin(\phi) + \hat{y} \cos(\phi) \quad (2.4.3)$$

where α is the angle between $\hat{\tau}$ and \hat{z} and $\hat{\rho}$ is the usual unit vector from the cylindrical coordinate system which is given by

$$\hat{\rho} = \hat{x} \cos(\phi) + \hat{y} \sin(\phi) \quad (2.4.4)$$

Also, the unit vectors $\hat{\tau}$ and $\hat{\phi}$ are tangent to the surface at the point P while the unit vector \hat{n} is normal to the surface at the point P . Note, since the generating curve for the body of revolution is defined by specifying two profile function $\rho(s)$ and $z(s)$ the angle α is also a function of s .

2.4.2 Electric Field Integral Equation

In this section the electric field integral equation derived in Section 2.3 for the case of an impedance body will be specialized for a scatterer with body of revolution symmetry. In the process, the vector integral equation for the unknown vector electric surface current density \mathbf{J}_{es} will be reduced to a pair of coupled scalar integral equations in terms of the vector components of \mathbf{J}_{es} .

The electric field integral is specialized by obtaining the components of the integral equation which are tangent to the surface of the body of revolution. In order to obtain the tangential components it is convenient to rewrite the electric field integral equation given by eq.(2.3.28) as follows

$$2\hat{n} \times \mathbf{E}^i(\mathbf{r}) = \eta(\mathbf{r})Z_0 \hat{n} \times \mathbf{J}_{es}(\mathbf{r}) - \mathfrak{S}_1^E(\mathbf{r}) - \mathfrak{S}_2^E(\mathbf{r}) - \mathfrak{S}_3^E(\mathbf{r}) \quad (2.4.5)$$

where

$$\mathfrak{S}_1^E(\mathbf{r}) = \frac{jZ_0}{2\pi k_0} \hat{\mathbf{n}} \times \int_S [\nabla' G(\mathbf{r}, \mathbf{r}')][\nabla' \cdot \mathbf{J}_{es}(\mathbf{r}')] dS' \quad (2.4.6)$$

$$\mathfrak{S}_2^E(\mathbf{r}) = -\frac{jk_0 Z_0}{2\pi} \hat{\mathbf{n}} \times \int_S G(\mathbf{r}, \mathbf{r}') \mathbf{J}_{es}(\mathbf{r}') dS' \quad (2.4.7)$$

$$\mathfrak{S}_3^E(\mathbf{r}) = -\frac{Z_0}{2\pi} \hat{\mathbf{n}} \times \int_S \nabla' G(\mathbf{r}, \mathbf{r}') \times [\eta(\mathbf{r}') \hat{\mathbf{n}}' \times \mathbf{J}_{es}(\mathbf{r}')] dS' \quad (2.4.8)$$

and

$$\begin{aligned} \mathbf{J}_{es}(\mathbf{r}') &= \hat{\tau}' J_\tau(\mathbf{r}') + \hat{\phi}' J_\phi(\mathbf{r}') \\ &= \hat{\rho} [\sin(\alpha') \cos(\Delta') J_\tau(\mathbf{r}') - \sin(\Delta') J_\phi(\mathbf{r}')] \\ &\quad + \hat{\phi} [\cos(\Delta') J_\phi(\mathbf{r}') - \sin(\alpha') \sin(\Delta') J_\tau(\mathbf{r}')] + \hat{z} \cos(\alpha') J_\tau(\mathbf{r}') \end{aligned} \quad (2.4.9)$$

where $\Delta' = \phi' - \phi$. Interchanging the cross product operation with the integration operation and making use of the following expression

$$\nabla' G = -\nabla G = (\mathbf{r} - \mathbf{r}') \frac{1 + jk_0 R}{R^3} e^{-jk_0 R} = (\mathbf{r} - \mathbf{r}') G_1 \quad (2.4.10)$$

where

$$G_1 = \frac{1 + jk_0 R}{R^3} e^{-jk_0 R} \quad (2.4.11)$$

the expressions for \mathfrak{S}_1^E , \mathfrak{S}_2^E and \mathfrak{S}_3^E can be written as

$$\mathfrak{S}_1^E(\mathbf{r}) = \frac{jZ_0}{2\pi k_0} \int_S G_1(\mathbf{r}, \mathbf{r}') [\hat{\mathbf{n}} \times (\mathbf{r} - \mathbf{r}')][\nabla' \cdot \mathbf{J}_{es}(\mathbf{r}')] dS' \quad (2.4.12)$$

$$\mathfrak{S}_2^E(\mathbf{r}) = -\frac{jk_0 Z_0}{2\pi} \int_S G(\mathbf{r}, \mathbf{r}') [\hat{\mathbf{n}} \times \mathbf{J}_{es}(\mathbf{r}')] dS' \quad (2.4.13)$$

$$\mathfrak{S}_3^E(\mathbf{r}) = -\frac{Z_0}{2\pi} \int_S \eta(\mathbf{r}') G_1(\mathbf{r}, \mathbf{r}') [\hat{\mathbf{n}} \times (\mathbf{r} - \mathbf{r}') \times (\hat{\mathbf{n}}' \times \mathbf{J}_{es}(\mathbf{r}'))] dS' \quad (2.4.14)$$

The τ and ϕ components are obtained by taking the dot product of eq (2.4.5) with $\hat{\tau}$ and $\hat{\phi}$ respectively.

The electric field integral equation given by eq. (2.3.28) can now be written as the following pair of coupled scalar integral equations.

$$\begin{aligned}
E_{\phi}^i(\mathbf{r}) = & \frac{1}{2}\eta(\mathbf{r})Z_0J_{\phi}(\mathbf{r}) \\
& + \frac{jZ_0}{4\pi k_0} \int_S G_1(\mathbf{r},\mathbf{r}')\rho'\sin(\Delta') \left[\frac{\partial J_{\tau}(\mathbf{r}')}{\partial s'} + \frac{\sin(\alpha')}{\rho'}J_{\tau}(\mathbf{r}') + \frac{1}{\rho'}\frac{\partial J_{\phi}(\mathbf{r}')}{\partial \phi'} \right] dS' \\
& + \frac{jk_0Z_0}{4\pi} \oint_S G(\mathbf{r},\mathbf{r}')\sin(\alpha')\sin(\Delta')J_{\tau}(\mathbf{r}')dS' \\
& + \frac{jk_0Z_0}{4\pi} \oint_S G(\mathbf{r},\mathbf{r}')\cos(\Delta')J_{\phi}(\mathbf{r}')dS' \\
& + \frac{Z_0}{4\pi} \int_S \eta(\mathbf{r}')G_1(\mathbf{r},\mathbf{r}') \left\{ [\chi\cos(\Delta') - 2\rho\sin^2(\Delta'/2)]\cos(\alpha') \right. \\
& \quad \left. - \xi\sin(\alpha')\cos(\Delta') \right\} J_{\phi}(\mathbf{r}')dS' \\
& - \frac{Z_0}{4\pi} \int_S \eta(\mathbf{r}')G_1(\mathbf{r},\mathbf{r}')\xi\sin(\Delta')J_{\tau}(\mathbf{r}')dS' \tag{2.4.15}
\end{aligned}$$

and

$$\begin{aligned}
E_{\tau}^i(\mathbf{r}) = & \frac{1}{2}\eta(\mathbf{r})Z_0J_{\tau}(\mathbf{r}) \\
& + \frac{jZ_0}{4\pi k_0} \int_S G_1(\mathbf{r},\mathbf{r}') \left\{ [\chi\cos(\Delta') - 2\rho\sin^2(\Delta'/2)]\sin(\alpha) + \xi\cos(\alpha) \right\} \\
& \quad \cdot \left[\frac{\partial J_{\tau}(\mathbf{r}')}{\partial s'} + \frac{\sin(\alpha')}{\rho'}J_{\tau}(\mathbf{r}') + \frac{1}{\rho'}\frac{\partial J_{\phi}(\mathbf{r}')}{\partial \phi'} \right] dS' \\
& - \frac{jk_0Z_0}{4\pi} \oint_S G(\mathbf{r},\mathbf{r}')\sin(\alpha)\sin(\Delta')J_{\phi}(\mathbf{r}')dS' \\
& + \frac{jk_0Z_0}{4\pi} \oint_S G(\mathbf{r},\mathbf{r}')[\sin(\alpha)\sin(\alpha')\cos(\Delta') + \cos(\alpha)\cos(\alpha')]J_{\tau}(\mathbf{r}')dS' \\
& - \frac{Z_0}{4\pi} \int_S \eta(\mathbf{r}')G_1(\mathbf{r},\mathbf{r}') \left\{ \rho'\sin(\alpha)\cos(\alpha') - \rho\cos(\alpha)\sin(\alpha') \right. \\
& \quad \left. - \xi\sin(\alpha)\sin(\alpha') \right\} \sin(\Delta')J_{\phi}(\mathbf{r}')dS' \\
& - \frac{Z_0}{4\pi} \int_S \eta(\mathbf{r}')G_1(\mathbf{r},\mathbf{r}') \left\{ \xi\sin(\alpha)\cos(\Delta') \right. \\
& \quad \left. - [\chi + 2\rho\sin^2(\Delta'/2)]\cos(\alpha) \right\} J_{\tau}(\mathbf{r}')dS' \tag{2.4.16}
\end{aligned}$$

where $\chi = \rho' - \rho$, $\xi = z' - z$ and $dS' = \rho' d\phi' ds'$ for a body of revolution.

Finally, from eq. (2.2.4) the τ and ϕ components of the incident electric field can be written as

$$E_{\tau}^i(\mathbf{r}) = \left\{ [\cos(\theta_i)\cos(\Delta_i)\cos(\nu) - \sin(\Delta_i)\sin(\nu)]\sin(\alpha) - \sin(\theta_i)\cos(\nu)\cos(\alpha) \right\} e^{-\mathbf{k}^i \cdot \mathbf{r}} \quad (2.4.17)$$

$$E_{\phi}^i(\mathbf{r}) = [\cos(\theta_i)\sin(\Delta_i)\cos(\nu) + \cos(\Delta_i)\sin(\nu)] e^{-\mathbf{k}^i \cdot \mathbf{r}} \quad (2.4.18)$$

where

$$\mathbf{k}^i \cdot \mathbf{r} = k_0 \hat{k}_i \cdot \mathbf{r} = k_0 [\rho \sin(\theta_i) \cos(\Delta_i) + z \cos(\theta_i)] \quad (2.4.19)$$

2.4.3 Magnetic Field Integral Equation

The magnetic field integral equation derived in Section 2.3 for an arbitrarily shaped impedance scatterer is now specialized for a scatterer with body of revolution symmetry. The method is virtually identical to that used for the electric field integral in the the previous section (Section 2.4.2).

The magnetic field integral equation given by eq. (2.3.29) can be written in a more convenient form as follows

$$2\hat{\mathbf{n}} \times \mathbf{H}^i(\mathbf{r}) = \mathbf{J}_{es}(\mathbf{r}) - \mathfrak{S}_1^H(\mathbf{r}) - \mathfrak{S}_2^H(\mathbf{r}) - \mathfrak{S}_3^H(\mathbf{r}) \quad (2.4.20)$$

where

$$\mathfrak{S}_1^H(\mathbf{r}) = -\frac{j}{2\pi k_0} \hat{\mathbf{n}} \times \oint_S [\nabla' G(\mathbf{r}, \mathbf{r}')][\nabla' \cdot (\eta(\mathbf{r}') \hat{\mathbf{n}}' \times \mathbf{J}_{es}(\mathbf{r}'))] dS' \quad (2.4.21)$$

$$\mathfrak{S}_2^H(\mathbf{r}) = \frac{jk_0}{2\pi} \hat{\mathbf{n}} \times \oint_S G(\mathbf{r}, \mathbf{r}') [\eta(\mathbf{r}') \hat{\mathbf{n}}' \times \mathbf{J}_{es}(\mathbf{r}')] dS' \quad (2.4.22)$$

$$\mathfrak{S}_3^H(\mathbf{r}) = -\frac{1}{2\pi} \hat{\mathbf{n}} \times \oint_S \nabla' G(\mathbf{r}, \mathbf{r}') \times \mathbf{J}_{es}(\mathbf{r}') dS' \quad (2.4.23)$$

and \mathbf{J}_{es} is given by eq. (2.4.9). Interchanging the cross product operation with the integration operation and making use of eq. (2.4.10) the expressions for \mathfrak{S}_1^H , \mathfrak{S}_2^H and \mathfrak{S}_3^H can be written as

$$\mathfrak{S}_1^H(\mathbf{r}) = -\frac{j}{2\pi k_0} \oint_S G_1(\mathbf{r}, \mathbf{r}') [\hat{\mathbf{n}} \times (\mathbf{r} - \mathbf{r}')] [\nabla' \cdot (\eta(\mathbf{r}') \hat{\mathbf{n}}' \times \mathbf{J}_{es}(\mathbf{r}'))] dS' \quad (2.4.24)$$

$$\mathfrak{S}_2^H(\mathbf{r}) = \frac{jk_0}{2\pi} \oint_S \eta(\mathbf{r}') G(\mathbf{r}, \mathbf{r}') [\hat{\mathbf{n}} \times (\hat{\mathbf{n}}' \times \mathbf{J}_{es}(\mathbf{r}'))] dS' \quad (2.4.25)$$

$$\mathfrak{S}_3^H(\mathbf{r}) = -\frac{1}{2\pi} \oint_S G_1(\mathbf{r}, \mathbf{r}') [\hat{\mathbf{n}} \times (\mathbf{r} - \mathbf{r}') \times \mathbf{J}_{es}(\mathbf{r}')] dS' \quad (2.4.26)$$

The τ and ϕ components are obtained by taking the dot product of eq (2.4.20) with $\hat{\boldsymbol{\tau}}$ and $\hat{\boldsymbol{\phi}}$ respectively.

The magnetic field integral equation given by eq. (2.3.29) can now be written as the following pair of coupled scalar integral equations.

$$\begin{aligned}
H_{\tau}^i(\mathbf{r}) = & -\frac{1}{2} J_{\phi}(\mathbf{r}) \\
& - \frac{j}{4\pi k_0} \int_S G_1(\mathbf{r}, \mathbf{r}') \{ [\chi \cos(\Delta') - 2\rho \sin^2(\Delta'/2)] \sin(\alpha) + \xi \cos(\alpha) \} \\
& \quad \bullet \left\{ \frac{\eta(\mathbf{r}') \sin(\alpha')}{\rho'} + \frac{\partial \eta(\mathbf{r}')}{\partial s'} \right\} J_{\phi}(\mathbf{r}') dS' \\
& + \frac{j}{4\pi k_0} \int_S G_1(\mathbf{r}, \mathbf{r}') \{ [\chi \cos(\Delta') - 2\rho \sin^2(\Delta'/2)] \sin(\alpha) + \xi \cos(\alpha) \} \\
& \quad \bullet \left\{ \frac{1}{\rho'} \frac{\partial \eta(\mathbf{r}')}{\partial \phi'} \right\} J_{\tau}(\mathbf{r}') dS' \\
& - \frac{j}{4\pi k_0} \int_S \eta(\mathbf{r}') G_1(\mathbf{r}, \mathbf{r}') \{ [\chi \cos(\Delta') - 2\rho \sin^2(\Delta'/2)] \sin(\alpha) + \xi \cos(\alpha) \} \\
& \quad \bullet \left\{ \frac{\partial J_{\phi}(\mathbf{r}')}{\partial s'} - \frac{1}{\rho'} \frac{\partial J_{\tau}(\mathbf{r}')}{\partial \phi'} \right\} dS' \\
& - \frac{jk_0}{4\pi} \int_S \eta(\mathbf{r}') G(\mathbf{r}, \mathbf{r}') [\cos(\alpha) \cos(\alpha') + \sin(\alpha) \sin(\alpha') \cos(\Delta')] J_{\phi}(\mathbf{r}') dS' \\
& - \frac{jk_0}{4\pi} \int_S \eta(\mathbf{r}') G(\mathbf{r}, \mathbf{r}') \sin(\alpha) \sin(\Delta') J_{\tau}(\mathbf{r}') dS' \\
& - \frac{1}{4\pi} \int_S G_1(\mathbf{r}, \mathbf{r}') [\rho' \sin(\alpha) \cos(\alpha') - \rho \sin(\alpha') \cos(\alpha) \\
& \quad - \xi \sin(\alpha) \sin(\alpha')] \sin(\Delta') J_{\tau}(\mathbf{r}') dS' \\
& - \frac{1}{4\pi} \int_S G_1(\mathbf{r}, \mathbf{r}') \{ [\chi \cos(\alpha) - \xi \sin(\alpha)] \cos(\Delta') \\
& \quad + 2\rho' \cos(\alpha') \sin^2(\Delta'/2) \} J_{\phi}(\mathbf{r}') dS'
\end{aligned} \tag{2.4.27}$$

and

$$\begin{aligned}
H_{\phi}^i(\mathbf{r}) = & \frac{1}{2} J_{\tau}(\mathbf{r}) \\
& - \frac{j}{4\pi k_0} \oint_s G_1(\mathbf{r}, \mathbf{r}') \rho' \sin(\Delta') \left\{ \frac{\eta(\mathbf{r}') \sin(\alpha')}{\rho'} + \frac{\partial \eta(\mathbf{r}')}{\partial s'} \right\} J_{\phi}(\mathbf{r}') dS' \\
& + \frac{j}{4\pi k_0} \oint_s G_1(\mathbf{r}, \mathbf{r}') \rho' \sin(\Delta') \left\{ \frac{1}{\rho'} \frac{\partial \eta(\mathbf{r}')}{\partial \phi'} \right\} J_{\tau}(\mathbf{r}') dS' \\
& - \frac{j}{4\pi k_0} \oint_s \eta(\mathbf{r}') G_1(\mathbf{r}, \mathbf{r}') \rho' \sin(\Delta') \left\{ \frac{\partial J_{\phi}(\mathbf{r}')}{\partial s'} - \frac{1}{\rho'} \frac{\partial J_{\tau}(\mathbf{r}')}{\partial \phi'} \right\} dS' \\
& - \frac{jk_0}{4\pi} \oint_s \eta(\mathbf{r}') G(\mathbf{r}, \mathbf{r}') \sin(\alpha') \sin(\Delta') J_{\phi}(\mathbf{r}') dS' \\
& + \frac{jk_0}{4\pi} \oint_s \eta(\mathbf{r}') G(\mathbf{r}, \mathbf{r}') \cos(\Delta') J_{\tau}(\mathbf{r}') dS' \\
& + \frac{1}{4\pi} \oint_s G_1(\mathbf{r}, \mathbf{r}') \xi \sin(\Delta') J_{\phi}(\mathbf{r}') dS' \\
& + \frac{1}{4\pi} \oint_s G_1(\mathbf{r}, \mathbf{r}') \left\{ [\chi \cos(\alpha') - \xi \sin(\alpha')] \cos(\Delta') \right. \\
& \quad \left. - 2\rho \cos(\alpha') \sin^2(\Delta'/2) \right\} J_{\tau}(\mathbf{r}') dS' \tag{2.4.28}
\end{aligned}$$

where $\chi = \rho' - \rho$, $\xi = z' - z$ and $dS' = \rho' d\phi' ds'$ for a body of revolution.

Finally, from eq. (2.2.5) the τ and ϕ components of the incident magnetic field can be written as

$$\begin{aligned}
H_{\tau}^i(\mathbf{r}) = & \frac{1}{Z_0} \left\{ \sin(\theta_i) \sin(\nu) \cos(\alpha) \right. \\
& \left. - \sin(\alpha) [\cos(\theta_i) \cos(\Delta_i) \sin(\nu) + \sin(\Delta_i) \cos(\nu)] \right\} e^{-j\mathbf{k}^i \cdot \mathbf{r}} \tag{2.4.29}
\end{aligned}$$

$$H_{\phi}^i(\mathbf{r}) = \frac{1}{Z_0} [\cos(\Delta_i) \cos(\nu) - \cos(\theta_i) \sin(\Delta_i) \sin(\nu)] e^{-j\mathbf{k}^i \cdot \mathbf{r}} \tag{2.4.30}$$

where $\mathbf{k}^i \cdot \mathbf{r}$ is given by eq. (2.4.19).

2.4.4 Combined Field Integral Equation

Since the combined field integral equation for an arbitrarily shaped scatterer, was constructed from the electric and magnetic field integral equations for an arbitrarily

shaped scatterer it is reasonable to assume that the combined field integral equation for a body of revolution can be derived from the appropriate combination of the electric and magnetic field integral equations for a body of revolution. In order to do this we must first determine the τ and ϕ components of the combined field integral equation.

The τ component of the right hand side of eq. (2.3.36) is given by

$$\begin{aligned} \left(2\hat{\mathbf{n}} \times \left(\mathbf{H}^i(\mathbf{r}) - \frac{\alpha_{\text{CFIE}}}{Z_0} \hat{\mathbf{n}} \times \mathbf{E}^i(\mathbf{r}) \right) \right)_{\tau} &= \hat{\boldsymbol{\tau}} \cdot \left(2\hat{\mathbf{n}} \times \left(\mathbf{H}^i(\mathbf{r}) - \frac{\alpha_{\text{CFIE}}}{Z_0} \hat{\mathbf{n}} \times \mathbf{E}^i(\mathbf{r}) \right) \right) \\ &= 2 \left(H_{\phi}^i(\mathbf{r}) + \frac{\alpha_{\text{CFIE}}}{Z_0} E_{\tau}^i(\mathbf{r}) \right) \end{aligned} \quad (2.4.31)$$

The τ component of the left hand side of eq. (2.3.36) is given by

$$\begin{aligned} (L_c[\mathbf{J}_{es}])_{\tau} &= \hat{\boldsymbol{\tau}} \cdot (L_c[\mathbf{J}_{es}]) \\ &= \hat{\boldsymbol{\tau}} \cdot \left(L_H[\mathbf{J}_{es}] - \frac{\alpha_{\text{CFIE}}}{Z_0} \hat{\mathbf{n}} \times L_E[\mathbf{J}_{es}] \right) \\ &= (L_H[\mathbf{J}_{es}])_{\tau} - \frac{\alpha_{\text{CFIE}}}{Z_0} (L_E[\mathbf{J}_{es}])_{\phi} \end{aligned} \quad (2.4.32)$$

Then, the τ components of the combined field integral equation is given by

$$Z_0 H_{\phi}^i(\mathbf{r}) + \alpha_{\text{CFIE}} E_{\tau}^i(\mathbf{r}) = \frac{Z_0}{2} (L_H[\mathbf{J}_{es}])_{\tau} - \frac{\alpha_{\text{CFIE}}}{2} (L_E[\mathbf{J}_{es}])_{\phi} \quad (2.4.33)$$

where $\frac{1}{2}(L_H[\mathbf{J}_{es}])_{\tau}$ is given by the right hand side of eq. (2.4.28) and $-\frac{1}{2}(L_E[\mathbf{J}_{es}])_{\phi}$ is given by the right hand side of eq. (2.4.16).

The ϕ component of the right hand side of eq. (2.3.36) is given by

$$\begin{aligned} \left(2\hat{\mathbf{n}} \times \left(\mathbf{H}^i(\mathbf{r}) - \frac{\alpha_{\text{CFIE}}}{Z_0} \hat{\mathbf{n}} \times \mathbf{E}^i(\mathbf{r}) \right) \right)_{\phi} &= \hat{\boldsymbol{\phi}} \cdot \left(2\hat{\mathbf{n}} \times \left(\mathbf{H}^i(\mathbf{r}) - \frac{\alpha_{\text{CFIE}}}{Z_0} \hat{\mathbf{n}} \times \mathbf{E}^i(\mathbf{r}) \right) \right) \\ &= 2 \left(-H_{\tau}^i(\mathbf{r}) + \frac{\alpha_{\text{CFIE}}}{Z_0} E_{\phi}^i(\mathbf{r}) \right) \end{aligned} \quad (2.4.34)$$

The ϕ component of the left hand side of eq. (2.3.36) is given by

$$\begin{aligned} (L_c[\mathbf{J}_{es}])_\phi &= \hat{\phi} \cdot (L_c[\mathbf{J}_{es}]) \\ &= \hat{\phi} \cdot \left(L_H[\mathbf{J}_{es}] - \frac{\alpha_{\text{CFIE}}}{Z_0} \hat{\mathbf{n}} \times L_E[\mathbf{J}_{es}] \right) \\ &= (L_H[\mathbf{J}_{es}])_\phi + \frac{\alpha_{\text{CFIE}}}{Z_0} (L_E[\mathbf{J}_{es}])_\tau \end{aligned} \quad (2.4.35)$$

Then, the ϕ components of the combined field integral equation is given by

$$Z_0 H_\tau^i(\mathbf{r}) - \alpha_{\text{CFIE}} E_\phi^i(\mathbf{r}) = -\frac{Z_0}{2} (L_H[\mathbf{J}_{es}])_\tau - \frac{\alpha_{\text{CFIE}}}{2} (L_E[\mathbf{J}_{es}])_\phi \quad (2.4.36)$$

where $-\frac{1}{2}(L_H[\mathbf{J}_{es}])_\phi$ is given by the right hand side of eq. (2.4.27) and $\frac{1}{2}(L_E[\mathbf{J}_{es}])_\tau$ is given by the right hand side of eq. (2.4.15).

2.5 Far Field and Radar Cross Section

2.5.1 Far Scattered Fields

In the far field the scattered electric and magnetic fields can be written much more simply [Elliott, 1981] as

$$\mathbf{E}^s(\mathbf{r}) = -j\omega(\mathbf{A}_{eT}(\mathbf{r}) - Z_0 \hat{\mathbf{r}} \times \mathbf{A}_{mT}(\mathbf{r})) \quad (2.5.1)$$

$$\mathbf{H}^s(\mathbf{r}) = -j\omega(\mathbf{A}_{mT}(\mathbf{r}) + Y_0 \hat{\mathbf{r}} \times \mathbf{A}_{eT}(\mathbf{r})) \quad (2.5.2)$$

where \mathbf{A}_{eT} and \mathbf{A}_{mT} are the transverse (to $\hat{\mathbf{r}}$) components of the electric and magnetic vector potentials and are given by the following expressions

$$\mathbf{A}_{eT}(\mathbf{r}) = \mathbf{A}_e(\mathbf{r}) - \hat{\mathbf{r}}(\hat{\mathbf{r}} \cdot \mathbf{A}_e(\mathbf{r})) = \hat{\theta}A_{e\theta}(\mathbf{r}) + \hat{\phi}A_{e\phi}(\mathbf{r}) \quad (2.5.3)$$

$$\mathbf{A}_{mT}(\mathbf{r}) = \mathbf{A}_m(\mathbf{r}) - \hat{\mathbf{r}}(\hat{\mathbf{r}} \cdot \mathbf{A}_m(\mathbf{r})) = \hat{\theta}A_{m\theta}(\mathbf{r}) + \hat{\phi}A_{m\phi}(\mathbf{r}) \quad (2.5.4)$$

where $\hat{\mathbf{r}}$, $\hat{\theta}$ and $\hat{\phi}$ are the usual unit vectors form the spherical coordinate system. The free space Green's function can also be simplified in the far field region . When $|\mathbf{r}|$ is

much larger than $|\mathbf{r}'|$ the $1/R$ factor, which represents the magnitude of the free space Green's function, can be simply approximated by $1/r$. For the R factor which appears in the complex exponential, the following more exact approximation must be used

$$R = |\mathbf{r} - \mathbf{r}'| \approx r - \hat{\mathbf{r}} \cdot \mathbf{r}' = r - \mathcal{L} \quad (2.5.5)$$

where, in cylindrical coordinates,

$$\mathcal{L} = \hat{\mathbf{r}} \cdot \mathbf{r}' = \rho' \cos(\Delta') \sin(\theta) + z' \cos(\theta) \quad (2.5.6)$$

Thus in the far field the vector potentials can be written as

$$\mathbf{A}_e(\mathbf{r}) = \frac{\mu_0}{4\pi} \frac{e^{-jk_0 r}}{r} \oint_S \mathbf{J}_{es}(\mathbf{r}') e^{jk_0 \mathcal{L}} dS' \quad (2.5.5)$$

$$\mathbf{A}_m(\mathbf{r}) = \frac{\epsilon_0}{4\pi} \frac{e^{-jk_0 r}}{r} \oint_S \mathbf{J}_{ms}(\mathbf{r}') e^{jk_0 \mathcal{L}} dS' \quad (2.5.6)$$

Substituting eqs. (2.5.3) and (2.5.4) into the far field expression for the scattered field given by eq. (2.5.1) the θ and ϕ components of the scattered electric field can be written as

$$E_\theta^s(\mathbf{r}) = -j\omega \mathbf{A}_{e\theta}(\mathbf{r}) - j\omega Z_0 \mathbf{A}_{m\phi}(\mathbf{r}) \quad (2.5.7)$$

$$E_\phi^s(\mathbf{r}) = -j\omega \mathbf{A}_{e\phi}(\mathbf{r}) + j\omega Z_0 \mathbf{A}_{m\theta}(\mathbf{r}) \quad (2.5.8)$$

Using the far field forms of the vector potentials given by eqs. (2.5.5) and (2.5.6) the components of the scattered electric field given by eqs. (2.5.7) and (2.5.8) can be written as

$$E_\theta^s(\mathbf{r}) = \frac{e^{-jk_0 r}}{k_0 r} \left[-\frac{jk_0^2}{4\pi} \oint_S [Z_0 J'_{e\theta}(\mathbf{r}') + J'_{m\phi}(\mathbf{r}')] e^{jk_0 \mathcal{L}} dS' \right] = \frac{e^{-jk_0 r}}{k_0 r} S_\theta(\theta, \phi) \quad (2.5.9)$$

$$E_\phi^s(\mathbf{r}) = \frac{e^{-jk_0 r}}{k_0 r} \left[-\frac{jk_0^2}{4\pi} \oint_S [Z_0 J'_{e\phi}(\mathbf{r}') - J'_{m\theta}(\mathbf{r}')] e^{jk_0 \mathcal{L}} dS' \right] = \frac{e^{-jk_0 r}}{k_0 r} S_\phi(\theta, \phi) \quad (2.5.10)$$

where

$$J'_{e\theta}(\mathbf{r}') = \hat{\theta} \cdot \mathbf{J}_{es}(\mathbf{r}') \quad (2.5.11)$$

$$J'_{e\phi}(\mathbf{r}') = \hat{\phi} \cdot \mathbf{J}_{es}(\mathbf{r}') \quad (2.5.12)$$

$$J'_{m\theta}(\mathbf{r}') = \hat{\theta} \cdot \mathbf{J}_{ms}(\mathbf{r}') \quad (2.5.13)$$

$$J'_{m\phi}(\mathbf{r}') = \hat{\phi} \cdot \mathbf{J}_{ms}(\mathbf{r}') \quad (2.5.14)$$

and $S_\theta(\theta, \phi)$ and $S_\phi(\theta, \phi)$ are called the far field scattering (pattern) coefficients.

Making use of the expression for $\mathbf{J}_{es}(\mathbf{r}')$ given by eq. (2.4.9) and the expression relating \mathbf{J}_{ms} to \mathbf{J}_{es} given by eq. (2.3.25) the transverse components of the scattered electric field can be written as

$$E_\theta^s(\mathbf{r}) = -\frac{jk_0^2 Z_0}{4\pi} \frac{e^{-jk_0 r}}{k_0 r} \oint_S \left\{ [\cos(\theta) \sin(\alpha') \cos(\Delta') - \sin(\theta) \cos(\alpha')] \right. \\ \left. + \eta(\mathbf{r}') \cos(\Delta') \right] J_\tau(\mathbf{r}') \\ - [\cos(\theta) \sin(\Delta') + \eta(\mathbf{r}') \sin(\alpha') \sin(\Delta')] J_\phi(\mathbf{r}') \} e^{jk_0 \rho} dS' \quad (2.5.15)$$

$$E_\phi^s(\mathbf{r}) = -\frac{jk_0^2 Z_0}{4\pi} \frac{e^{-jk_0 r}}{k_0 r} \oint_S \left\{ [\sin(\alpha') \sin(\Delta') + \eta(\mathbf{r}') \cos(\theta) \sin(\Delta')] J_\tau(\mathbf{r}') \right. \\ \left. + [\cos(\Delta') + \eta(\mathbf{r}') \cos(\theta) \sin(\alpha') \cos(\Delta')] \right. \\ \left. - \eta(\mathbf{r}') \sin(\theta) \cos(\alpha') \right] J_\phi(\mathbf{r}') \} e^{jk_0 \rho} dS' \quad (2.5.16)$$

2.5.2 Radar Cross Section

In the far field, the scattered fields can be written in spherical coordinates as

$$\mathbf{E}^s(\mathbf{r}) = \hat{\theta} E_\theta^s(\mathbf{r}) + \hat{\phi} E_\phi^s(\mathbf{r}) = \frac{e^{-k_0 r}}{k_0 r} \left[\hat{\theta} S_\theta(\theta, \phi) + \hat{\phi} S_\phi(\theta, \phi) \right] \quad (2.5.17)$$

where $S_\theta(\theta, \phi)$ and $S_\phi(\theta, \phi)$ follow from either eqs. (2.5.9) and (2.5.10) or eqs. (2.5.15) and (2.5.16). The bistatic radar cross section (differential scattering cross section) is defined as [Bowman et. al., 1987]

$$\sigma(\theta, \phi) = \lim_{r \rightarrow \infty} 4\pi r^2 \frac{|\mathbf{E}^s|^2}{|\mathbf{E}^i|^2} \quad (2.5.18)$$

Assume a unit amplitude for the incident electric field (i.e. $|\mathbf{E}^i|=1$). From eq. (2.5.17) the magnitude of the scattered field is given by

$$|\mathbf{E}^s|^2 = \mathbf{E}^s \cdot \mathbf{E}^{s*} = \frac{1}{(k_0 r)^2} \left[|S_\theta(\theta, \phi)|^2 + |S_\phi(\theta, \phi)|^2 \right] \quad (2.5.19)$$

Then, the radar cross section can be written as

$$\sigma(\theta, \phi) = \lim_{r \rightarrow \infty} 4\pi r^2 \frac{\left[|S_\theta(\theta, \phi)|^2 + |S_\phi(\theta, \phi)|^2 \right]}{(k_0 r)^2} = \frac{4\pi}{k_0^2} \left[|S_\theta(\theta, \phi)|^2 + |S_\phi(\theta, \phi)|^2 \right] \quad (2.5.20)$$

3. NUMERICAL METHODOLOGY

3.1 Introduction

This section covers the techniques used to find a numerical solution of the integral equations derived in Chapter 1. The integral equations are solved using the method of moments [Harrington, 1968]. Since the scatterer is a body of revolution the surface of the scatterer can be mapped to a rectangular region in the s - ϕ plane where s is the arclength coordinate and ϕ is the usual cylindrical coordinate. The rectangular region in the s - ϕ plane is subdivided into many smaller rectangular subregions or patches. On each patch the components of the surface current $\mathbf{J}_{\alpha}(s, \phi)$ are expressed in terms of a linear combination of two-dimensional Hermite expansion functions. This choice for the expansion functions permits the use of delta functions for the testing (weighting) functions in the method of moments.

3.2 Method of Moments

The electric field integral equation, the magnetic field integral equation and the combined field integral equation as by eqs. (2.3.32), (2.3.33) and (2.3.36) all have the following general form [Poggio and Miller, 1973]

$$L[\mathbf{F}(\mathbf{x}')] = \mathbf{G}(\mathbf{x}) \quad (3.2.1)$$

where \mathbf{F} is an unknown vector function, \mathbf{G} is a known vector function and L is a linear operator. Construct an approximate solution for $\mathbf{F}(\mathbf{x})$ from a linear combination of known expansion functions as follows

$$\mathbf{F}(\mathbf{x}) \approx \mathbf{f}(\mathbf{x}) = \sum_{n=1}^N a_n \mathbf{f}_n(\mathbf{x}) \quad (3.2.2)$$

where a_n are constants to be determined and $\{\mathbf{f}_n(\mathbf{x})\}$ is a set of N known expansion (basis) functions.

Define a residual error function $\mathfrak{R}(\mathbf{x})$ as

$$\mathfrak{R}(\mathbf{x}) = L[\mathbf{f}(\mathbf{x}')] - \mathbf{G}(\mathbf{x}) \quad (3.2.3)$$

Substituting eq. (3.2.2) for \mathbf{f} in eq. (3.2.3) and interchanging the summation and the integration the residual error can be written as

$$\mathfrak{R}(\mathbf{x}) = \sum_{n=1}^N a_n L[\mathbf{f}_n(\mathbf{x}')] - \mathbf{G}(\mathbf{x}) \quad (3.2.4)$$

Next, define an inner product over S of two vectors \mathbf{x} and \mathbf{y} as

$$\langle \mathbf{x}, \mathbf{y} \rangle = \iint_S \mathbf{x} \cdot \mathbf{y} \, dS \quad (3.2.5)$$

Now choose a set of M weighting (testing) functions $\{\mathbf{w}_m\}$ and require that the inner product of the weighting functions and the residual error satisfy the following condition.

$$\langle \mathbf{w}_m, \mathfrak{R} \rangle = \sum_{n=1}^N \langle \mathbf{w}_m, L[\mathbf{f}_n(\mathbf{x}')] \rangle - \langle \mathbf{w}_m, \mathbf{G} \rangle = 0 \quad (3.2.6)$$

Eq. (3.2.6) can be written in matrix form as

$$\mathbf{Z}\mathbf{I} = \mathbf{V} \quad (3.2.7)$$

where the elements of \mathbf{Z} , \mathbf{I} and \mathbf{V} are given by

$$Z_{mn} = \langle \mathbf{w}_m, L[\mathbf{f}_n(\mathbf{x}')] \rangle \quad (3.2.8)$$

$$I_n = a_n \quad (3.2.9)$$

$$V_n = \langle \mathbf{w}_m, \mathbf{G} \rangle \quad (3.2.10)$$

The solution to the integral equation can now be found by solving the linear system of equations given by eq. (3.2.7)

The set of expansion functions $\{\mathbf{f}_n\}$ can be completely arbitrary as long as they exist in the domain of the operator L . Similarly, the testing functions $\{\mathbf{w}_n\}$ can be completely arbitrary as long as they exist in the range of the operator L . In the problem

under consideration evaluating the linear operator applied to an expansion function $L[f_n(\mathbf{x}')]$ and evaluating the inner product $\langle \mathbf{w}_m, L[f_n(\mathbf{x}')] \rangle$ both involve an integration over the domain S where S is the surface of the scatterer. Therefore, the conditions on the expansion and testing functions can be stated more simply as a requirement that they be either non-zero over the entire surface of the scatterer (i.e. entire domain S) or at least non-zero over a small portion (i.e. subdomain) of the surface of the scatterer. When the expansion or testing functions are defined over the entire domain S they are called *entire-domain basis functions*. When the expansion or testing functions are defined over a subdomain of S they are called *subsectional basis functions*. The actual selection of the expansion and testing functions is influenced by such factors as the desired numerical accuracy, geometry of the problem and expected behavior of the unknown function.

3.3 Description of Scatterer Geometry and Surface Impedance

In the computer program implementing the solution of eqs. (2.3.46), (2.3.47) and (2.3.50) the two profile functions and the relative surface impedance are numerically represented by cubic spline interpolation functions [deBoor, 1978]. Since a cubic spline interpolation has continuous first and second derivatives it can not be used to describe a function which is discontinuous or has discontinuous derivatives. For these cases, it is necessary to use more than one spline function to represent the desired function. When a function is represented by more than one spline function, the individual spline functions are referred to as spline meta-segments. The use of spline meta-segments permits the use of a generating curve which produces a surface having geometrical discontinuities (i.e. edges) and allows for the use of a discontinuous surface impedance. Note, the spline functions used for the generating curve and the spline function used for the surface impedance need not be defined over the same set of spline meta-segments. For example, for a spherical scatterer with a relative surface impedance $\eta = 1$ for the hemisphere $z > 0$

and $\eta = 0$ for the hemisphere $z < 0$ the profile functions $\rho(s)$ and $z(s)$ would be defined using a single meta-segment while the relative surface impedance $\eta = \eta(s)$ would require two meta-segments.

Finally, the spline description used for the profile functions and the surface impedance is particularly useful when it is necessary to evaluate the first and second derivatives of the profile functions. For example, it is not necessary to explicitly provide the function $\alpha(s)$ since it only appears in the integral equations in the form of $\sin(\alpha)$ and $\cos(\alpha)$ and these functions are readily available if one makes use of the following:

$$\cos(\alpha) = \frac{dz}{ds} \quad (3.3.1)$$

$$\sin(\alpha) = \frac{d\rho}{ds} \quad (3.3.2)$$

Similarly, where needed the derivatives of the surface impedance can be easily evaluated.

3.4 Hermite Expansion Functions

Suppose that for some unknown function $f(x)$ we are given the values of $f(x)$, df/dx and possibly higher order derivatives evaluated at a set of points $\{x_n\}$. The process of determining a polynomial interpolation of $f(x)$ which matches these conditions is called Hermitian interpolation [Lancaster and Salkauskas, 1986].

Consider the problem of finding an interpolation for $f(x)$ on a single interval $[x_n, x_{n+1}]$. Given the following values

$$\begin{aligned} f_n &= f(x_n), & f'_n &= \left(\frac{df}{dx}\right)_n = \frac{df}{dx}\bigg|_{x=x_n} \\ f_{n+1} &= f(x_{n+1}), & f'_{n+1} &= \left(\frac{df}{dx}\right)_{n+1} = \frac{df}{dx}\bigg|_{x=x_{n+1}} \end{aligned} \quad (3.4.1)$$

the function $f(x)$ can be approximated in the interval $[x_n, x_{n+1}]$ by the following expression

$$f(x) = f_n \phi_n(x) + f'_n \psi_n(x) + f_{n+1} \phi_{n+1}(x) + f'_{n+1} \psi_{n+1}(x) \quad (3.4.2)$$

where $\phi_n(x)$ and $\psi_n(x)$ are cubic Hermite expansion functions given by

$$\phi_n(x) = \begin{cases} 1 - 3\left(\frac{x-x_n}{\Delta x_{n-1}}\right)^2 - 2\left(\frac{x-x_n}{\Delta x_{n-1}}\right)^3 & \text{if } x_{n-1} \leq x \leq x_n \\ 1 - 3\left(\frac{x-x_n}{\Delta x_n}\right)^2 + 2\left(\frac{x-x_n}{\Delta x_n}\right)^3 & \text{if } x_n \leq x \leq x_{n+1} \end{cases} \quad (3.4.3)$$

$$\psi_n(x) = \begin{cases} (x-x_n)\left(\frac{x-x_{n-1}}{\Delta x_{n-1}}\right)^2 & \text{if } x_{n-1} \leq x \leq x_n \\ (x-x_n)\left(\frac{x-x_{n+1}}{\Delta x_n}\right)^2 & \text{if } x_n \leq x \leq x_{n+1} \end{cases} \quad (3.4.4)$$

and $\Delta x_n = x_{n+1} - x_n$. This is the simplest polynomial interpolation for $f(x)$ which satisfies the boundary conditions given by eq. (3.4.1).

Using the following properties for $\phi_n(x)$ and $\psi_n(x)$ it is easy to show that the expansion for $f(x)$ given by eq. (3.4.2) satisfies the boundary conditions specified in eq. (3.4.1).

$$\begin{aligned} \phi_n(x_n) &= 1 \\ \phi_n(x_{n-1}) &= \phi_n(x_{n+1}) = 0 \\ \psi_n(x_{n-1}) &= \psi_n(x_n) = \psi_n(x_{n+1}) = 0 \\ \left(\frac{d\phi_n}{dx}\right)_{n-1} &= \left(\frac{d\phi_n}{dx}\right)_n = \left(\frac{d\phi_n}{dx}\right)_{n+1} = 0 \\ \left(\frac{d\psi_n}{dx}\right)_n &= 1 \\ \left(\frac{d\psi_n}{dx}\right)_{n-1} &= \left(\frac{d\psi_n}{dx}\right)_{n+1} = 0 \end{aligned} \quad (3.4.5)$$

If the values of $f(x)$ and df/dx are given for a set of values $\{x_n\}$ the Hermitian interpolation for $f(x)$ is given by

$$f(x) = \sum_n F_n(x) = \sum_n f_n \phi_n(x) + f'_n \psi_n(x) \quad (3.4.6)$$

where

$$F_n(x) = f_n \phi_n(x) + f'_n \psi_n(x) \quad (3.4.7)$$

is the Hermite expansion of $f(x)$ at the point (node) $x = x_n$. Note, the forms of eqs. (3.4.2) and (3.4.6) appear to be quite different but they are fundamentally the same. Eq. (3.4.2) is simply an expansion for a single interval while eq. (3.4.6) is an expansion over multiple intervals. Associating the expansion functions with the nodes makes it possible to construct an expansion for a function which is discontinuous or has discontinuous derivatives. For example, if $f(x)$ is known to have a discontinuous first derivative at $x = x_n$ then $F_n(x)$ can be written as

$$F_n(x) = \begin{cases} f_n \phi_n(x) + f'_{n,l} \psi_n(x) & \text{if } x < x_n \\ f_n \phi_n(x) + f'_{n,r} \psi_n(x) & \text{if } x > x_n \end{cases} \quad (3.4.8)$$

where

$$f'_{n,l} = \lim_{x \rightarrow x_n^-} \frac{df}{dx}, \quad \text{and} \quad f'_{n,r} = \lim_{x \rightarrow x_n^+} \frac{df}{dx} \quad (3.4.9)$$

Similarly, if $f(x)$ is discontinuous at $x = x_n$ then $F_n(x)$ can be written as

$$F_n(x) = \begin{cases} f_{n,l} \phi_n(x) + f'_{n,l} \psi_n(x) & \text{if } x < x_n \\ f_{n,r} \phi_n(x) + f'_{n,r} \psi_n(x) & \text{if } x > x_n \end{cases} \quad (3.4.10)$$

where

$$f_{n,l} = \lim_{x \rightarrow x_n^-} f(x), \quad f_{n,r} = \lim_{x \rightarrow x_n^+} f(x) \quad (3.4.11)$$

and $f'_{n,l}$ and $f'_{n,r}$ are given by eq. (3.4.9).

3.5 Hermite Expansion Functions on Rectangles

For the rectangular region shown in Figure 3.5.1 two-dimensional Hermite expansion functions can be obtained from the products of the one-dimensional Hermite expansion functions. Define the two-dimensional Hermite expansion functions as follows

$$H_{n,m}^1(x, y) = \phi_n(x)\phi_m(x) \quad (3.5.1)$$

$$H_{n,m}^2(x, y) = \phi_n(x)\psi_m(x) \quad (3.5.2)$$

$$H_{n,m}^3(x, y) = \psi_n(x)\phi_m(x) \quad (3.5.3)$$

$$H_{n,m}^4(x, y) = \psi_n(x)\psi_m(x) \quad (3.5.4)$$

where ϕ_n and ψ_n are the one-dimensional Hermite expansion functions given by eqs. (3.4.3) and (3.4.4). The two subscripts n and m indicate that these expansion functions are associated with the point (x_n, y_m) (n, m 'th node). The superscripts 1, 2, 3 and 4 are used to indicate that a particular expansion function is associated with the following values

$$f, \quad \frac{\partial f}{\partial y}, \quad \frac{\partial f}{\partial x}, \quad \frac{\partial^2 f}{\partial x \partial y}$$

evaluated at the n, m 'th node.

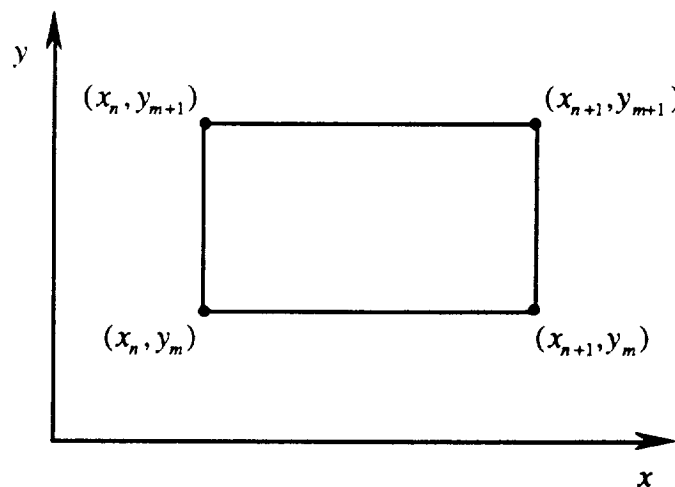


Figure 3.5.1 Domain of two-dimensional Hermite expansion functions.

Let

$$f_{i,j} = f(x, y)|_{x=x_i, y=y_j} \quad (3.5.5)$$

$$\left(\frac{\partial f}{\partial x}\right)_{i,j} = \frac{\partial f}{\partial x}|_{x=x_i, y=y_j} \quad (3.5.6)$$

$$\left(\frac{\partial f}{\partial y}\right)_{i,j} = \frac{\partial f}{\partial y}\bigg|_{x=x_i, y=y_j} \quad (3.5.7)$$

$$\left(\frac{\partial^2 f}{\partial x \partial y}\right)_{i,j} = \frac{\partial^2 f}{\partial x \partial y}\bigg|_{x=x_i, y=y_j} \quad (3.5.8)$$

Using the expansion functions defined by eqs. (3.5.1), (3.5.2), (3.5.3) and (3.5.4) a function $f(x,y)$ can be approximated in the region $x_n \leq x \leq x_{n+1}$, $y_m \leq y \leq y_{m+1}$ by the expansion

$$\begin{aligned} f(x,y) &= F_{n,m}(x,y) + F_{n,m+1}(x,y) + F_{n+1,m}(x,y) + F_{n+1,m+1}(x,y) \\ &= \sum_{k=0}^1 \sum_{l=0}^1 F_{n+k,m+l}(x,y) \end{aligned} \quad (3.5.9)$$

where

$$\begin{aligned} F_{i,j}(x,y) &= f_{i,j} H_{i,j}^1(x,y) + \left(\frac{\partial f}{\partial y}\right)_{i,j} H_{i,j}^2(x,y) \\ &\quad + \left(\frac{\partial f}{\partial x}\right)_{i,j} H_{i,j}^3(x,y) + \left(\frac{\partial^2 f}{\partial x \partial y}\right)_{i,j} H_{i,j}^4(x,y) \end{aligned} \quad (3.5.10)$$

is the Hermite expansion of $f(x,y)$ at the i,j 'th node.

As was the case with the Hermite expansion of a function of one variable, it is possible to construct a Hermite expansion for a function of two variable which is discontinuous or has discontinuous first derivatives. The only restrictions is that the discontinuities must lie along values of constant x or constant y . For example, if $\partial f/\partial x$ is discontinuous along $x = x_i$, then the expansions at nodes along $x = x_i$ have the following form

$$F_{i,j}(x,y) = \begin{cases} f_{i,j}H_{i,j}^1(x,y) + \left(\frac{\partial f}{\partial y}\right)_{i,j} H_{i,j}^2(x,y) \\ \quad + \left(\frac{\partial f}{\partial x}\right)_{i,j,l} H_{i,j}^3(x,y) + \left(\frac{\partial^2 f}{\partial x \partial y}\right)_{i,j,l} H_{i,j}^4(x,y) & \text{if } x < x_n \\ f_{i,j}H_{i,j}^1(x,y) + \left(\frac{\partial f}{\partial y}\right)_{i,j} H_{i,j}^2(x,y) \\ \quad + \left(\frac{\partial f}{\partial x}\right)_{i,j,r} H_{i,j}^3(x,y) + \left(\frac{\partial^2 f}{\partial x \partial y}\right)_{i,j,r} H_{i,j}^4(x,y) & \text{if } x > x_n \end{cases} \quad (3.5.11)$$

where

$$\left(\frac{\partial f}{\partial x}\right)_{i,j,l} = \lim_{\substack{x \rightarrow x_i^- \\ y=y_j}} \frac{\partial f}{\partial x} \quad \left(\frac{\partial^2 f}{\partial x \partial y}\right)_{i,j,l} = \lim_{\substack{x \rightarrow x_i^- \\ y=y_j}} \frac{\partial^2 f}{\partial x \partial y} \quad (3.5.12)$$

$$\left(\frac{\partial f}{\partial x}\right)_{i,j,r} = \lim_{\substack{x \rightarrow x_i^+ \\ y=y_j}} \frac{\partial f}{\partial x} \quad \left(\frac{\partial^2 f}{\partial x \partial y}\right)_{i,j,r} = \lim_{\substack{x \rightarrow x_i^+ \\ y=y_j}} \frac{\partial^2 f}{\partial x \partial y} \quad (3.5.13)$$

Similarly, if $f(x,y)$ is discontinuous along $x = x_i$, the Hermite expansions at nodes along $x = x_i$ have the form

$$F_{i,j}(x,y) = \begin{cases} f_{i,j,l}H_{i,j}^1(x,y) + \left(\frac{\partial f}{\partial y}\right)_{i,j,l} H_{i,j}^2(x,y) \\ \quad + \left(\frac{\partial f}{\partial x}\right)_{i,j,l} H_{i,j}^3(x,y) + \left(\frac{\partial^2 f}{\partial x \partial y}\right)_{i,j,l} H_{i,j}^4(x,y) & \text{if } x < x_n \\ f_{i,j,r}H_{i,j}^1(x,y) + \left(\frac{\partial f}{\partial y}\right)_{i,j,r} H_{i,j}^2(x,y) \\ \quad + \left(\frac{\partial f}{\partial x}\right)_{i,j,r} H_{i,j}^3(x,y) + \left(\frac{\partial^2 f}{\partial x \partial y}\right)_{i,j,r} H_{i,j}^4(x,y) & \text{if } x > x_n \end{cases} \quad (3.5.14)$$

where

$$f_{i,j,l} = \lim_{\substack{x \rightarrow x_i^- \\ y=y_j}} f(x,y) \quad \left(\frac{\partial f}{\partial y}\right)_{i,j,l} = \lim_{\substack{x \rightarrow x_i^- \\ y=y_j}} \frac{\partial f}{\partial y} \quad (3.5.15)$$

$$f_{i,j,r} = \lim_{\substack{x \rightarrow x_i^+ \\ y=y_j}} f(x,y) \quad \left(\frac{\partial f}{\partial y}\right)_{i,j,r} = \lim_{\substack{x \rightarrow x_i^+ \\ y=y_j}} \frac{\partial f}{\partial y} \quad (3.5.16)$$

Similar expressions can be found for the cases when $f(x,y)$ or $\partial f/\partial y$ are discontinuous along $y = y_j$ or discontinuous along both $x = x_i$ and $y = y_j$.

3.6 Expansion of Surface Currents

Using s - ϕ coordinates the surface of the scatterer can be mapped to the region $0 \leq s \leq s_{\max}$, $0 \leq \phi \leq 2\pi$ in the s - ϕ plane. Keep in mind that since we are considering bodies of revolution the points $(s,0)$ and $(s,2\pi)$ in the s - ϕ plane correspond to the same point on the surface of the scatterer. This is a result of the surface of the scatterer being periodic in ϕ with period 2π . Therefore, we also expect any function defined over the surface of the scatterer, such as the components of the surface current, to be periodic in ϕ with period 2π . Also, note that points along $s = 0$ represent the same physical point on the scatterer. However, the components of the surface current, J_τ and J_ϕ are in general not constant along $s = 0$ since the unit vectors $\hat{\tau}$ and $\hat{\phi}$ and hence J_τ and J_ϕ are functions of ϕ . These same considerations also apply to points along $s = s_{\max}$.

The domains(patches) over which the expansion functions for the components of the surface are defined are constructed by dividing the region $0 \leq s \leq s_{\max}$, $0 \leq \phi \leq 2\pi$ as shown in Figure 3.6.1. There are $N_s - 1$ intervals along the s -axis and $N_\phi - 1$ intervals along the ϕ -axis for a total of $(N_s - 1)(N_\phi - 1)$ patches and a total of $N_s N_\phi$ nodes. The patches are numbered so that the upper left hand corner of the i,j 'th patch as shown in Figure 3.6.1 has the coordinates (s_i, ϕ_j) . The components of the surface current can be written as

$$J_\tau(s, \phi) = \sum_{i=1}^{N_s} \sum_{j=1}^{N_\phi} J_{\tau,i,j}(s, \phi) \quad (3.6.1)$$

$$J_\phi(s, \phi) = \sum_{i=1}^{N_s} \sum_{j=1}^{N_\phi} J_{\phi,i,j}(s, \phi) \quad (3.6.2)$$

where $J_{\tau,i,j}$ and $J_{\phi,i,j}$ are the Hermite expansions of J_{τ} and J_{ϕ} at the point (s_i, ϕ_j) (i.e. i,j 'th node) and have a form similar to either eq. (3.5.10), (3.5.11) or (3.5.14). The particular form of the nodal expansion functions will depend upon both the local geometry of the scatterer and the continuity of the surface surface at each of the nodes.

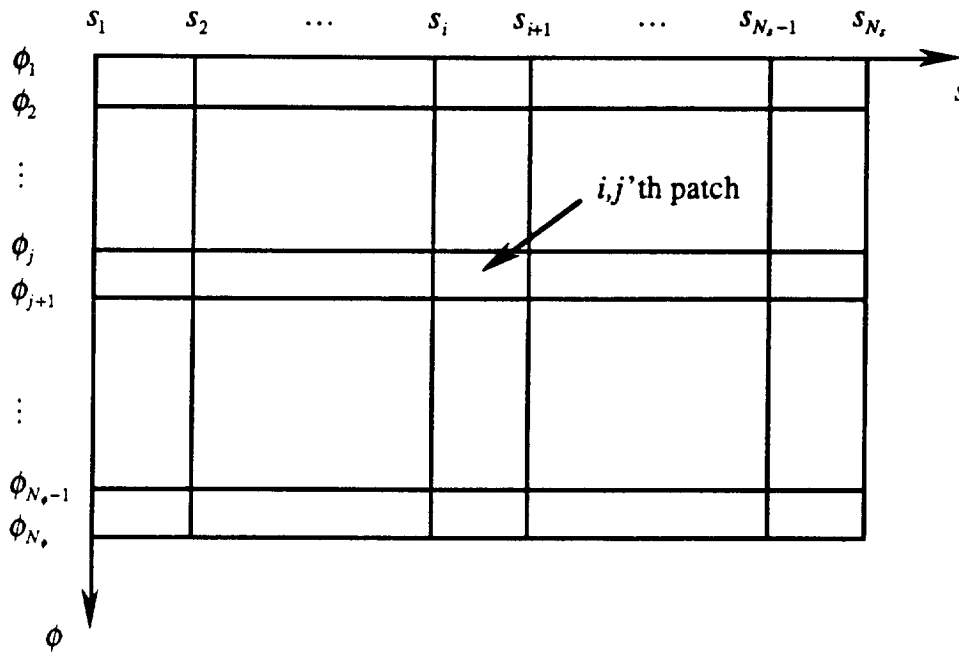


Figure 3.6.1 Expansion function domains for components of the surface current.

Now consider the nodes along the line $s = 0$ in the s - ϕ plane when $\alpha(0) = \pi/2$. For this case the scatterer is smooth and has a well defined normal at the point $s = 0$. The point $s = 0$ on the surface of the scatterer maps to the line $s = 0$ in the s - ϕ plane. This is due to the fact that the unit vectors $\hat{\tau}$ and $\hat{\phi}$ are not uniquely defined at the point $s = 0$. However, since all the points along $s = 0$ represent the same physical point on the scatterer it is reasonable to assume that the coefficients for the expansion functions associated with nodes along $s = 0$ are not completely independent. The relationships between the coefficients can be determined by selecting one or more coordinate systems which have uniquely defined coordinate vectors at $s = 0$.

Construct a new local coordinate system on the surface of the scatterer in the neighborhood of $s = 0$ as shown in Figure 3.6.2. Define a new arclength parameter s^* and a new tangent vector $\hat{\tau}^*$ as follows

$$s^* = \begin{cases} s & \text{when } \phi = \phi_0 \\ -s & \text{when } \phi = \phi_0 + \pi \end{cases} \quad (3.6.3)$$

$$\hat{\tau}^* = \begin{cases} \hat{\tau} & \text{when } \phi = \phi_0 \\ -\hat{\tau} & \text{when } \phi = \phi_0 + \pi \end{cases} \quad (3.6.4)$$

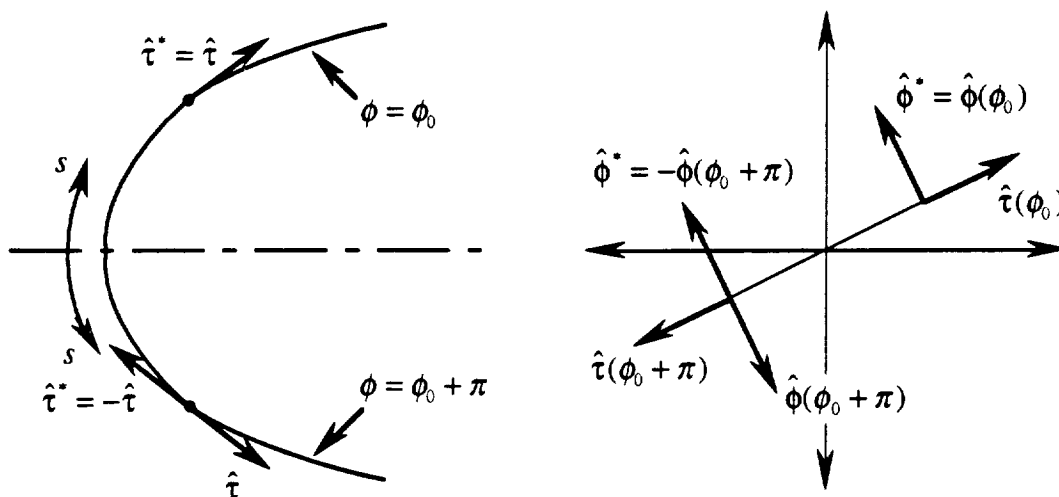


Figure 3.6.2 Construction of local coordinate system at $s = 0$.

Since the generating curve is smooth at $s^* = 0$ the τ^* component of \mathbf{J}_{es} must be continuous at $s^* = 0$. This condition can be stated mathematically as

$$\lim_{\substack{s^* \rightarrow 0^- \\ \phi = \phi_0 + \pi}} \hat{\tau}^* \cdot \mathbf{J}_{es}(s^*, \phi) = \lim_{\substack{s^* \rightarrow 0^+ \\ \phi = \phi_0}} \hat{\tau}^* \cdot \mathbf{J}_{es}(s^*, \phi) \quad (3.6.5)$$

Using the definitions of s^* and $\hat{\tau}^*$ eq. (3.6.5) reduces to

$$\lim_{\substack{s \rightarrow 0^+ \\ \phi = \phi_0 + \pi}} J_\tau(s, \phi) = - \lim_{\substack{s \rightarrow 0^+ \\ \phi = \phi_0}} J_\tau(s, \phi) \quad (3.6.6)$$

Since $\alpha(0) = \pi/2$ $d\alpha/ds^*$ is continuous at $s^* = 0$. Therefore, the derivative of the $\hat{\tau}^*$ component of \mathbf{J}_{es} with respect to s^* at $s^* = 0$ must also be continuous. This condition can be written as

$$\lim_{\substack{s^* \rightarrow 0^- \\ \phi = \phi_0 + \pi}} \frac{\partial}{\partial s^*} \hat{\tau}^* \cdot \mathbf{J}_{es}(s^*, \phi) = \lim_{\substack{s^* \rightarrow 0^+ \\ \phi = \phi_0}} \frac{\partial}{\partial s^*} \hat{\tau}^* \cdot \mathbf{J}_{es}(s^*, \phi) \quad (3.6.7)$$

For $s^* < 0$ we have $\hat{\tau}^* = -\hat{\tau}$, $s^* = -s$ and $\partial/\partial s^* = -\partial/\partial s$ and for $s^* > 0$ we have $\hat{\tau}^* = \hat{\tau}$, $s^* = s$ and $\partial/\partial s^* = \partial/\partial s$. Therefore, eq. (3.6.7) reduces to

$$\lim_{\substack{s \rightarrow 0^+ \\ \phi = \phi_0 + \pi}} \frac{\partial}{\partial s} J_\tau(s, \phi) = \lim_{\substack{s \rightarrow 0^+ \\ \phi = \phi_0}} \frac{\partial}{\partial s} J_\tau(s, \phi) \quad (3.6.8)$$

The results given in eqs. (3.6.6) and (3.6.8) imply the following:

$$\lim_{\substack{s \rightarrow 0^+ \\ \phi = \phi_0 + \pi}} \frac{\partial}{\partial \phi} J_\tau(s, \phi) = - \lim_{\substack{s \rightarrow 0^+ \\ \phi = \phi_0}} \frac{\partial}{\partial \phi} J_\tau(s, \phi) \quad (3.6.9)$$

$$\lim_{\substack{s \rightarrow 0^+ \\ \phi = \phi_0 + \pi}} \frac{\partial^2}{\partial s \partial \phi} J_\tau(s, \phi) = \lim_{\substack{s \rightarrow 0^+ \\ \phi = \phi_0}} \frac{\partial^2}{\partial s \partial \phi} J_\tau(s, \phi) \quad (3.6.10)$$

For the ϕ component of the surface current define a new angular vector $\hat{\phi}^*$ as follows

$$\hat{\phi}^* = \begin{cases} \hat{\phi} & \text{when } \phi = \phi_0 \\ -\hat{\phi} & \text{when } \phi = \phi_0 + \pi \end{cases} \quad (3.6.11)$$

Like the component of the surface current in the τ^* direction the component in the ϕ^* direction must also be continuous at $s^* = 0$.

$$\lim_{\substack{s^* \rightarrow 0^- \\ \phi = \phi_0 + \pi}} \hat{\phi}^* \cdot \mathbf{J}_{es}(s^*, \phi) = \lim_{\substack{s^* \rightarrow 0^+ \\ \phi = \phi_0}} \hat{\phi}^* \cdot \mathbf{J}_{es}(s^*, \phi) \quad (3.6.12)$$

Using the definition for $\hat{\phi}^*$ the condition on the continuity of the ϕ^* component can be written as

$$\lim_{\substack{s \rightarrow 0^+ \\ \phi = \phi_0 + \pi}} J_\phi(s, \phi) = - \lim_{\substack{s \rightarrow 0^+ \\ \phi = \phi_0}} J_\phi(s, \phi) \quad (3.6.13)$$

Since the geometry of the scatterer is smooth at $s = 0$ the derivative of the $\hat{\phi}^*$ component of \mathbf{J}_{es} with respect to s^* should be continuous at $s^* = 0$.

$$\lim_{\substack{s^* \rightarrow 0^- \\ \phi = \phi_0 + \pi}} \frac{\partial}{\partial s^*} \hat{\phi}^* \cdot \mathbf{J}_{es}(s^*, \phi) = \lim_{\substack{s^* \rightarrow 0^- \\ \phi = \phi_0}} \frac{\partial}{\partial s^*} \hat{\phi}^* \cdot \mathbf{J}_{es}(s^*, \phi) \quad (3.6.14)$$

Since $\hat{\phi}^* = \hat{\phi}$ and $\frac{\partial}{\partial s^*} = -\frac{\partial}{\partial s}$ for $s^* < 0$ and $\hat{\phi}^* = \hat{\phi}$ and $\frac{\partial}{\partial s^*} = \frac{\partial}{\partial s}$ for $s^* > 0$ eq. (3.6.14) simplifies to

$$\lim_{\substack{s \rightarrow 0^+ \\ \phi = \phi_0 + \pi}} \frac{\partial}{\partial s} J_\phi(s, \phi) = \lim_{\substack{s \rightarrow 0^+ \\ \phi = \phi_0}} \frac{\partial}{\partial s} J_\phi(s, \phi) \quad (3.6.15)$$

The results given in eqs. (3.6.13) and (3.6.15) imply that the following is also true.

$$\lim_{\substack{s \rightarrow 0^+ \\ \phi = \phi_0 + \pi}} \frac{\partial}{\partial \phi} J_\phi(s, \phi) = - \lim_{\substack{s \rightarrow 0^+ \\ \phi = \phi_0}} \frac{\partial}{\partial \phi} J_\phi(s, \phi) \quad (3.6.16)$$

$$\lim_{\substack{s \rightarrow 0^+ \\ \phi = \phi_0 + \pi}} \frac{\partial^2}{\partial s \partial \phi} J_\phi(s, \phi) = \lim_{\substack{s \rightarrow 0^+ \\ \phi = \phi_0}} \frac{\partial^2}{\partial s \partial \phi} J_\phi(s, \phi) \quad (3.6.17)$$

If $\alpha(s_{\max}) = -\pi/2$ then the results given by eqs. (3.6.6, 8-10, 13, 15-17) also apply in the limit $s \rightarrow s_{\max}^-$, that is, at the point $s = s_{\max}$. For nodes along $s = 0$ ($s = s_{\max}$) whenever $\alpha(0) = \pi/2$ ($\alpha(s_{\max}) = -\pi/2$) eqs. (3.6.6), (3.6.8), (3.6.9) and (3.6.10) can be used to reduce the number of unknowns per node associated with J_r from 4 to 2. Similarly, eqs. (3.6.13), (3.6.15), (3.6.16) and (3.6.17) can be used to reduce the number of unknowns per node associated with J_ϕ from 4 to 2 for all nodes along $s = 0$ ($s = s_{\max}$) whenever $\alpha(0) = \pi/2$ ($\alpha(s_{\max}) = -\pi/2$).

If $\alpha(0) \neq \pi/2$ the scatterer starts with a sharp point. This geometrical singularity will result in a possible singularity in J_ϕ at $s = 0$ while J_r will remain continuous at $s = 0$. However, since there is not a well defined surface normal at $s = 0$

we can not construct a local coordinate system at $s=0$ and hence we can not geometrically determine the behavior of either J_ϕ , J_τ or their derivatives in the limit $s \rightarrow 0^+$. These same considerations also apply at $s = s_{\max}$ when $\alpha(s_{\max}) \neq -\pi/2$. In either of the two cases eqs. (3.6.6, 8-10, 13, 15-17) can not be used to reduce the number of unknowns and 4 unknowns per current component must be used at each node along $s = 0$ or $s = s_{\max}$.

3.7 Selection of Sampling and Integration Points

Since Hermite expansion functions belong to the class of functions with C^1 continuity (i.e. continuous first derivatives) the use of delta functions as the testing functions is allowed [Chap. 11, Vichnevetsky, 1981]. From eq. (3.2.13) it can be seen that employing delta functions as the testing functions is equivalent to sampling the integral equation at some arbitrary point on the surface of the scatterer. Since the domain of the testing functions is the surface of the scatterer the sampling points must be located on the surface of the scatterer. In addition, since the domains of the expansion functions are a subregion of the entire surface, the locations of the sampling points must be distributed over the surface of the scatterer in order to include the effects of all the expansion functions. That is, if there are N unknown coefficients then the sampling points must be chosen to produce N linearly independent equations in terms of the unknown coefficients.

Using delta functions as the testing functions, consider the method of moments solution to eq. (3.2.7) for the simple case where \mathbf{F} and \mathbf{G} are the scalar functions $f(x)$ and $g(x)$ respectively. For the interval $[x_1, x_N]$ let the expansion of $f(x)$ have the form given by eq. (3.4.6). Assume that at each node x_n , $n = 1, \dots, N$ in the interval $[x_1, x_N]$ the function f is continuous so that the nodal expansion functions F_n have the form given in eq. (3.4.7). Since there are two unknowns per nodal expansion function, the total number of unknowns is $2N$. The elements of \mathbf{Z} and \mathbf{V} given in eqs. (3.2.8) and (3.2.10) are determined by sampling $L[f(x')]$ and $g(x)$ respectively at $2N$ points in the interval

$[x_1, x_N]$. Since the expansion function at the n 'th node is only defined for the interval $[x_{n-1}, x_{n+1}]$ the two sampling points associated with the unknown coefficients from the nodal expansion function at $x = x_n$ must be located somewhere in the interval $[x_{n-1}, x_{n+1}]$. Since a nodal expansion function contributes to the overall value of $f(x)$ on both sides of the corresponding node, the locations of the sampling points associated with the n 'th node are chosen so that one sampling point is located in the interval $[x_{n-1}, x_n]$ while the other is located in the interval $[x_n, x_{n+1}]$. The exception to this rule occurs for the first and last intervals. Since a solution is desired only for the interval $[x_1, x_N]$ it is not logical to locate sampling points outside of this interval. Therefore, the sampling points associated with the first and N 'th nodes can only be located in the intervals $[x_1, x_2]$ and $[x_{N-1}, x_N]$ respectively. The required distribution of sampling points is shown in Figure 3.7.1. If the values of f or df/dx are known at the endpoints or boundary conditions for f and df/dx are specified at the endpoints then it may be possible to reduce the number of total number of sampling points in the first and last intervals from three to two.

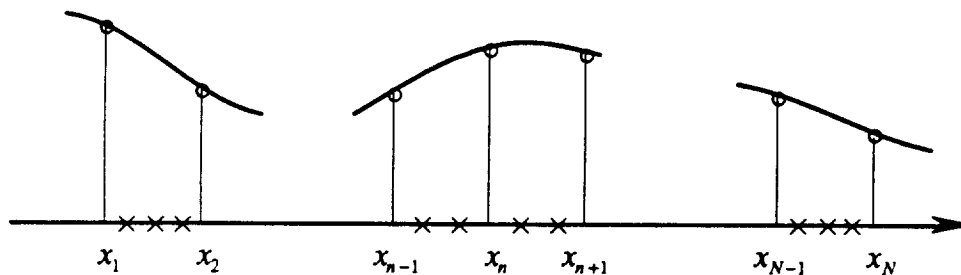


Figure 3.7.1 Location of sampling points for a continuous function. Circles represent nodes; crosses represent sampling points.

If df/dx is discontinuous at $x = x_i$, then a nodal expansion function of the form given in eq. (3.4.8) must be used at the i 'th node. This introduces an additional unknown coefficient for which an additional sampling point must be chosen. This additional sampling point must be located at the point $x = x_i$ as shown in Figure 3.7.2a. If $f(x)$ is discontinuous at $x = x_i$, then the nodal expansion function at the i 'th node has the form

given by eq. (3.4.10). This choice for the nodal expansion function introduces two additional unknown coefficients into the problem. While there are four unknown coefficients associated with the i 'th node two of the coefficients only contribute to f in the interval $[x_{i-1}, x_i]$ and the other two coefficients only contribute to f in the interval $[x_i, x_{i+1}]$. Therefore, the two of the four sampling points associated with the i 'th node are located in the interval $[x_{i-1}, x_i]$ while the other two sampling points are located in $[x_i, x_{i+1}]$ as shown in Figure 3.7.2b.

The distribution of sampling points for the two-dimensional problem is based on the distributions found for the one-dimensional problem. For example, consider a two-dimensional function $f(x, y)$ where f and $\partial f / \partial y$ are always continuous in y , $\partial f / \partial x$ is discontinuous in x at $x = x_i$ and f is discontinuous in x at $x = x_j$. Construct a new one-dimensional function $f_1(y) = f(x_0, y)$, where x_0 is a constant. Since $f(x, y)$ and $\partial f / \partial y$ are always continuous in y , f_1 and $\partial f_1 / \partial y$ are also continuous in y . Therefore, the distribution of sampling point along the y direction should be chosen as shown in Figure 3.7.1. For the sampling points in the x direction construct a new function $f_2(x) = f(x, y_0)$ where y_0 is a constant. Since $\partial f / \partial x$ and $f(x, y)$ are discontinuous at $x = x_i$ and $x = x_j$ respectively $\partial f_2 / \partial x$ and f_2 will also be discontinuous at $x = x_i$ and $x = x_j$ respectively. Therefore, at nodes where f_2 and $\partial f_2 / \partial x$ are both continuous choose the sampling points as shown in Figure 3.7.1; at nodes where $\partial f_2 / \partial x$ is discontinuous choose the sampling points as shown in Figure 3.7.2a; and at nodes where f_2 is discontinuous choose the sampling points as shown in Figure 3.7.2b.

In principle, the sampling points can be located anywhere in the interval. Numerical accuracy is improved if they are located at the points used for Gaussian integration [Chap. 11, Vichnevetsky, 1981]. Sampling at the Gaussian points is referred to as orthogonal collocation. The drawback in using orthogonal collocation results from the complexity it introduces to the choice for the numerical integration rule.

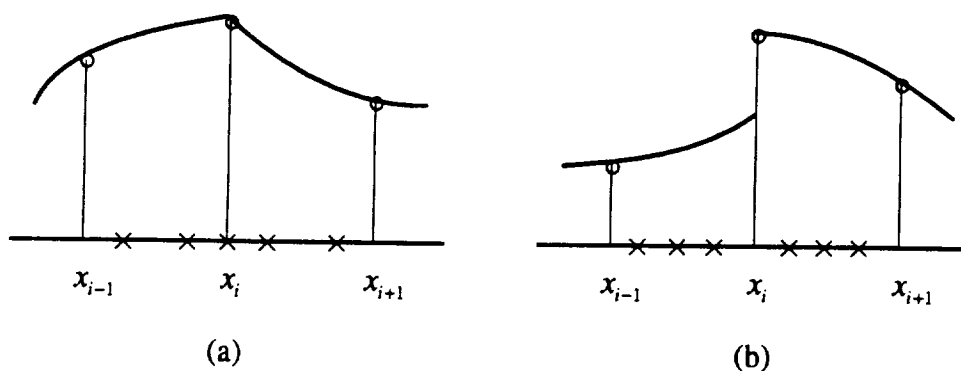


Figure 3.7.2 Location of sampling points for discontinuous functions. (a) df/dx is discontinuous at $x = x_i$, (b) $f(x)$ is discontinuous at $x = x_i$. Circles represent nodes; crosses represent sampling points.

The free space Green's function, G , which appears in the integral equations is singular whenever the observation point (i.e. sampling point) and integration point coincide. The free space Green's function appears in three forms in the integral equation, as GF the scalar product of G and a vector function F , as $f\nabla G$ the product of the scalar function f and ∇G and as $\nabla G \times F$ the vector cross product of ∇G and a vector function F . Analytically, if F is non-singular then the integral of GF over a surface is always convergent [Kellogg, 1953]. However, there are convergence problems associated the numerical integration of a function such as GF even when it has been established analytically to be integrable. Analytically, the integrals of $f\nabla G$ and $\nabla G \times F$ over a surface are, in general, not convergent. However, the problems associated with these two singular integrals have been accounted for through the use of the concept of principle value integrals.

With this in mind, there are two general possibilities for the choice of the locations of the sampling points and integration points. The sampling points and integration points can be chosen so that there is a possibility that they will be coincident or they can be chosen so that they are never coincident. If the sampling and integration points are allowed to be coincident then some provisions must be made in the numerical

integration routine to detect the case where the two points are coincident. For the integrals of GF the integration in the vicinity of the singularity is either replaced by a numerical integration rule specifically designed to handle this type of singularity or evaluated using an approximate analytical expression for the integral. For the integrals of $f\nabla G$ and $\nabla G \times \mathbf{F}$, since the effects of their singularities have already been accounted for through the use of the principle value integrals, the integrands can simply be set to zero whenever the integration and sampling points are coincident. A simpler procedure is to select the sampling and integration points so that they are never coincident. Then, the numerical integration does not have to check for the possibility of a singular integrand. There is some loss of numerical accuracy if the singularity of GF is not considered explicitly. However, this effect can be minimized by selecting the integration points so that they are symmetrically placed around the sampling points.

It is relatively easy to construct a numerical integration rule which will avoid selecting integration points which are coincident with the sampling points. Integration over a surface patch is performed by dividing the patch into a number of square subpatches. The center point of each patch is referred to as an integration point. On each integration subpatch the value of the integral is approximated as the product of the area of the subpatch times the value of the integrand evaluated at the integration point for the subpatch. Let N_{int} be the number of integration intervals along the x and y axes. Assuming that the integration is being performed over the normalized patch $-1 \leq x \leq 1$ and $-1 \leq y \leq 1$ the numerical integration rule just described corresponds to selecting the two sets of weighting coefficients $\{w_{xk}\}$ and $\{w_{yj}\}$ for a two-dimensional numerical integration rule as

$$w_{xk} = w_{yk} = \frac{2}{N_{\text{int}}} \quad (3.7.1)$$

where $k = 1, \dots, N_{\text{int}}$ and selecting the two sets of integration points $\{x_k\}$ and $\{y_j\}$ as

$$x_k = y_k = \frac{2k-1}{N_{\text{int}}} - 1 \quad (3.7.2)$$

where $k = 1, \dots, N_{\text{int}}$. If the value of N_{int} is restricted to a multiple of 4 and the possible x and y coordinates of the sampling points in the normalized patch are restricted to the values $-1/2$, 0 and $1/2$ then the integration points and the sampling points will never be coincident. Note, using this scheme for the selection of the sampling and integration points does not permit the construction of a solution which is discontinuous at both ends of an interval.

4. NUMERICAL RESULTS

4.1 Organization of Computer Code

The computer code is divided into five distinct programs. Depending on the choice of the geometry, a total of four programs will actually be used. The programs are:

1. CNSPH3
2. CNCL3
3. PREMOM3
4. MOM3
5. PSTMOM3

The first two programs, CNSPH3 and CNCL3, are used to define the geometry for the cone-sphere and cone-cylinder scatterers respectively. The cross sections for both of these geometries are shown in Figures 4.1.1 and 4.1.2. Note that a spherical scatterer is a special case of both these geometries. Also, the cone-cylinder-sphere geometry can be generated as a particular case of the cone-cylinder geometry. The output from each of the two geometry programs is the cubic spline description for the generating curve and a cubic spline description for the surface impedance.

The program PREMOM3 reads the output file generated by one of the geometry programs, generates a surface patch model of the scatterer and then generates any remaining information needed to solve any of the three integral equations. PREMOM3 also generates some additional information used in the calculation of the far field scattering coefficients and the bistatic radar cross sections. The function of PREMOM3 is very similar to the mesh generating function found in commercial finite element programs. However, as a mesh generator PREMOM3 is limited to generating a single type of curved surface element only for geometries with body of revolution symmetry. PREMOM3 generates two output files. The first file is an unformatted file containing the surface patch model used by both MOM3 and PSTMOM3. This file also contains

information used only by PSTMOM3 in the calculation of the radar cross sections. The second file is a formatted file containing a Fortran PARAMETER statement which defines the absolute minimum array sizes needed by MOM3 and PSTMOM3. Using the PARAMETER statement generated for a particular problem in MOM3 and PSTMOM3 will always result in the use of the absolute minimum amount of memory.

As it's name suggests, MOM3 implements a method of moments solution of any one of the three integral equations presented in Chapter 2 using Hermite expansion functions with delta function testing. MOM3 reads the surface patch model generated by PREMOM3, generates the impedance matrix \mathbf{Z} for the desired integral equation and then solves the matrix equation given by eq. (3.2.7) for both TE and TM polarizations. Finally, MOM3 generates an unformatted file containing the coefficient vectors for the surface current belonging to the two orthogonal polarizations and a copy of the surface patch model generated by PREMOM3.

PSTMOM3 reads the file generated by MOM3 and computes, for both polarizations, the surface current at all integration points used in the evaluation of the scattering coefficients. The far field scattering coefficients are then calculated for a specified number of values for θ and ϕ . The scattering coefficients are then used to calculate the bistatic radar cross section at the same values of θ and ϕ . Finally, the results of all these calculations, the surface currents, the scattering coefficients and the radar cross sections are written to a formatted file.

An attempt has been made to write the programs so that they adhere as closely as possible to the Fortran-77 standard. The programs have been successfully compiled without modification by a large number of Fortran compilers ranging from Watfor-77 and Microsoft Fortran under MS-DOS to the cf77 compiler system under UNICOS. Additionally, some time has been spent improving the computational efficiency of the routine in MOM3 which generates the elements of \mathbf{Z} (i.e. matrix fill routine). This effort has been aimed mainly at writing a matrix fill routine which can be easily ported to vector

supercomputers like the Cray Y-MP. Future plans include the parallelization of the code for shared memory parallel processor systems like the Cray Y-MP and also for massively parallel processor systems like the Thinking Machines CM5.

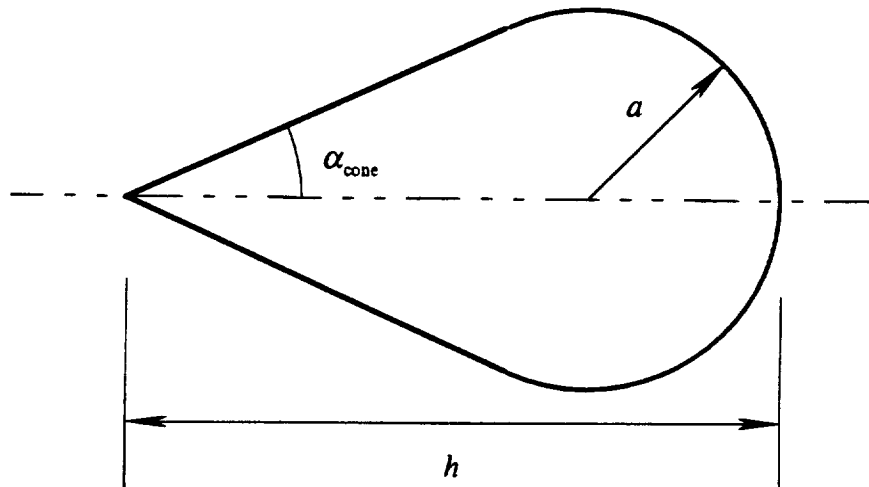


Figure 4.1.1 Cross section of cone-sphere geometry

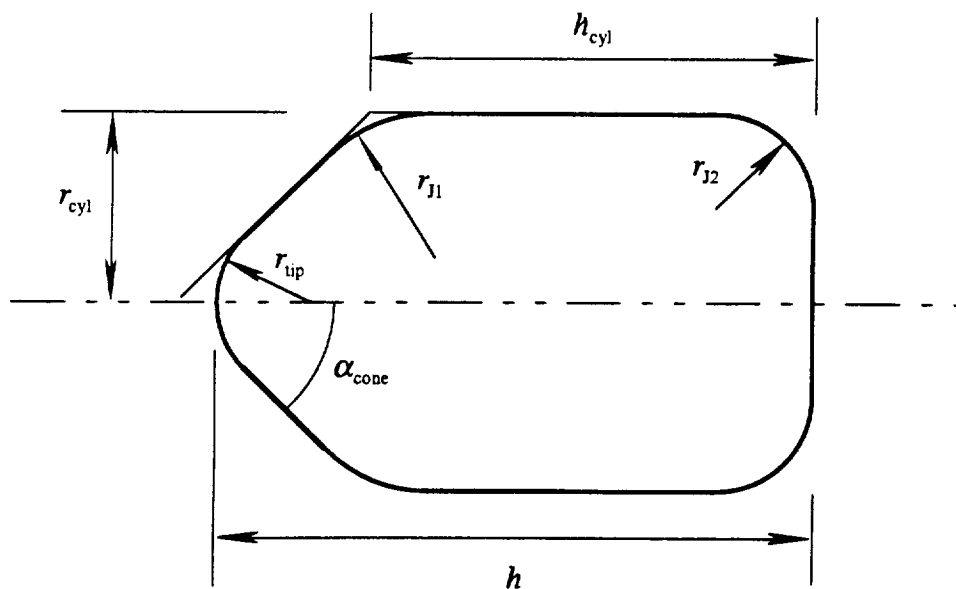


Figure 4.1.2 Cross section of cone-cylinder geometry

4.2 Sample Results

In this section the bistatic radar cross sections for two different cone-cylinder scatterers with surface impedances which vary along both the s and ϕ directions will be presented. All results have been obtained by solving the magnetic field integral equation. Additionally, all solutions have used 4 integration points per interval in both the s and ϕ directions for a total of 16 integration points per surface patch.

The first three examples are for a cone-cylinder (see Figure 4.1.2) with normalized dimensions $k_0 h_{\text{cyl}} = 3.0$, $k_0 r_{\text{cyl}} = 0.5$, $\alpha_{\text{cone}} = 21^\circ$, $k_0 r_{\text{up}} = 0.1875$, $k_0 r_{J1} = 2.0$ and $k_0 r_{J2} = 0.0$. This geometry will be referred to as cone-cylinder 1. The normalized arclength for this scatterer's generating curve is $k_0 s_{\text{max}} = 4.6242$. Results for three different variations in the surface impedance of cone-cylinder 1 will be presented. For all three examples the surface patches are generated using $N_s = 13$ nodes in the s direction and $N_\phi = 9$ nodes in the ϕ direction. For the first example, the relative surface impedance has a constant value of $\eta = 0$ (i.e. perfectly conducting). The bistatic radar cross sections for this constant surface impedance are shown in Figures 4.2.3 and 4.2.4. The radar cross sections are for the case of oblique incidence with angles of incidence $\phi_i = 0^\circ$ and $\theta_i = 45^\circ$ and both TE and TM polarizations.

For the second and third examples using cone-cylinder 1 the relative surface impedance is piecewise constant with two step discontinuities, one at $k_0 s = 0.7619$ and another at $k_0 s = 1.4949$. The surface impedance for the second example is given by

$$\eta(k_0 s) = \begin{cases} 0 & 0.0 < k_0 s < 0.7619 \\ 1 & 0.7619 < k_0 s < 1.4949 \\ 0 & 1.4949 < k_0 s < 4.6242 \end{cases} \quad (4.2.1)$$

while the surface impedance for the third example is given by

$$\eta(k_0s) = \begin{cases} 1 & 0.0 < k_0s < 0.7619 \\ 2 & 0.7619 < k_0s < 1.4949 \\ 1 & 1.4949 < k_0s < 4.6242 \end{cases} \quad (4.2.2)$$

A graphical picture of the surface impedances given by eqs. (4.2.1) and (4.2.2) are shown in Figures 4.2.1 and 4.2.2 respectively. It can be seen from Figures 4.2.1 and 4.2.2 that points with a normalized arclength coordinate k_0s in the range $0.7619 < k_0s < 1.4949$ are located on the rounded joint between the cone and the cylinder. The bistatic radar cross sections for cone-cylinder 1 with a relative surface impedance given by eq. (4.2.1) are shown in Figures 4.2.5 and 4.2.6. The bistatic radar cross sections for cone-cylinder 1 with a relative surface impedance given by eq. (4.2.2) are shown in Figures 4.2.7 and 4.2.8. The results presented are for TE and TM polarizations and angles of incidence $\phi_i = 0^\circ$ and $\theta_i = 45^\circ$.

The second cone-cylinder geometry has normalized dimensions $k_0h_{\text{cyl}} = 4$, $k_0r_{\text{cyl}} = 1$, $\alpha_{\text{cone}} = 26.565^\circ$, $k_0r_{\text{tip}} = k_0r_{J2} = 0.25$ and $k_0r_{J1} = 0.75$. This geometry will be referred to as cone-cylinder 2. The normalized height for cone-cylinder 2 is $h = 5.6910$ and the normalized arclength of its generating curve is $s_{\text{max}} = 6.8992$. Two different examples for the surface impedance will be used with this geometry. The first example uses a constant relative surface impedance $\eta = 1$ (i.e. perfectly absorbing). For this case the surface patches have been generated using $N_s = 15$ and $N_\phi = 13$ which results in a total of 168 surface patches and a total of 1584 unknowns in the method of moments program. Results for the bistatic radar cross sections for this scatterer due to both TE and TM polarized incident fields with angles of incidence $\phi_i = 270^\circ$ and $\theta_i = 0^\circ, 45^\circ, 90^\circ, 135^\circ$ and 180° are shown in Figures 4.2.10-19. The reason for choosing $\phi_i = 270^\circ$ is so that the results for cone-cylinder 2 with $\eta = 1$ can be directly compared with the results obtained for the next example.

The second example using cone-cylinder 2 uses a relative surface impedance $\eta = 1$ for the entire surface except for a rectangular region where the relative surface

impedance is $\eta = 0$. The surface impedance for this example is given by the following expression

$$\eta(k_0s, \phi) = 1 - f_r(k_0s)f_\phi(\phi) \quad (4.2.3)$$

where the functions f_r and f_ϕ are given by

$$f_r(k_0s) = \begin{cases} 0 & 0 < k_0s < 3.1835 \\ 1 & 3.1835 < k_0s < 4.6835 \\ 0 & 4.6835 < k_0s < 6.8992 \end{cases} \quad (4.2.4)$$

$$f_\phi(\phi) = \begin{cases} 0 & 0 < \phi < \pi/4 \\ 1 & \pi/4 < \phi < 3\pi/4 \\ 0 & 3\pi/4 < \phi < 2\pi \end{cases} \quad (4.2.5)$$

A side view of cone-cylinder 2 with the surface impedance given by eq. (4.2.3) is shown in Figure 4.2.9. Results for the bistatic radar cross sections for cone-cylinder 2 with the relative surface impedance given by eq. (4.2.3) due to both TE and TM polarized incident fields with angles of incidence $\phi_i = 270^\circ$ and $\theta_i = 0^\circ, 45^\circ, 90^\circ, 135^\circ$ and 180° are shown in Figures (4.2.20-29). The reason for selecting $\phi_i = 270^\circ$ is so that an observer looking at the scatterer along the propagation vector \mathbf{k}^i , where $\mathbf{k}^i = k_0\hat{\mathbf{k}}_i = k_0\hat{\mathbf{z}}_i$ and $\hat{\mathbf{z}}_i$ is given by eq. (2.2.3), will see the impedance patch.

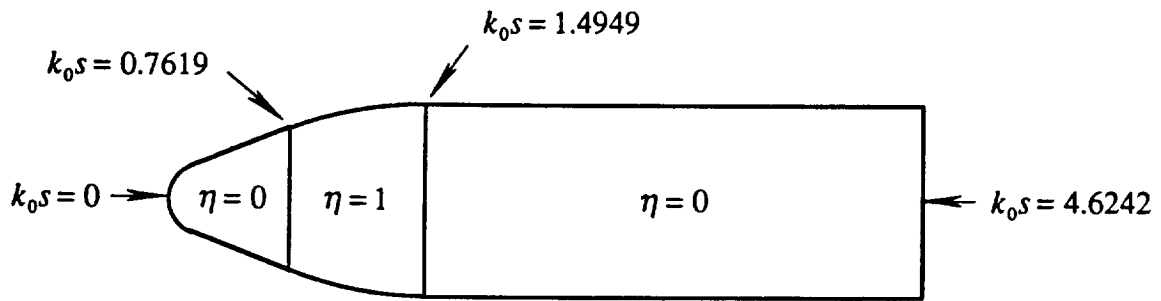


Figure 4.2.1 Graphical representation of relative surface impedance given by eq. (4.2.1)

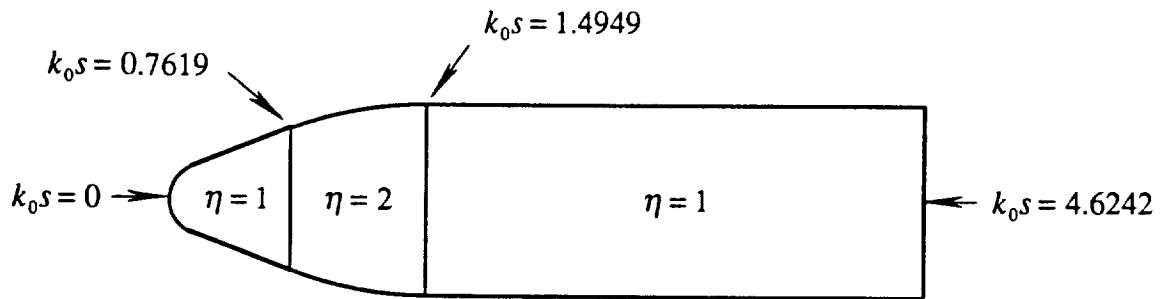


Figure 4.2.2 Graphical representation of relative surface impedance given by eq. (4.2.2)

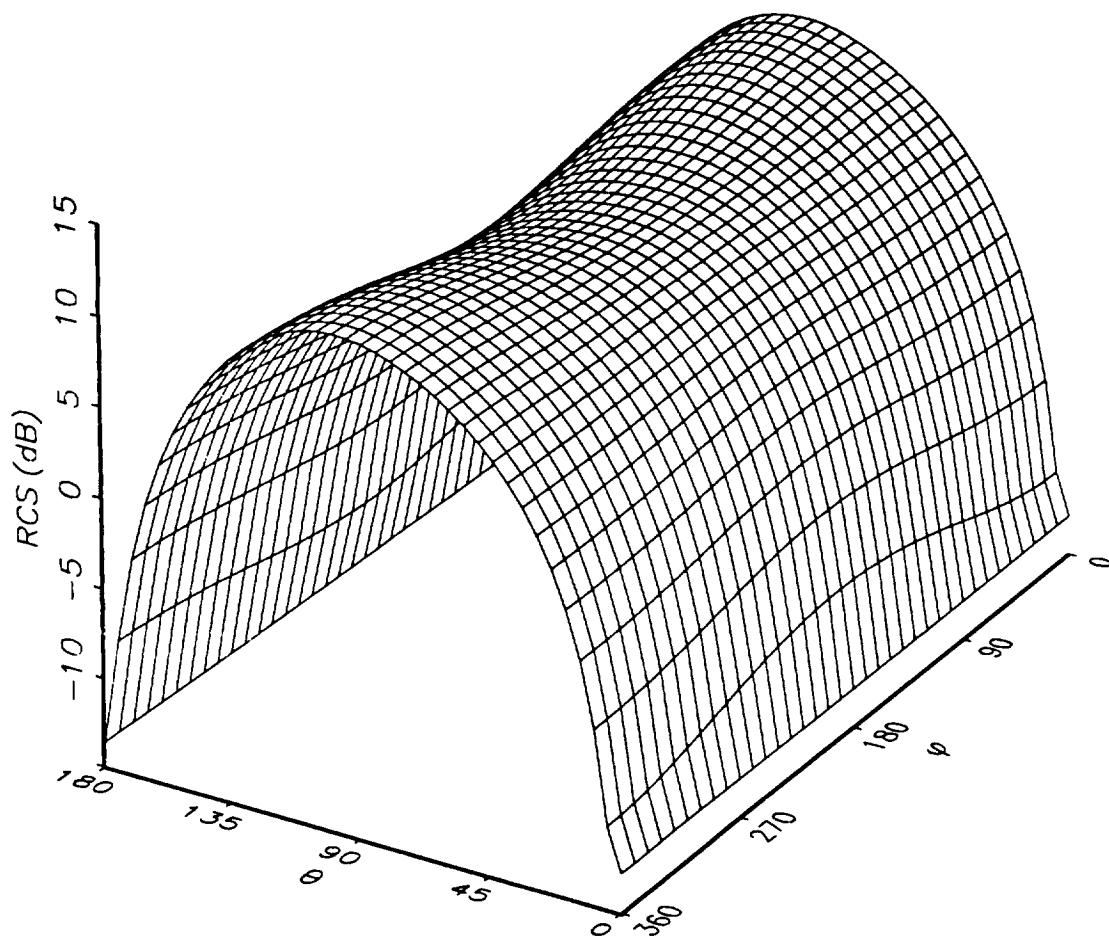


Figure 4.2.3 Bistatic radar cross section for perfectly conducting cone-cylinder: TE polarization, $\phi_i = 0^\circ$ and $\theta_i = 45^\circ$ - $k_0 h_{\text{cyl}} = 3.0$, $k_0 r_{\text{cyl}} = 0.5$, $\alpha_{\text{cone}} = 21^\circ$, $k_0 r_{\text{tip}} = 0.1875$, $k_0 r_{J1} = 2.0$, $k_0 r_{J2} = 0.0$, $N_s = 13$, and $N_\phi = 9$.

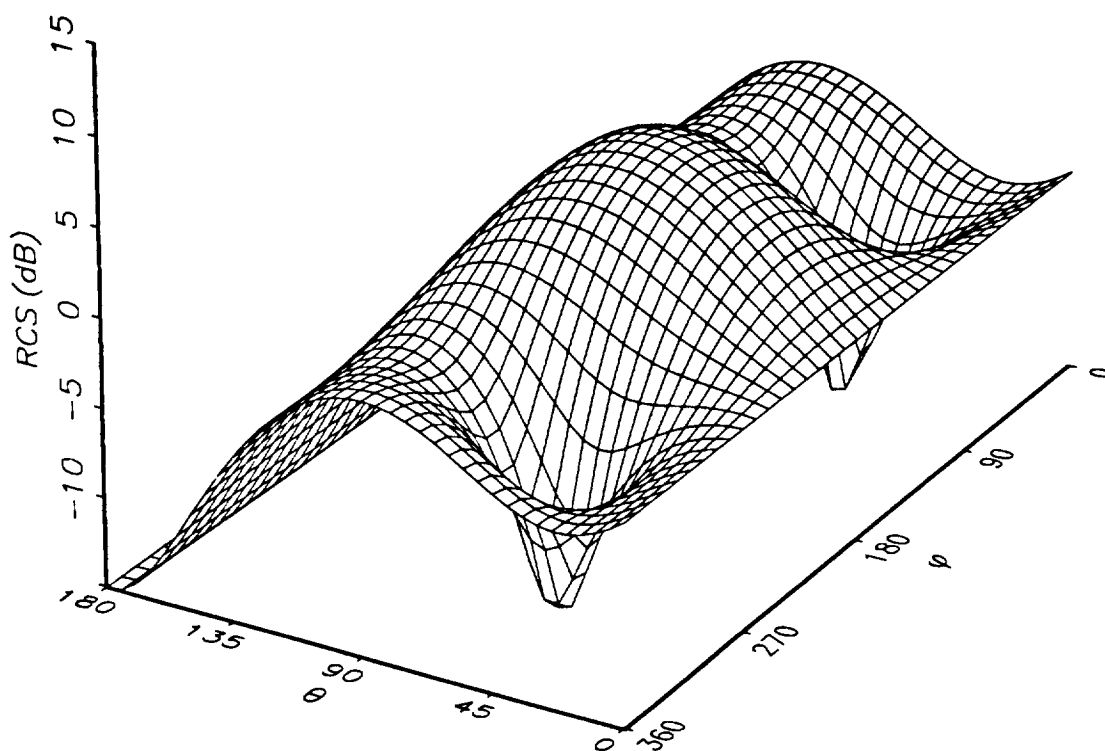


Figure 4.2.4 Bistatic radar cross section for perfectly conducting cone-cylinder: TM polarization, $\phi_i = 0^\circ$ and $\theta_i = 45^\circ$ - $k_0 h_{\text{cyl}} = 3.0$, $k_0 r_{\text{cyl}} = 0.5$, $\alpha_{\text{conc}} = 21^\circ$, $k_0 r_{\text{tip}} = 0.1875$, $k_0 r_{J1} = 2.0$, $k_0 r_{J2} = 0.0$, $N_s = 13$, and $N_\phi = 9$.

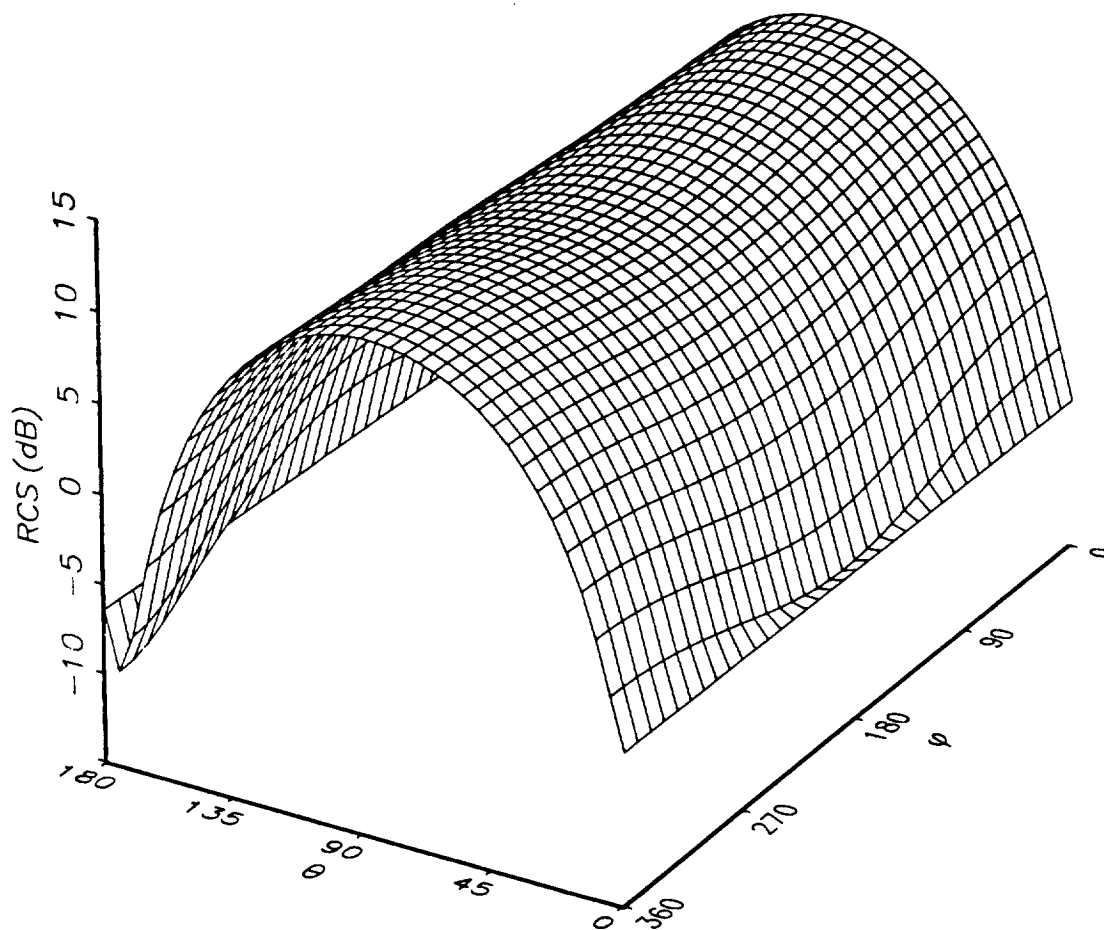


Figure 4.2.5 Bistatic radar cross section for cone-cylinder with piecewise constant surface impedance: TE polarization, $\phi_i = 0^\circ$ and $\theta_i = 45^\circ$ - $k_0 h_{\text{cyl}} = 3.0$, $k_0 r_{\text{cyl}} = 0.5$, $\alpha_{\text{cone}} = 21^\circ$, $k_0 r_{\text{tip}} = 0.1875$, $k_0 r_{J1} = 2.0$, $k_0 r_{J2} = 0.0$, $N_s = 13$ and $N_\phi = 9$ with relative surface impedance given by eq. (4.2.1).

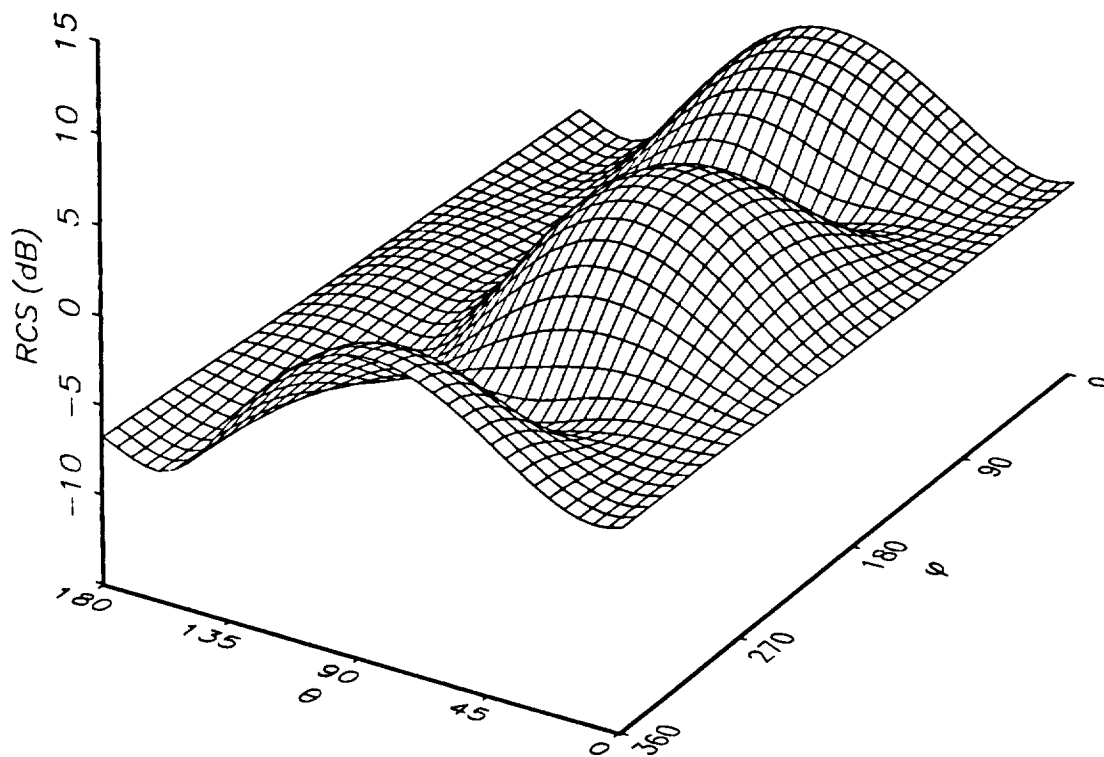


Figure 4.2.6 Bistatic radar cross section for cone-cylinder with piecewise constant surface impedance: TM polarization, $\phi_i = 0^\circ$ and $\theta_i = 45^\circ$ - $k_0 h_{\text{cyl}} = 3.0$, $k_0 r_{\text{cyl}} = 0.5$, $\alpha_{\text{cone}} = 21^\circ$, $k_0 r_{\text{tip}} = 0.1875$, $k_0 r_{J1} = 2.0$, $k_0 r_{J2} = 0.0$, $N_z = 13$, and $N_\phi = 9$ with relative surface impedance given by eq. (4.2.1).

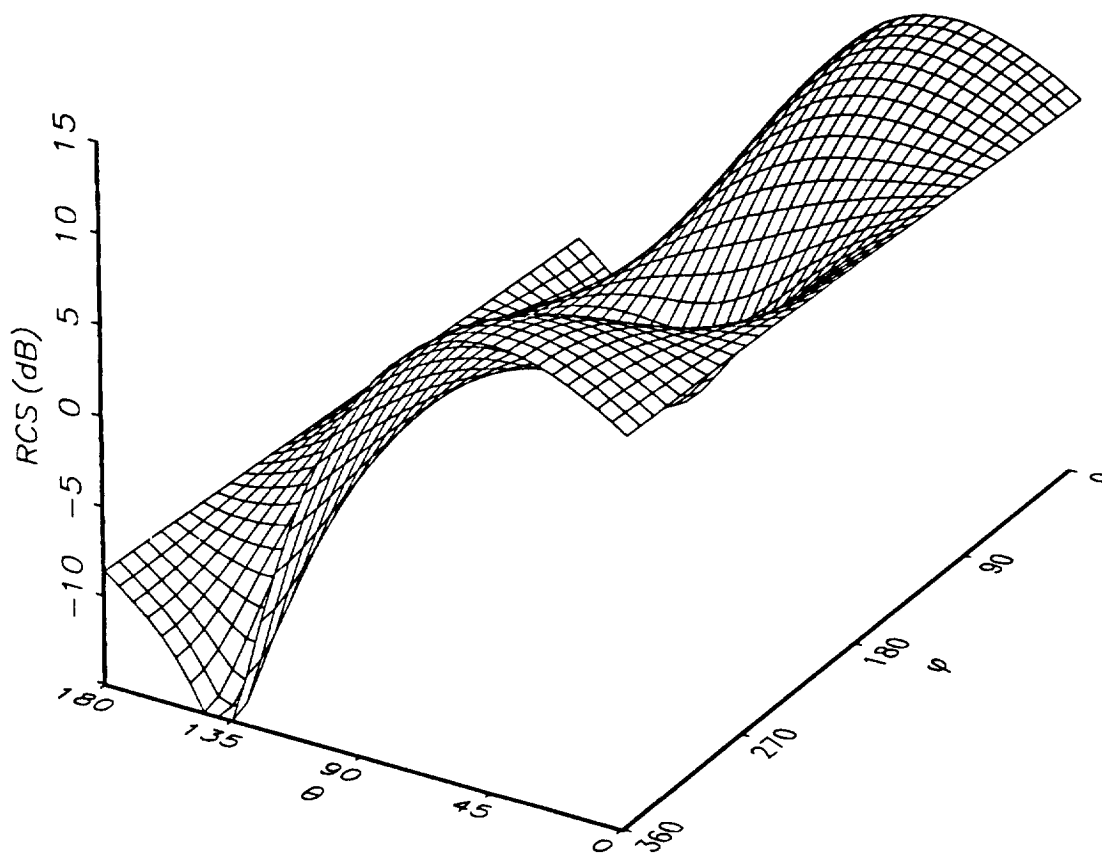


Figure 4.2.7 Bistatic radar cross section for cone-cylinder with piecewise constant surface impedance: TE polarization, $\phi_i = 0^\circ$ and $\theta_i = 45^\circ$ - $k_0 h_{\text{cyl}} = 3.0$, $k_0 r_{\text{cyl}} = 0.5$, $\alpha_{\text{cone}} = 21^\circ$, $k_0 r_{\text{tip}} = 0.1875$, $k_0 r_{j1} = 2.0$, $k_0 r_{j2} = 0.0$, $N_s = 13$, and $N_\phi = 9$ with relative surface impedance given by eq. (4.2.2).

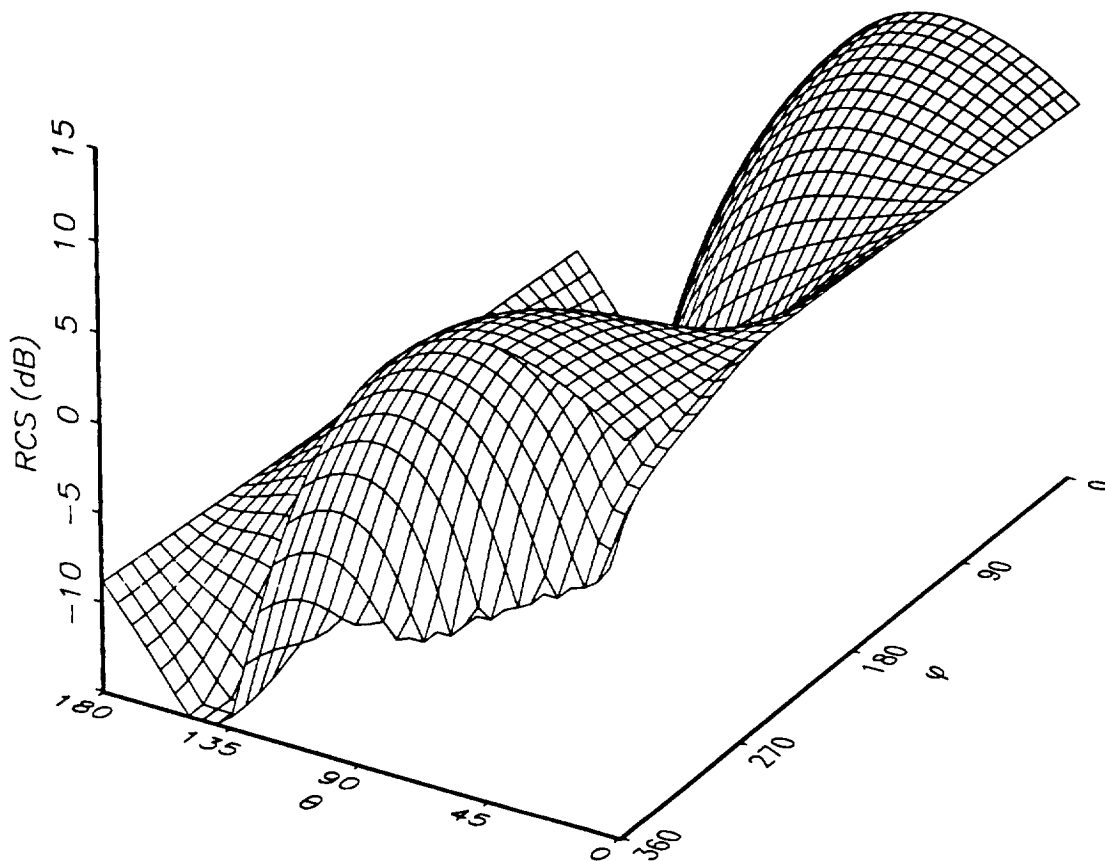


Figure 4.2.8 Bistatic radar cross section for cone-cylinder with piecewise constant surface impedance: TM polarization, $\phi_i = 0^\circ$ and $\theta_i = 45^\circ$ - $k_0 h_{\text{cyl}} = 3.0$, $k_0 r_{\text{cyl}} = 0.5$, $\alpha_{\text{cone}} = 21^\circ$, $k_0 r_{\text{tip}} = 0.1875$, $k_0 r_{J1} = 2.0$, $k_0 r_{J2} = 0.0$, $N_r = 13$, $N_\phi = 9$, $\phi_i = 0^\circ$, and $\theta_i = 45^\circ$ with relative surface impedance given by eq. (4.2.2).

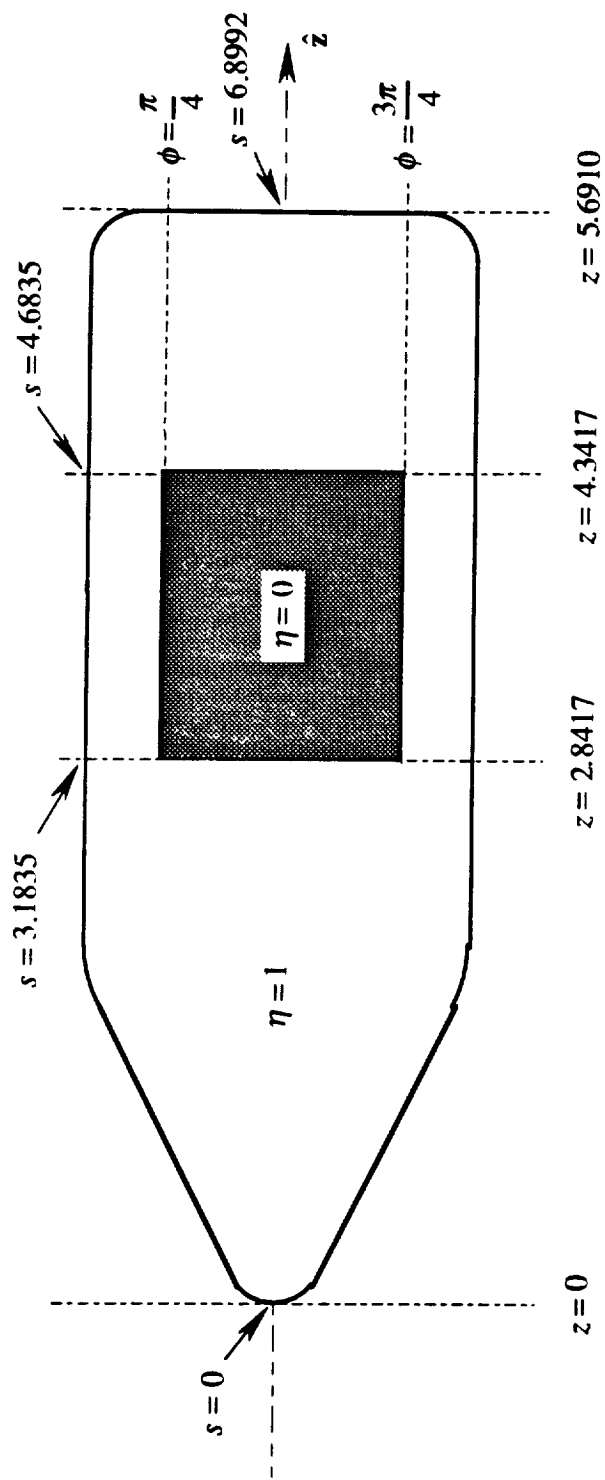


Figure 4.2.9 Side view of cone-cylinder 2 with surface impedance given by eq. (4.2.3) showing the impedance patch.

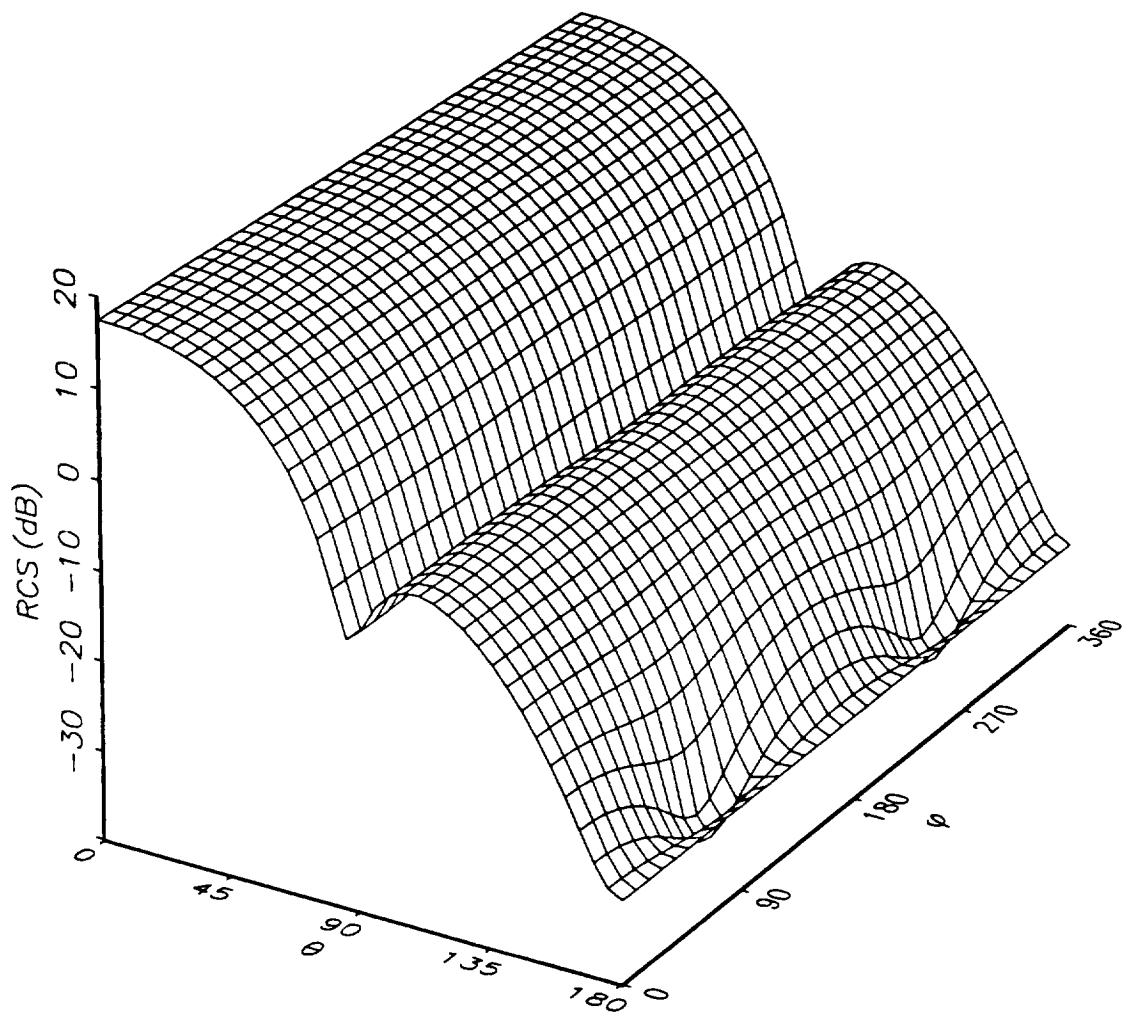


Figure 4.2.10 Bistatic radar cross section for perfectly absorbing cone-cylinder: TE polarization, $\phi_i = 270^\circ$ and $\theta_i = 0^\circ$ - $k_0 h_{\text{cyl}} = 4$, $k_0 r_{\text{cyl}} = 1$, $\alpha_{\text{cone}} = 26.565^\circ$, $k_0 r_{\text{up}} = k_0 r_{\text{J2}} = 0.25$, $k_0 r_{\text{J1}} = 0.75$, $N_s = 15$ and $N_\phi = 13$.

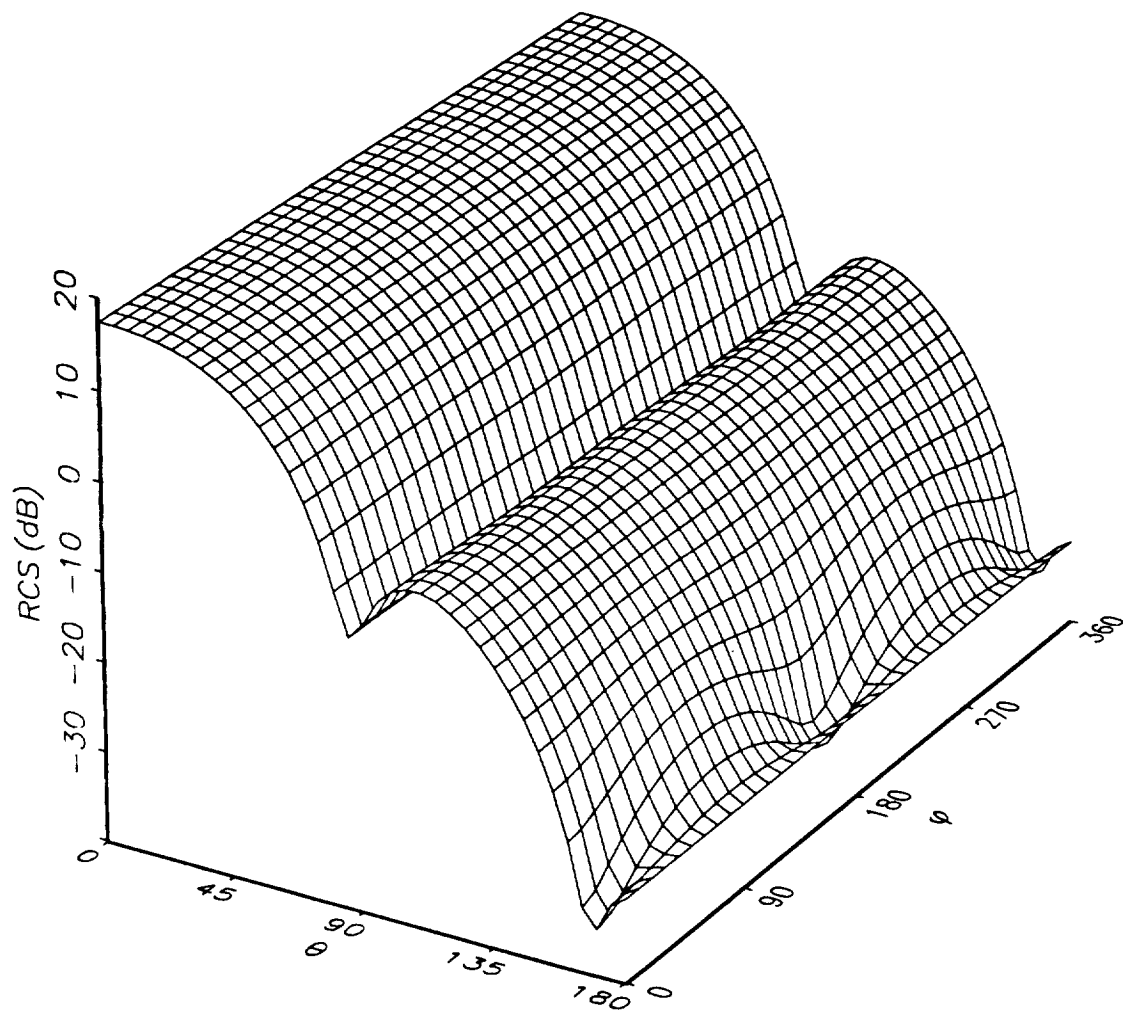


Figure 4.2.11 Bistatic radar cross section for perfectly absorbing cone-cylinder: TM polarization, $\phi_i = 270^\circ$ and $\theta_i = 0^\circ$ - $k_0 h_{\text{cyl}} = 4$, $k_0 r_{\text{cyl}} = 1$, $\alpha_{\text{cone}} = 26.565^\circ$, $k_0 r_{\text{up}} = k_0 r_{\text{J2}} = 0.25$, $k_0 r_{\text{J1}} = 0.75$, $N_s = 15$ and $N_\phi = 13$.

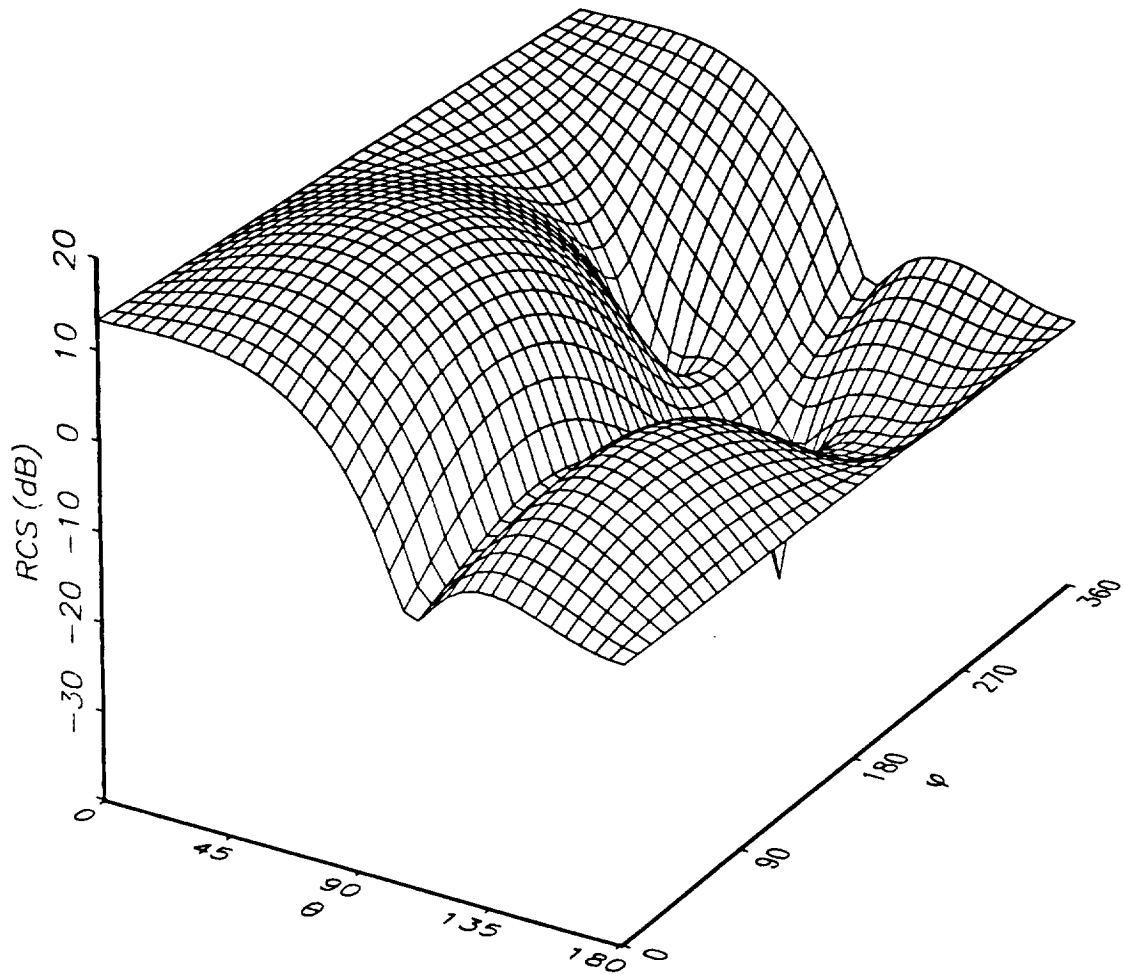


Figure 4.2.12 Bistatic radar cross section for perfectly absorbing cone-cylinder: TE polarization, $\phi_i = 270^\circ$ and $\theta_i = 45^\circ$ - $k_0 h_{\text{cyl}} = 4$, $k_0 r_{\text{cyl}} = 1$, $\alpha_{\text{conc}} = 26.565^\circ$, $k_0 r_{\text{up}} = k_0 r_{\text{J2}} = 0.25$, $k_0 r_{\text{J1}} = 0.75$, $N_s = 15$ and $N_\phi = 13$.

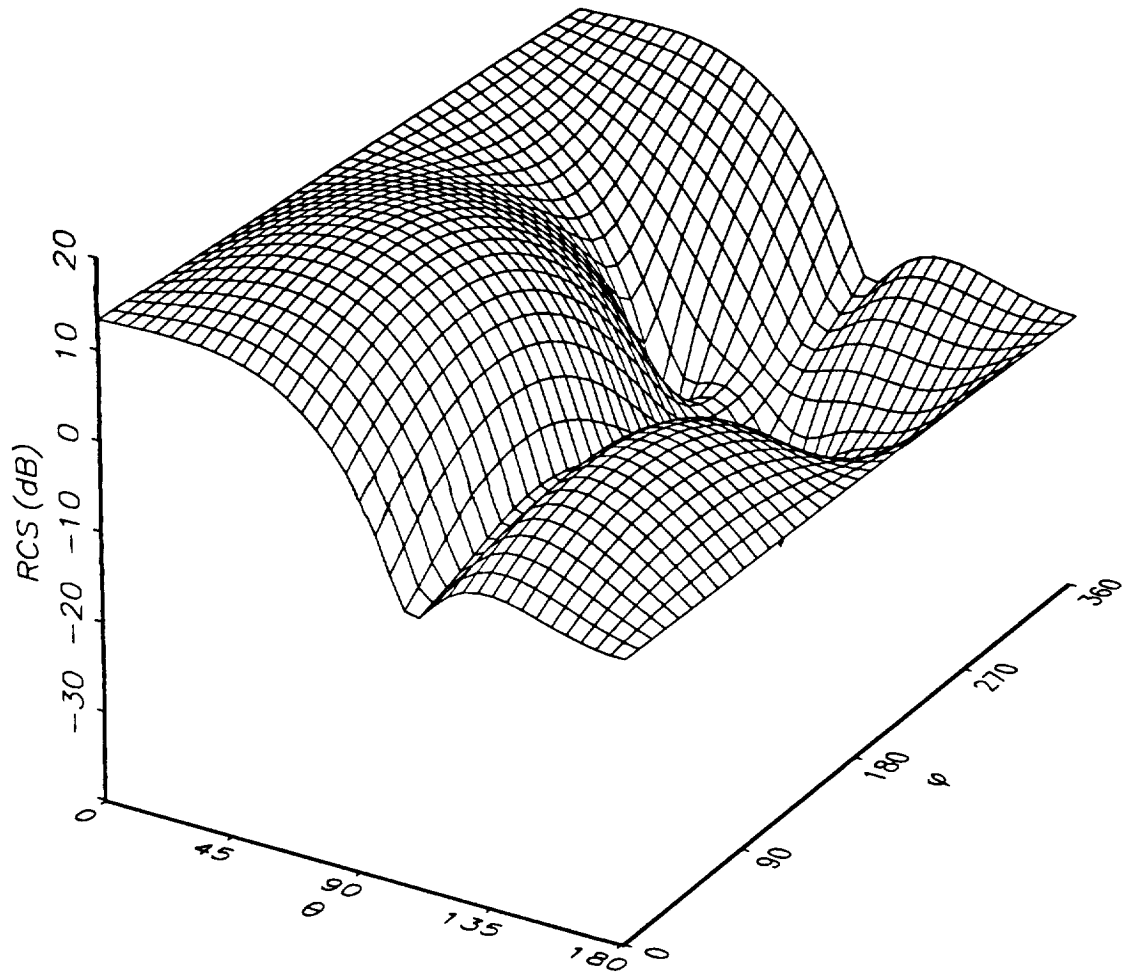


Figure 4.2.13 Bistatic radar cross section for perfectly absorbing cone-cylinder: TM polarization, $\phi_i = 270^\circ$ and $\theta_i = 45^\circ$ - $k_0 h_{\text{cyl}} = 4$, $k_0 r_{\text{cyl}} = 1$, $\alpha_{\text{cone}} = 26.565^\circ$, $k_0 r_{\text{tip}} = k_0 r_{\text{J2}} = 0.25$, $k_0 r_{\text{J1}} = 0.75$, $N_r = 15$ and $N_\phi = 13$.

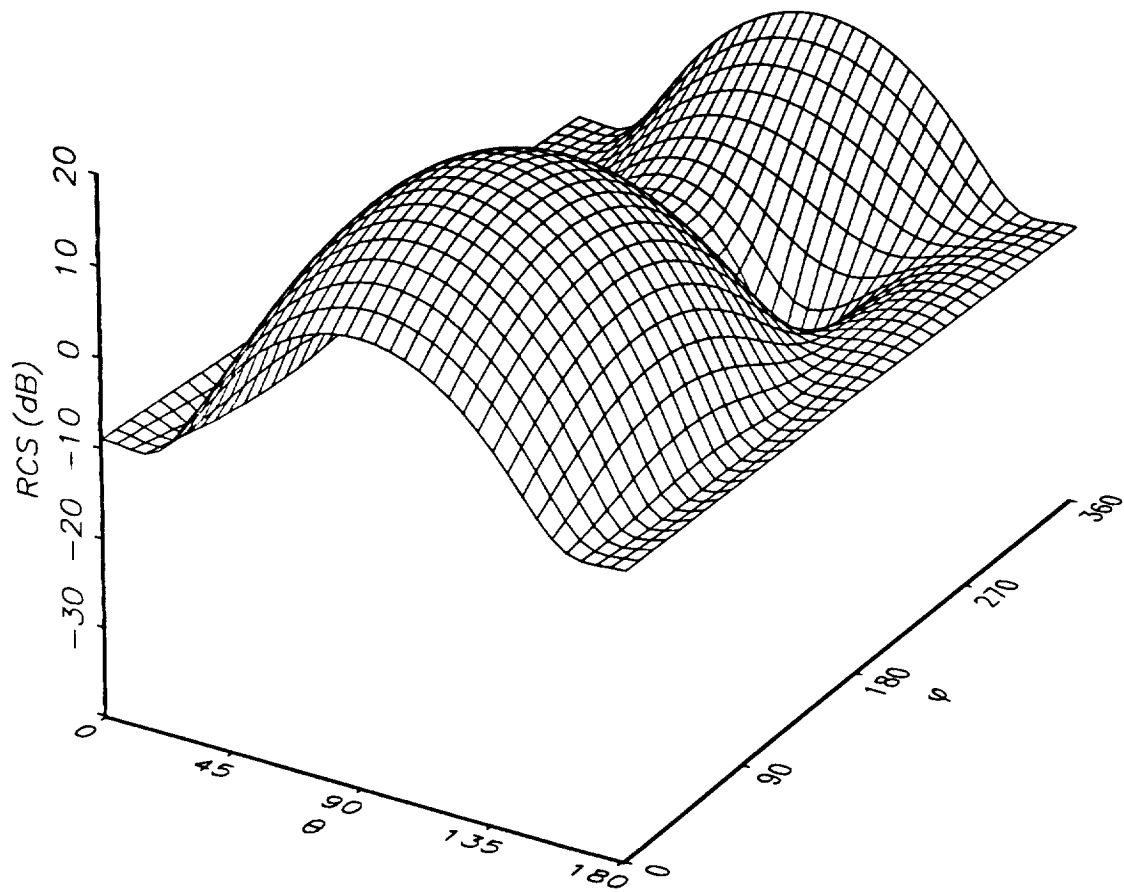


Figure 4.2.14 Bistatic radar cross section for perfectly absorbing cone-cylinder: TE polarization, $\phi_i = 270^\circ$ and $\theta_i = 90^\circ$ - $k_0 h_{\text{cyl}} = 4$, $k_0 r_{\text{cyl}} = 1$, $\alpha_{\text{cone}} = 26.565^\circ$, $k_0 r_{\text{tip}} = k_0 r_{j2} = 0.25$, $k_0 r_{j1} = 0.75$, $N_s = 15$ and $N_\phi = 13$.

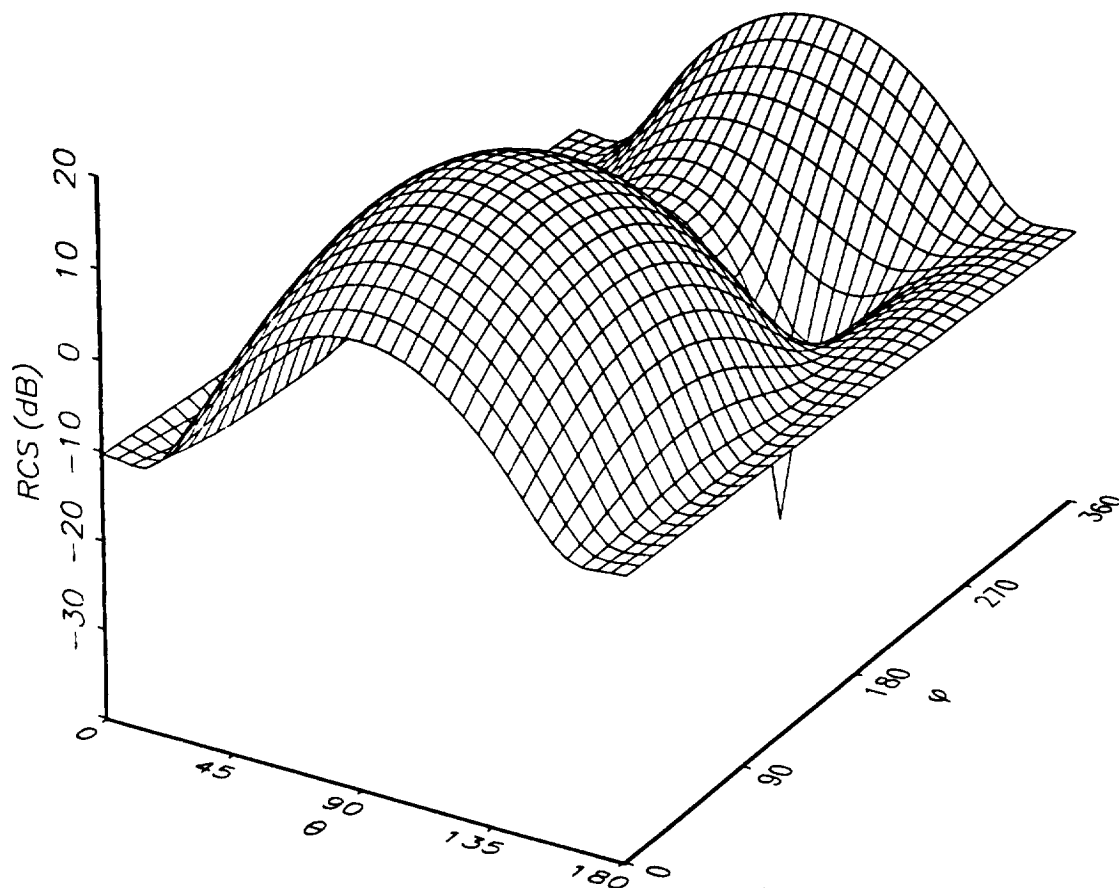


Figure 4.2.15 Bistatic radar cross section for perfectly absorbing cone-cylinder:
 TM polarization, $\phi_i = 270^\circ$ and $\theta_i = 90^\circ$ - $k_0 h_{\text{cyl}} = 4$, $k_0 r_{\text{cyl}} = 1$,
 $\alpha_{\text{cone}} = 26.565^\circ$, $k_0 r_{\text{tip}} = k_0 r_{J2} = 0.25$, $k_0 r_{J1} = 0.75$. $N_s = 15$ and $N_\phi = 13$.

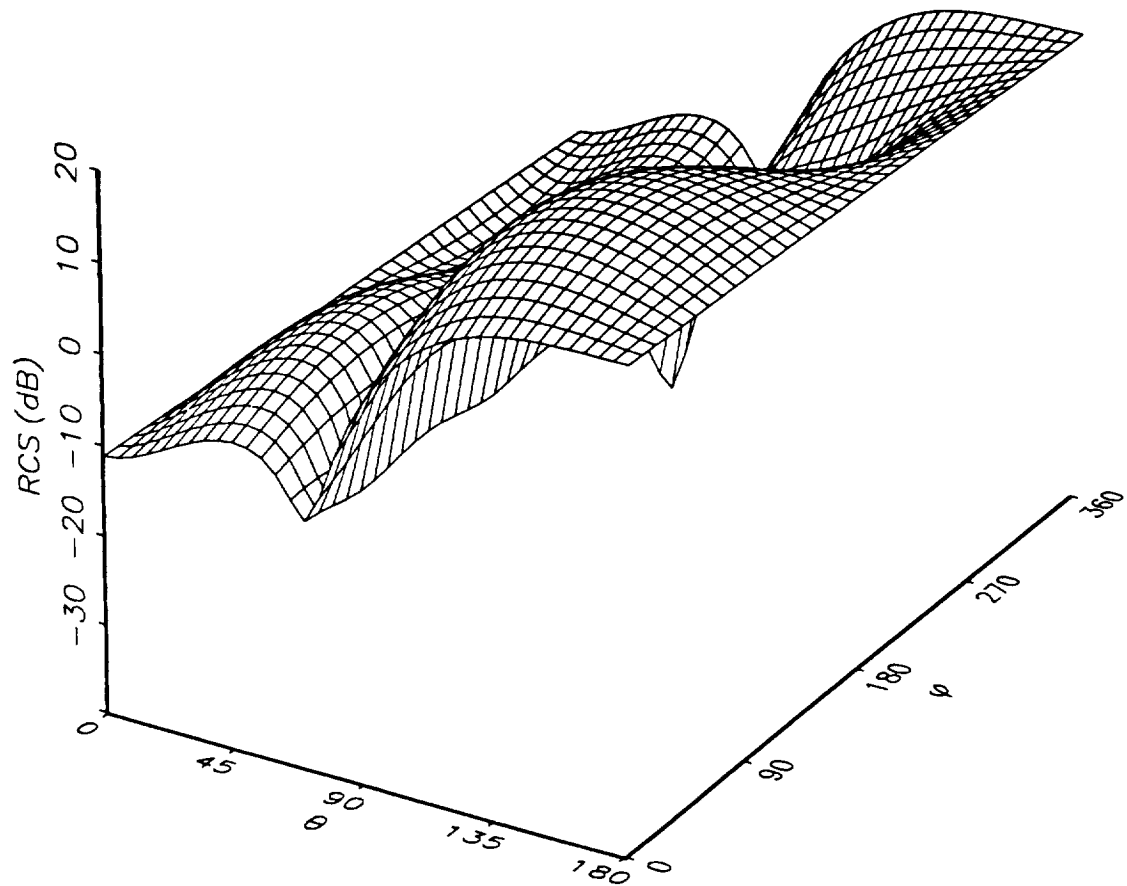


Figure 4.2.16 Bistatic radar cross section for perfectly absorbing cone-cylinder:
 TE polarization, $\phi_i = 270^\circ$ and $\theta_i = 135^\circ$ - $k_0 h_{\text{cyl}} = 4$, $k_0 r_{\text{cyl}} = 1$,
 $\alpha_{\text{cone}} = 26.565^\circ$, $k_0 r_{\text{up}} = k_0 r_{\text{J2}} = 0.25$, $k_0 r_{\text{J1}} = 0.75$, $N_z = 15$ and $N_\phi = 13$.

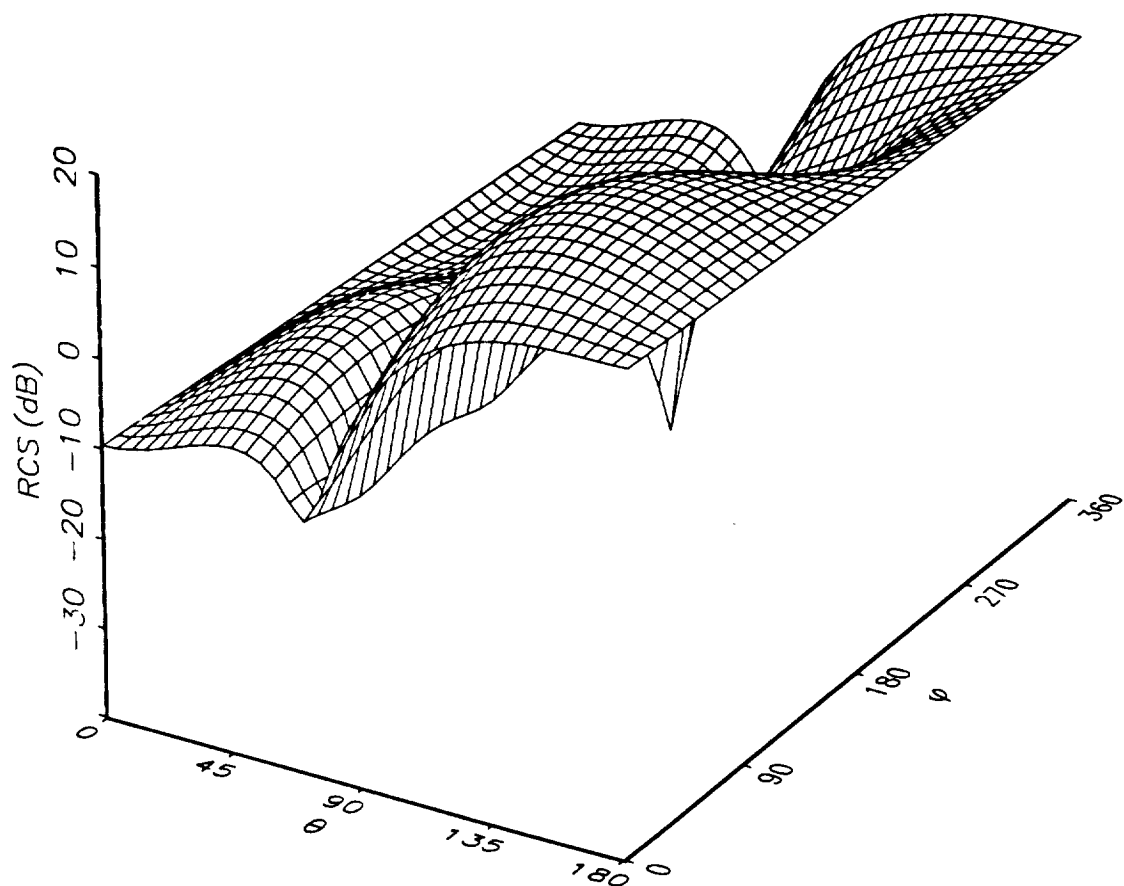


Figure 4.2.17 Bistatic radar cross section for perfectly absorbing cone-cylinder: TM polarization, $\phi_i = 270^\circ$ and $\theta_i = 135^\circ$ - $k_0 h_{\text{cyl}} = 4$, $k_0 r_{\text{cyl}} = 1$, $\alpha_{\text{cone}} = 26.565^\circ$, $k_0 r_{i1} = k_0 r_{i2} = 0.25$, $k_0 r_{j1} = 0.75$, $N_s = 15$ and $N_\phi = 13$.

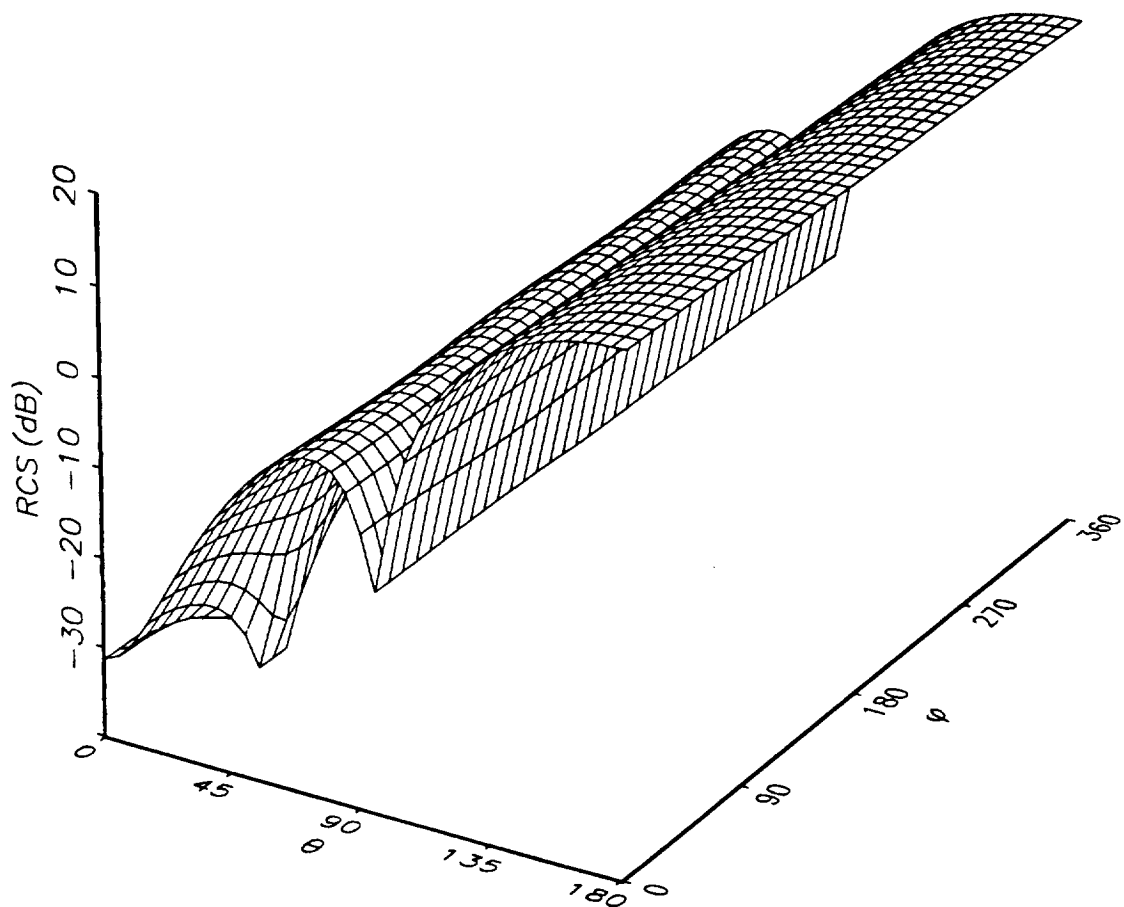


Figure 4.2.18 Bistatic radar cross section for perfectly absorbing cone-cylinder: TE polarization, $\phi_i = 270^\circ$ and $\theta_i = 180^\circ$ - $k_0 h_{\text{cyl}} = 4$, $k_0 r_{\text{cyl}} = 1$, $\alpha_{\text{cone}} = 26.565^\circ$, $k_0 r_{\text{up}} = k_0 r_{\text{J2}} = 0.25$, $k_0 r_{\text{J1}} = 0.75$, $N_s = 15$ and $N_\phi = 13$.

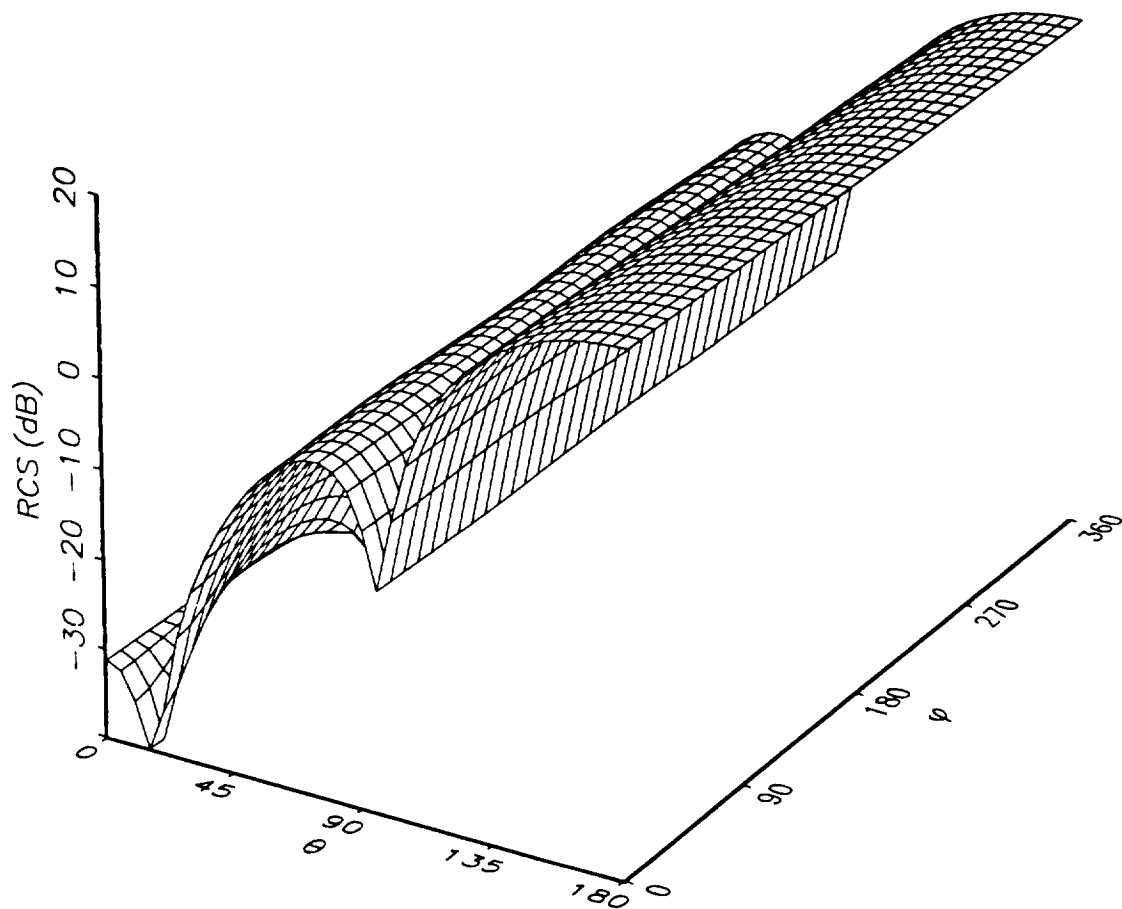


Figure 4.2.19 Bistatic radar cross section for perfectly absorbing cone-cylinder: TM polarization, $\phi_i = 270^\circ$ and $\theta_i = 180^\circ$ - $k_0 h_{\text{cyl}} = 4$, $k_0 r_{\text{cyl}} = 1$, $\alpha_{\text{cone}} = 26.565^\circ$, $k_0 r_{\text{tip}} = k_0 r_{\text{J2}} = 0.25$, $k_0 r_{\text{J1}} = 0.75$, $N_s = 15$ and $N_\phi = 13$.

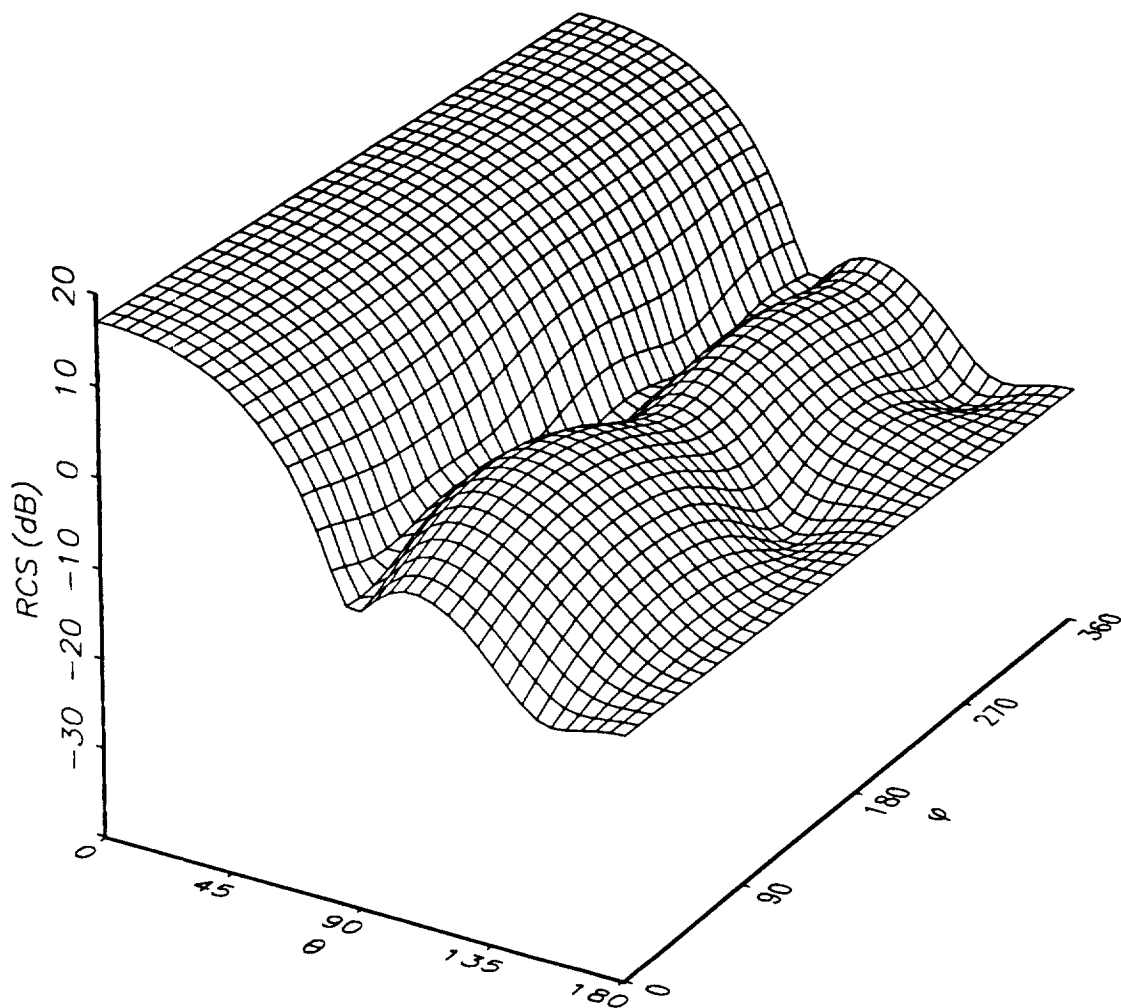


Figure 4.2.20 Bistatic radar cross section for cone-cylinder with impedance patch: TE polarization, $\phi_i = 270^\circ$ and $\theta_i = 0^\circ$ - $k_0 h_{\text{cyl}} = 4$, $k_0 r_{\text{cyl}} = 1$, $\alpha_{\text{cone}} = 26.565^\circ$, $k_0 r_{\text{tip}} = k_0 r_{j2} = 0.25$, $k_0 r_{j1} = 0.75$, $N_s = 16$ and $N_\phi = 11$; with η given by eq. (4.2.3).

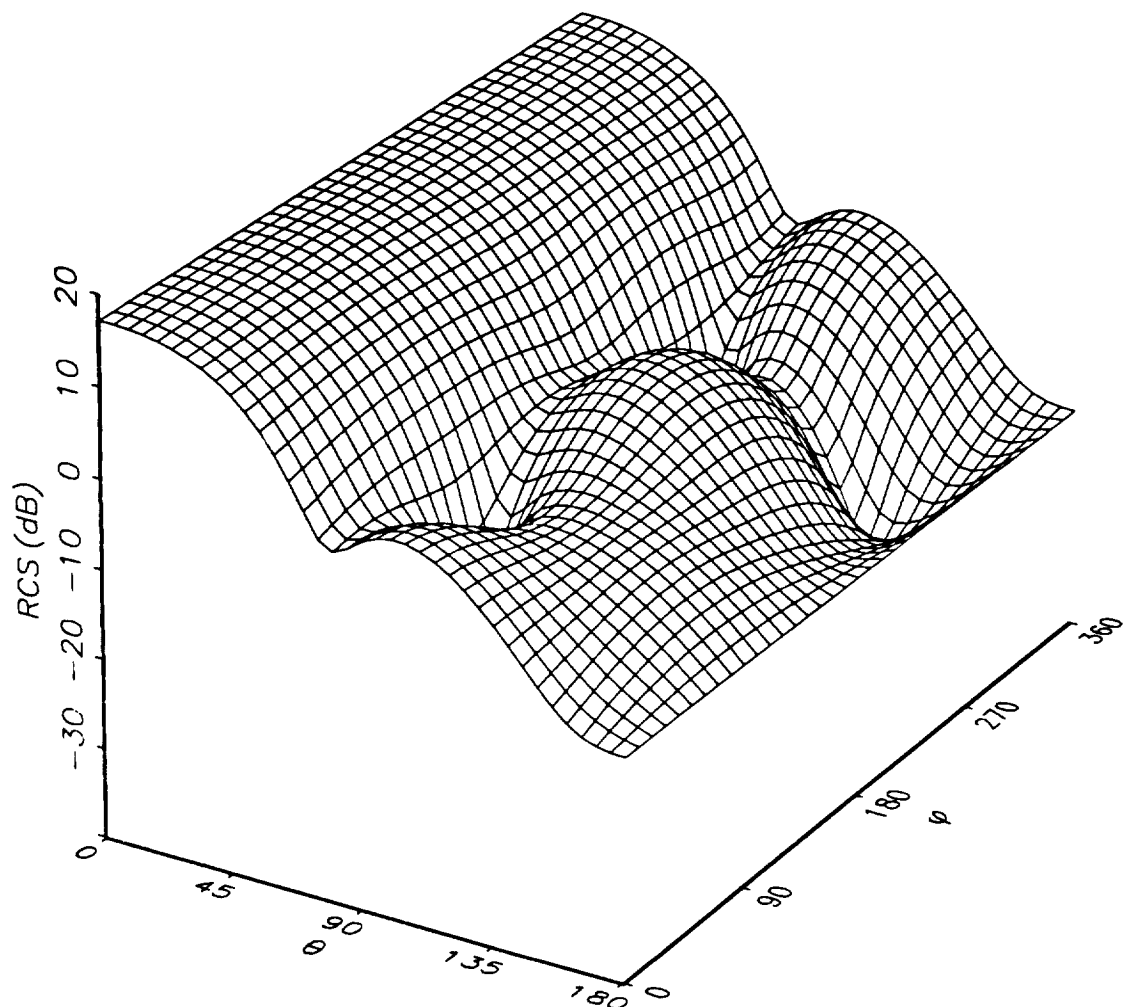


Figure 4.2.21 Bistatic radar cross section for cone-cylinder with impedance patch: TM polarization, $\phi_i = 270^\circ$ and $\theta_i = 0^\circ$ - $k_0 h_{\text{cyl}} = 4$, $k_0 r_{\text{cyl}} = 1$, $\alpha_{\text{cone}} = 26.565^\circ$, $k_0 r_{\text{up}} = k_0 r_{12} = 0.25$, $k_0 r_{11} = 0.75$, $N_s = 16$ and $N_\phi = 11$; with η given by eq. (4.2.3).

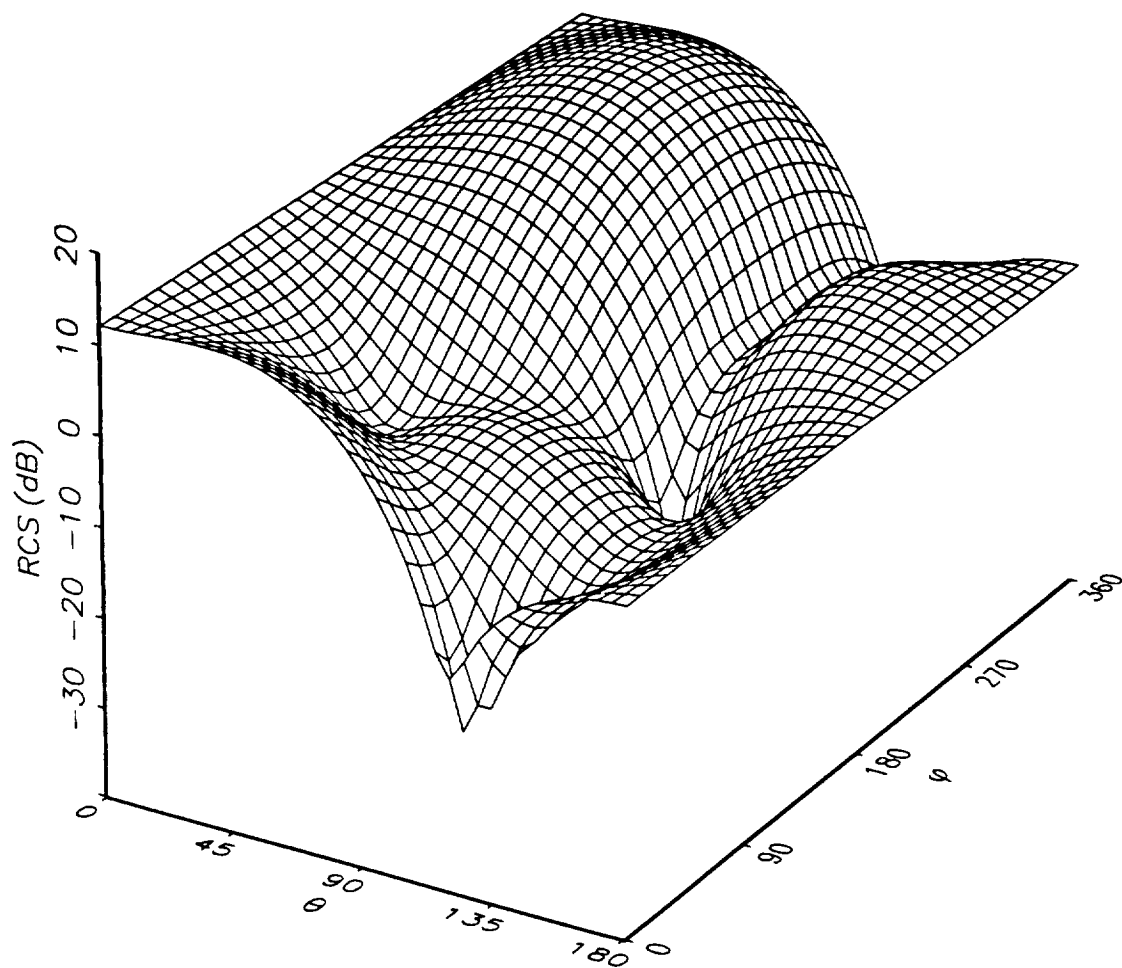


Figure 4.2.22 Bistatic radar cross section for cone-cylinder with impedance patch: TE polarization, $\phi_i = 270^\circ$ and $\theta_i = 45^\circ$ - $k_0 h_{\text{cyl}} = 4$, $k_0 r_{\text{cyl}} = 1$, $\alpha_{\text{cone}} = 26.565^\circ$, $k_0 r_{\text{up}} = k_0 r_{12} = 0.25$, $k_0 r_{11} = 0.75$, $N_s = 16$ and $N_\phi = 11$; with η given by eq. (4.2.3).

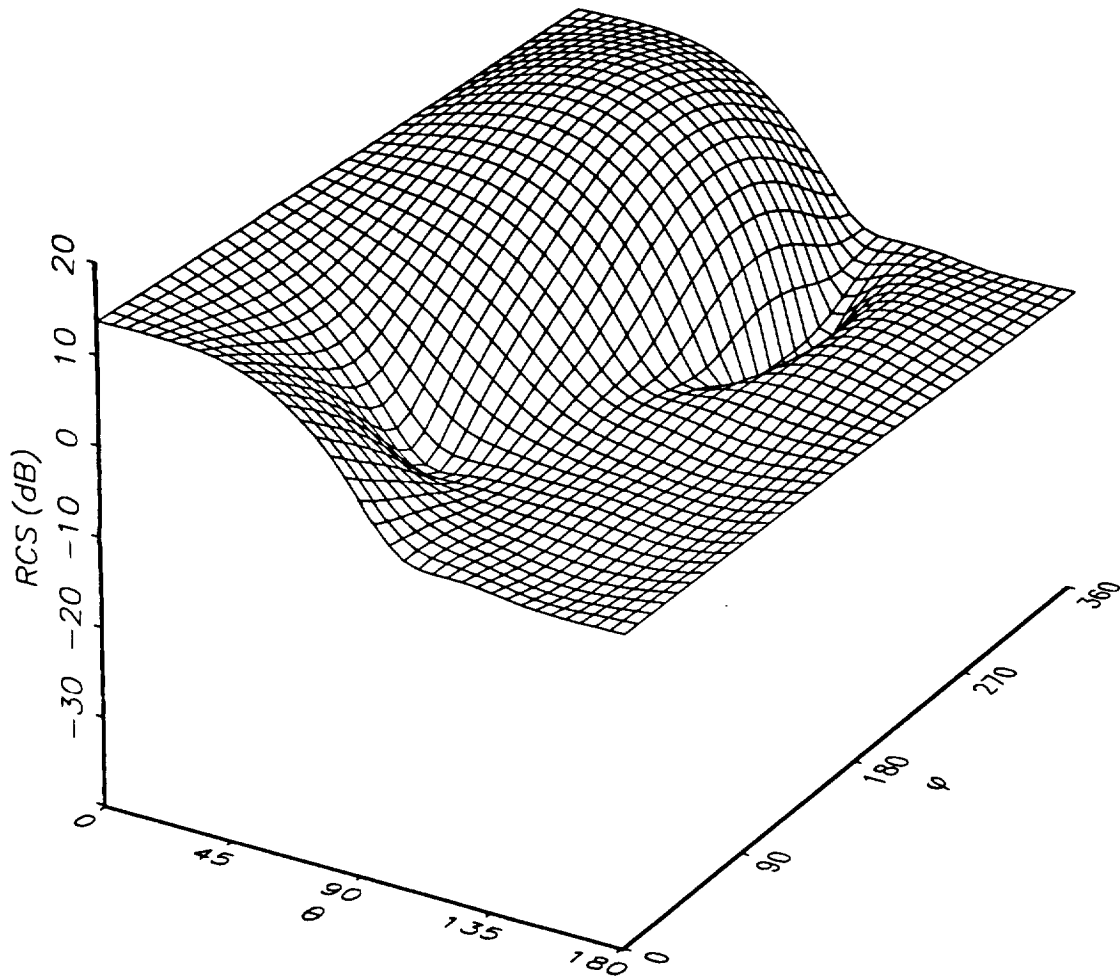


Figure 4.2.23 Bistatic radar cross section for cone-cylinder with impedance patch: TM polarization, $\phi_i = 270^\circ$ and $\theta_i = 45^\circ$ - $k_0 h_{\text{cyl}} = 4$, $k_0 r_{\text{cyl}} = 1$, $\alpha_{\text{cone}} = 26.565^\circ$, $k_0 r_{\text{tip}} = k_0 r_{12} = 0.25$, $k_0 r_{11} = 0.75$, $N_s = 16$ and $N_\phi = 11$; with η given by eq. (4.2.3).

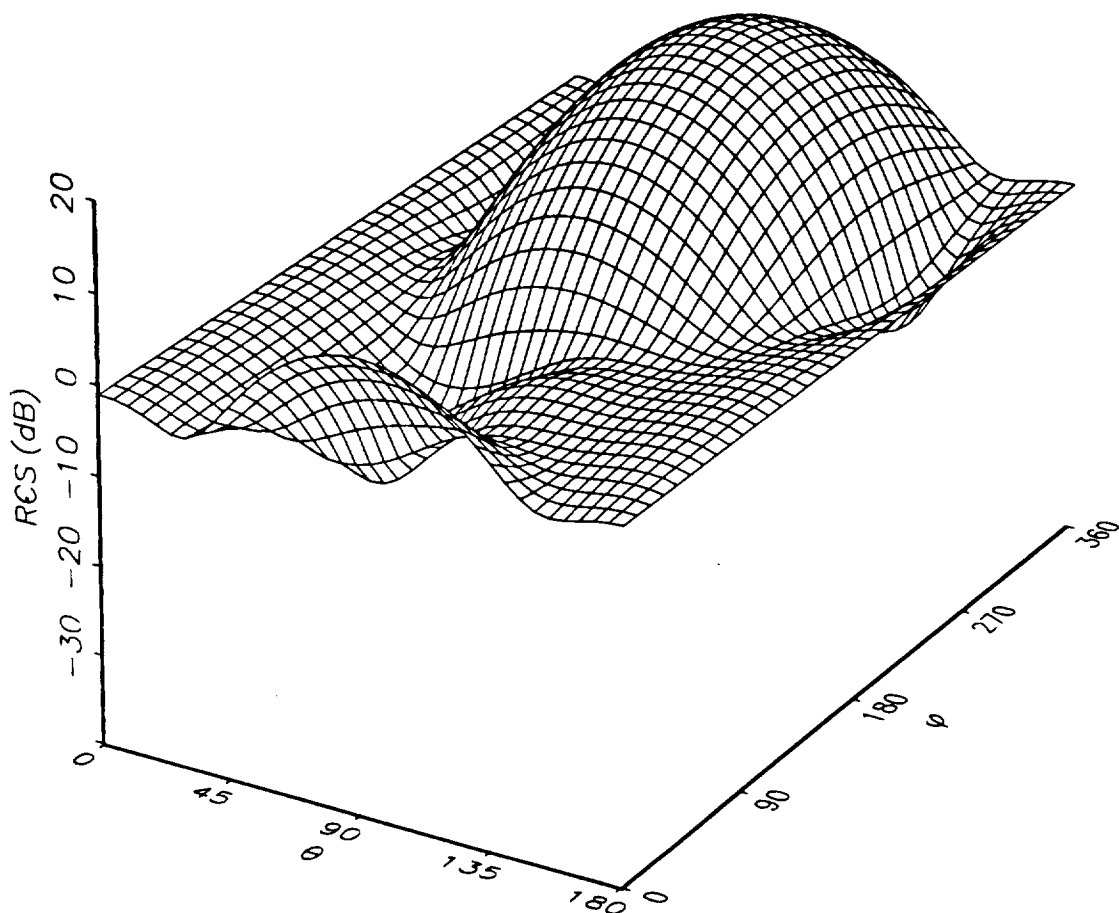


Figure 4.2.24 Bistatic radar cross section for cone-cylinder with impedance patch: TE polarization, $\phi_i = 270^\circ$ and $\theta_i = 90^\circ$ - $k_0 h_{\text{cyl}} = 4$, $k_0 r_{\text{cyl}} = 1$, $\alpha_{\text{cone}} = 26.565^\circ$, $k_0 r_{\text{up}} = k_0 r_{\text{j2}} = 0.25$, $k_0 r_{\text{j1}} = 0.75$, $N_s = 16$ and $N_\phi = 11$; with η given by eq. (4.2.3).

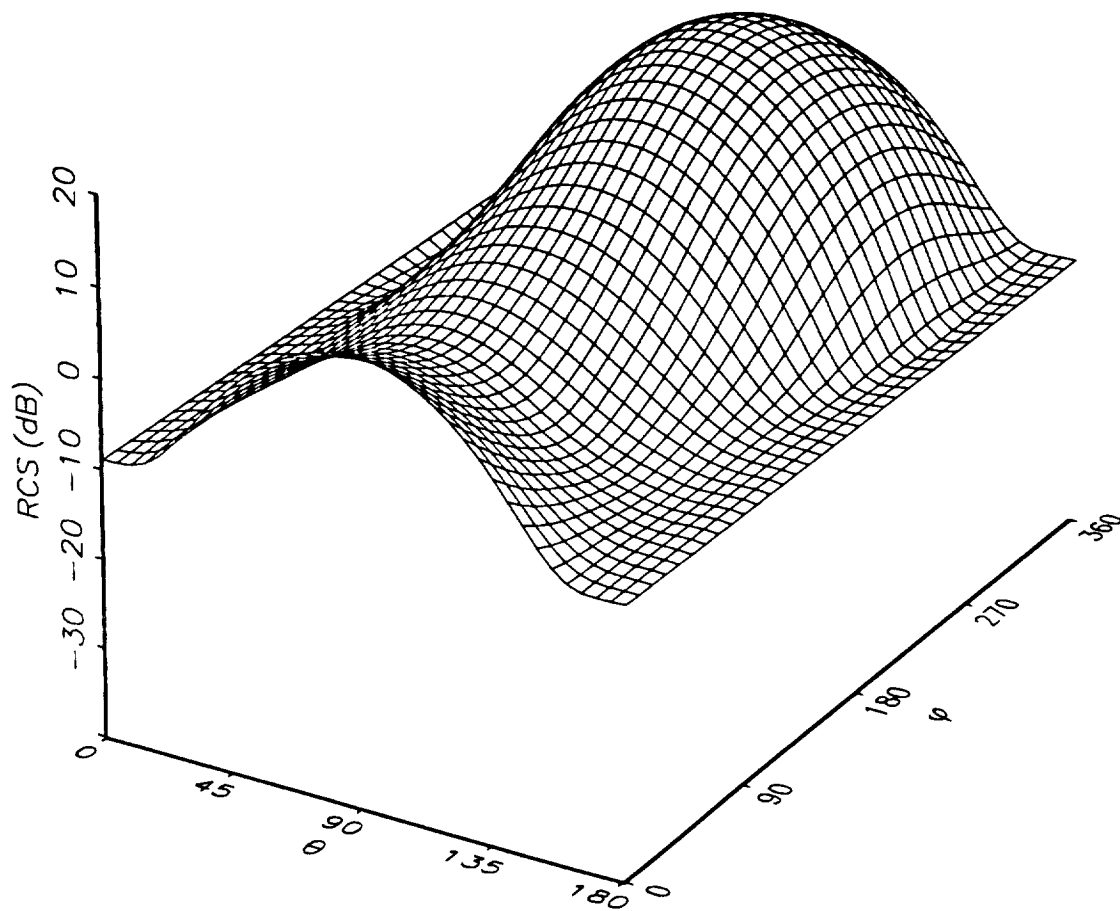


Figure 4.2.25 Bistatic radar cross section for cone-cylinder with impedance patch: TM polarization, $\phi_i = 270^\circ$ and $\theta_i = 90^\circ$ - $k_0 h_{\text{cyl}} = 4$, $k_0 r_{\text{cyl}} = 1$, $\alpha_{\text{cone}} = 26.565^\circ$, $k_0 r_{\text{tip}} = k_0 r_{12} = 0.25$, $k_0 r_{11} = 0.75$, $N_s = 16$ and $N_\phi = 11$; with η given by eq. (4.2.3).

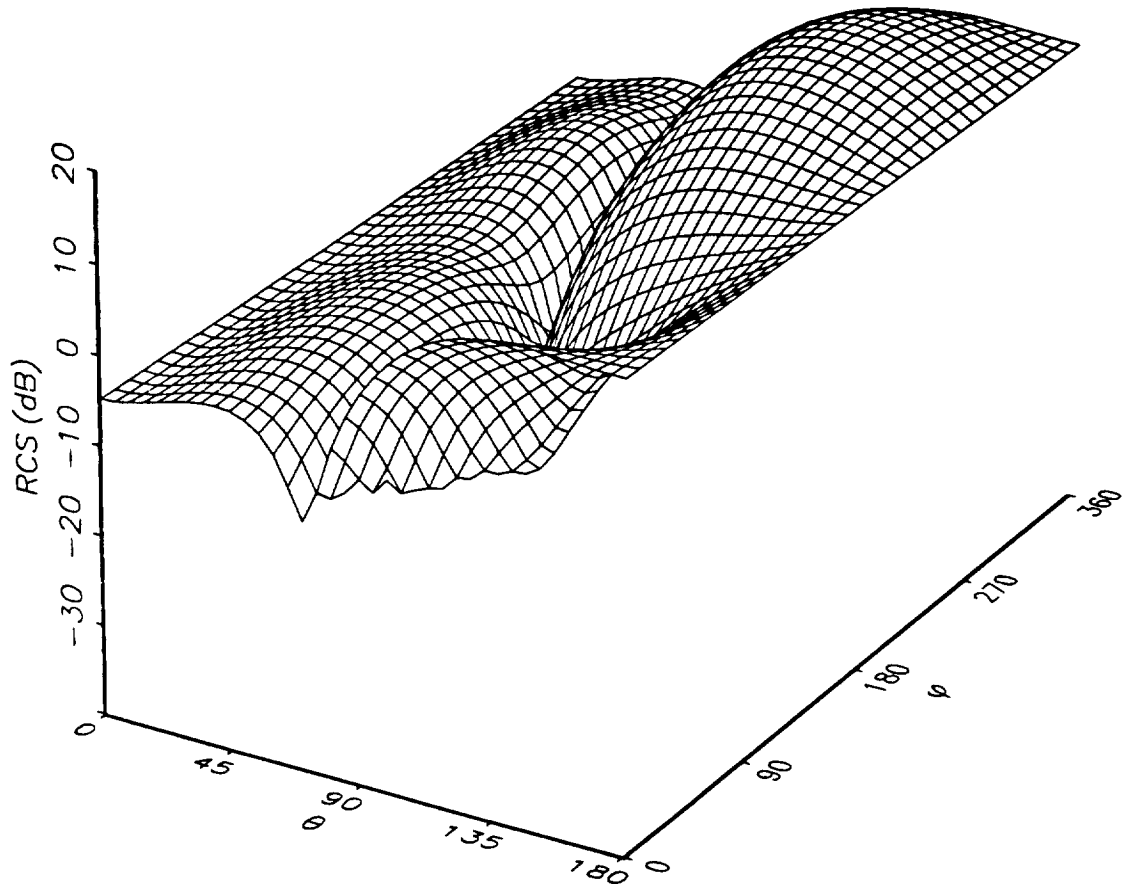


Figure 4.2.26 Bistatic radar cross section for cone-cylinder with impedance patch: TE polarization, $\phi_i = 270^\circ$ and $\theta_i = 135^\circ$ - $k_0 h_{\text{cyl}} = 4$, $k_0 r_{\text{cyl}} = 1$, $\alpha_{\text{cone}} = 26.565^\circ$, $k_0 r_{\text{up}} = k_0 r_{12} = 0.25$, $k_0 r_{j1} = 0.75$, $N_s = 16$ and $N_\phi = 11$; with η given by eq. (4.2.3).

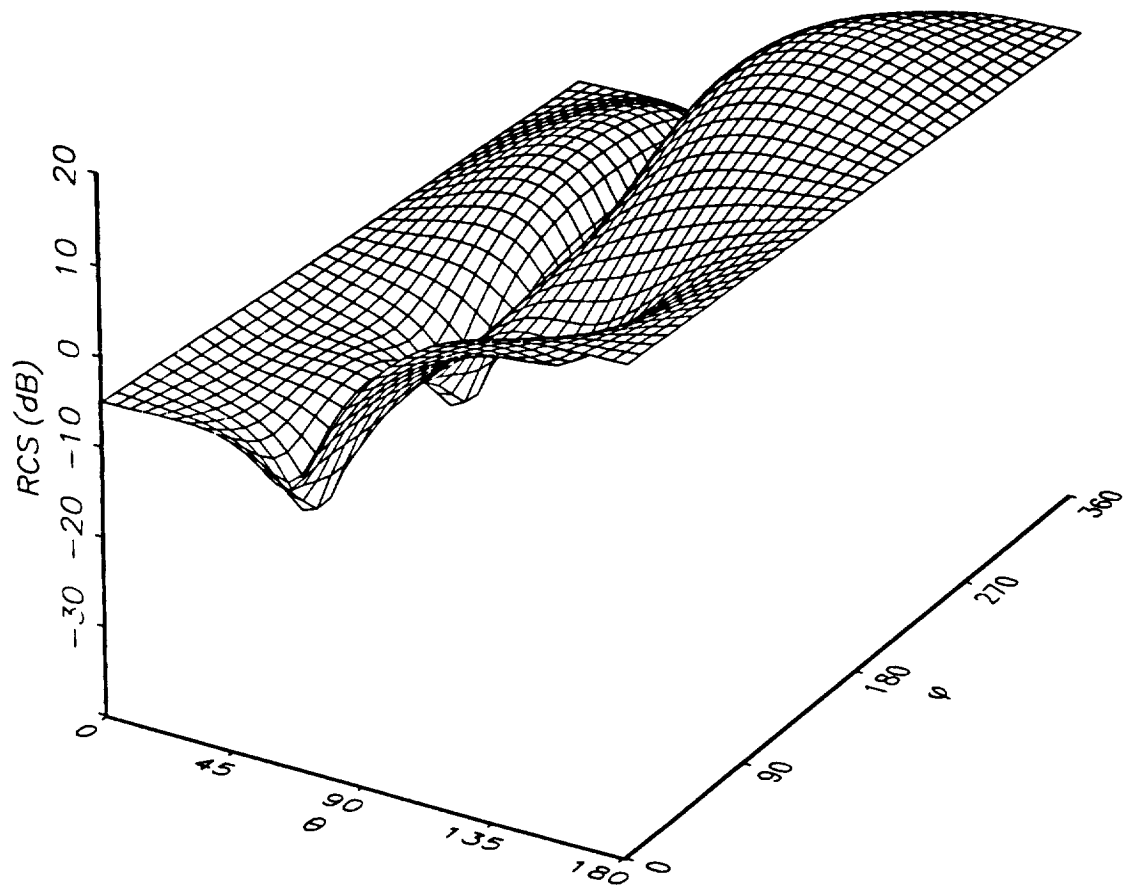


Figure 4.2.27 Bistatic radar cross section for cone-cylinder with impedance patch: TM polarization, $\phi_i = 270^\circ$ and $\theta_i = 135^\circ$ - $k_0 h_{\text{cyl}} = 4$, $k_0 r_{\text{cyl}} = 1$, $\alpha_{\text{cone}} = 26.565^\circ$, $k_0 r_{\text{up}} = k_0 r_{\text{J2}} = 0.25$, $k_0 r_{\text{J1}} = 0.75$, $N_r = 16$ and $N_\phi = 11$; with η given by eq. (4.2.3).

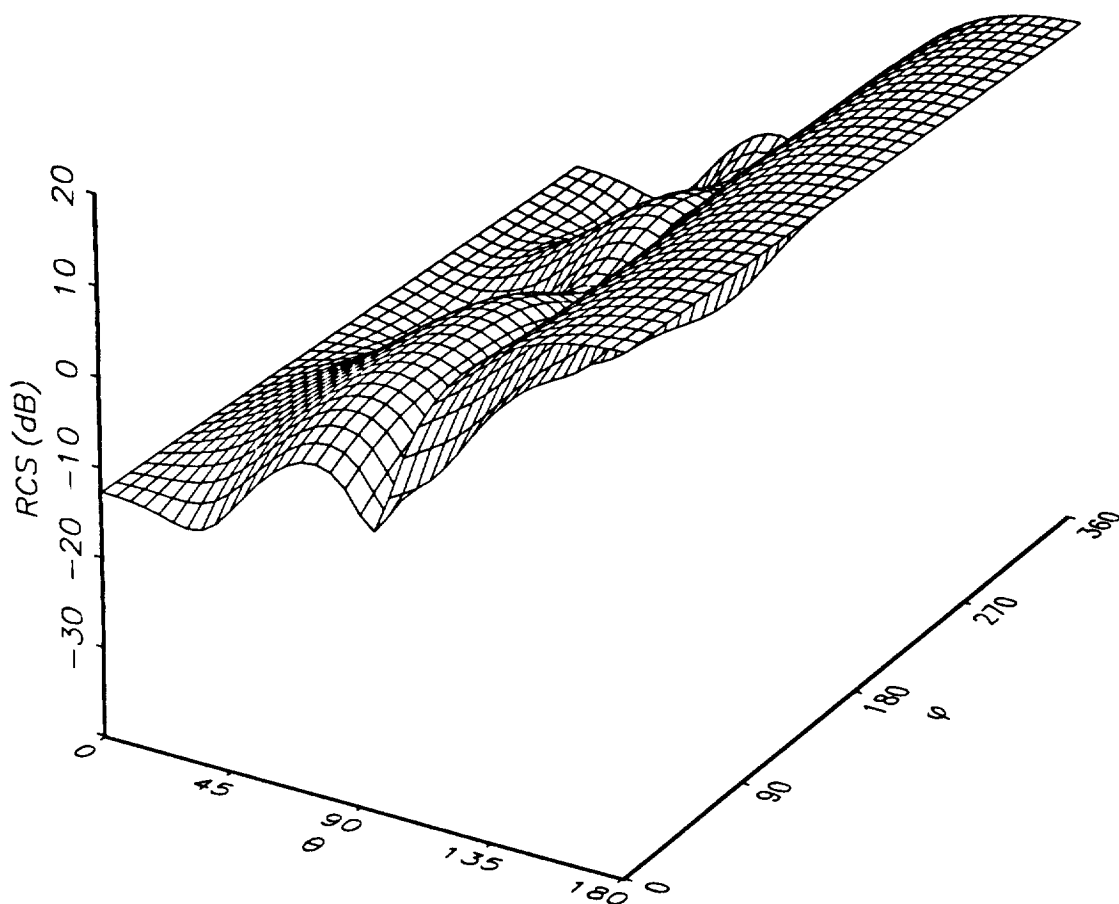


Figure 4.2.28 Bistatic radar cross section for cone-cylinder with impedance patch: TE polarization, $\phi_i = 270^\circ$ and $\theta_i = 180^\circ$ - $k_0 h_{\text{cyl}} = 4$, $k_0 r_{\text{cyl}} = 1$, $\alpha_{\text{cone}} = 26.565^\circ$, $k_0 r_{\text{tip}} = k_0 r_{12} = 0.25$, $k_0 r_{11} = 0.75$, $N_r = 16$ and $N_\phi = 11$; with η given by eq. (4.2.3).

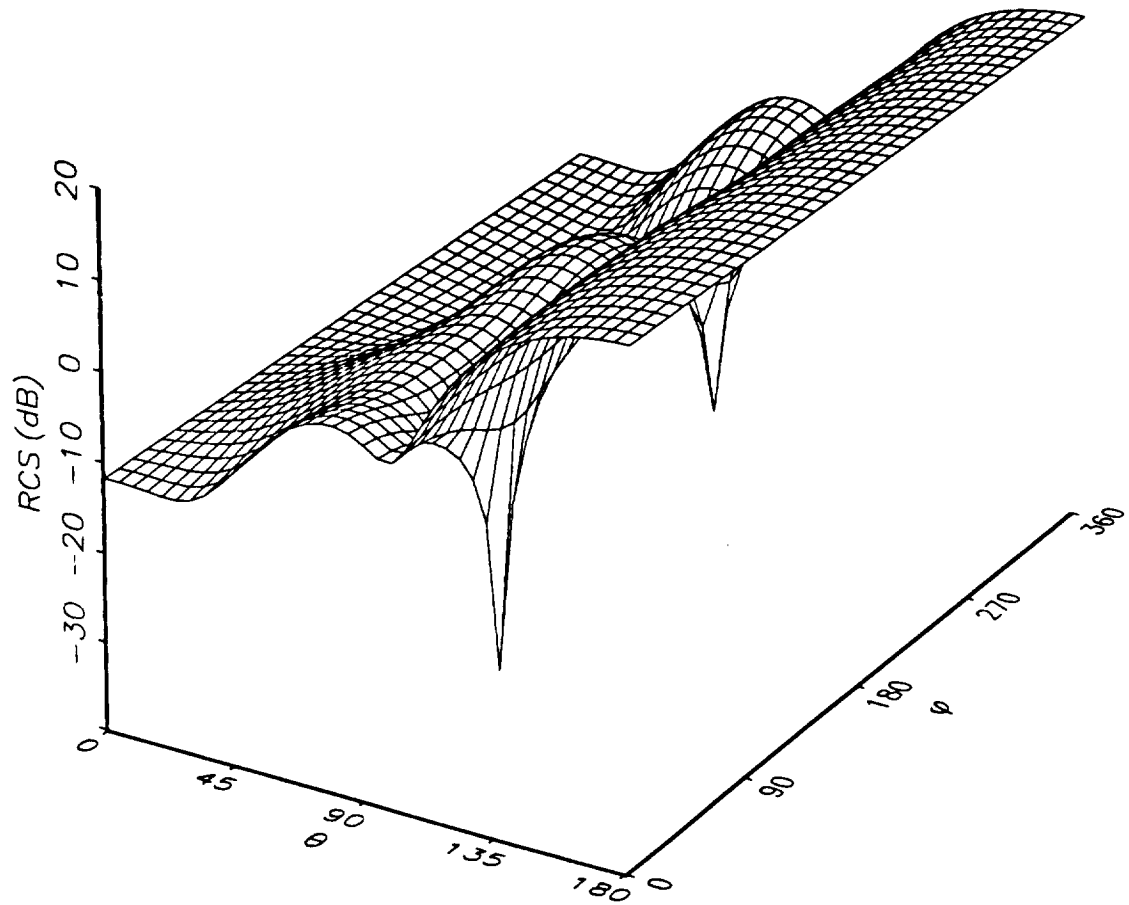


Figure 4.2.29 Bistatic radar cross section for cone-cylinder with impedance patch: TM polarization, $\phi_i = 270^\circ$ and $\theta_i = 180^\circ$ - $k_0 h_{\text{cyl}} = 4$, $k_0 r_{\text{cyl}} = 1$, $\alpha_{\text{conc}} = 26.565^\circ$, $k_0 r_{\text{up}} = k_0 r_{\text{J2}} = 0.25$, $k_0 r_{\text{J1}} = 0.75$, $N_s = 16$ and $N_\phi = 11$; with η given by eq. (4.2.3).

BIBLIOGRAPHY

Bowman, J. J., Senior, T. B. A. and Uslenghi, P. L. E., 'Electromagnetic and Acoustical Scattering by Simple Shapes', Hemisphere Publishing Corporation, New York, 1987

deBoor, C., 'A Practical Guide to Splines', Springer-Verlag, New York, 1978

Elliott, Robert S., 'Antenna Theory and Design', Prentice-Hall Inc., 1981.

Graglia, R. D., and Uslenghi, P. L. E., 'Electromagnetic Scattering from Anisotropic Materials, Part I: General Theory', IEEE Trans. Antenna Propagat., Vol. AP-32, no. 8, p867-869, August, 1984.

Graglia, R. D., and Uslenghi, P. L. E., 'Electromagnetic Scattering from Anisotropic Materials, Part II: General Theory', IEEE Trans. Antenna Propagat., Vol. AP-35, no. 2, p225-232, February, 1987.

Graglia, R. D., and Uslenghi, P. L. E., 'Anisotropic Layered Absorbers on Cylindrical Structures', Electromagnetics, Vol. 7, no. 2, p117-127, 1987.

Graglia, R. D., 'The Use of Parametric Elements in the Moment Method Solution of Static and Dynamic Volume Integral Equations', IEEE Trans. Antennas Propagat., Vol. AP-36, pp. 636-646, May 1988.

Graglia, R. D., and Uslenghi, P. L. E., 'Surface Currents on Impedance Bodies of Revolution', IEEE Trans. Antennas Propagat., Vol. AP-36, no. 9, pp. 1313-1317, September, 1988.

Graglia, R. D., Uslenghi, P. L. E., and Zich, R. S., 'Moment Method with Isoparametric Elements for Three-Dimensional Anisotropic Scatterers', Proc. IEEE., Vol. 77, no. 5, p750-760, May, 1989.

Harrington, R. F., 'Field Computation by Moment Methods', MacMillan Publishing Company, New York, 1968

Harrington, R. F., 'Time-Harmonic Electromagnetic Fields', McGraw-Hill, New York, 1961

Jones, D. S., 'Methods in Electromagnetic Wave Propagation', Clarendon Press, Oxford, 1979.

Kellog, O. D., 'Foundations of Potential Theory', Dover, New York, 1953

Lancaster, P. and Salkauskas, K., 'Curve and Surface Fitting: An Introduction', Academic Press, New York, 1986

Mitzner, K. M., 'Numerical Solution of the Exterior Scattering Problem at the Eigenfrequencies of the Interior Problem', Fall URSI Meeting, Boston MA, 1968.

Oshiro, F. K., Mitzner, K. M. and Locus, S. S., 'Calculation of Radar Cross-section', Air Force Avionics Laboratory Technical Report. AFAL-TR-70-21, Part II, April 1970.

Poggio, A. J. and Miller, E. K., 'Integral Equation Solutions of Three-dimensional Scattering Problems' in R. Mittra (ed), Computer Techniques for Electromagnetics, Chap. 4, Pergamon Press, London, 1973

Uslenghi, P.L.E., Laxpati, S.R. and Kawalko, S.F., 'Computer Code For Scattering From Impedance Bodies of Revolution Part I: Axial Incidence', Department of Electrical Engineering and Computer Science, University of Illinois at Chicago, Chicago, Illinois, Report EML-91-02-01, Feb. 1991.

Uslenghi, P.L.E., Laxpati, S.R. and Kawalko, S.F., 'Computer Code For Scattering From Impedance Bodies of Revolution Part II: Oblique Incidence', Department of Electrical Engineering and Computer Science, University of Illinois at Chicago, Chicago, Illinois, Report EML-91-11-01, Nov. 1991.

Vichnevetsky, R., 'Computer Methods for Partial Differential Equations, Volume 1', Prentice-Hall, Inc., 1981